Universitat Internacional de Catalunya
Facultat d'Odontologia

Tesis doctoral

Influence of custom made titanium meshes surface on bone regeneration using calcium phosphates

Nuno Pimentel Peito Cruz

Influence of custom made titanium meshes surface on bone regeneration using calcium phosphates

Nuno Pimentel Peito Cruz

DOCTORAL THESIS

Universitat Internacional de Catalunya, 2022

Supervisors:

Dr. Javier Gil Mur

Dr. João Paulo Tondela

Doctoral Programme in Health Sciences

Line of Research Basic and Applied Dentistry Research

Influence of custom made titanium meshes surface on bone regeneration using calcium phosphates

Dedicated to

To my wife, Andrea, and my daughters Francisca, Carolina and Teresa for the unconditional love and support, the type that can´t be drawn, measured or weighted. Everything I do is to try to make you proud and to be worthy of the family I was blessed with.

To my mother and father… no words needed!

ACKNOWLEDGEMENTS

I´m truly grateful to my Directors, my mentors and my dearest friends, Dr. Javier Gil Mur and Dr. João Paulo Tondela. Your knowledge and ability to teach and guide are truly inspiring. Thank you for your patience, support and friendship in such a generous and unselfish way that will mark me for the rest of my life.

Thank you to all my masters and Professors that I was lucky to came across throughout my student life. Every single of them were a piece in my learning process puzzle.

Thank you to Rui Coelho, dear friend and mentor, for all the long conversations and science discussions.

Thank you to my “brothers in arms”, Nuno Oliveira and Joaquim Reis, for putting up with me for so long. True friendship never ends!

Thank you to Inês Martins for the effort putted in our work here presented.

Thank you to BoneEasy for the contribution to our work here presented.

Thank you to Klockner for the contribution to our work here presented.

Thank you to Hospital da Luz Coimbra, its Administrator and Clinical Director for the trust and support.

Table of Contents

1. Introduction

Oral and maxillofacial reconstructive attempts strongly developed and evolved over the last five decades to meet both patients demands and health professionals needs.

The use of dental implants in oral rehabilitation became a regular base treatment option for partial or total edentulism, in most cases requested by the patient himself.

Nowadays there is no doubt that rehabilitation of edentulism using osseointegrated implants has revolutionized the field of dentistry and improved patients' quality of life (1), allowing an extension of treatment options to prosthetically rehabilitate patients suffering from partial or total edentulism, with or without the presence of maxillary atrophy (2).

The quality and volume of alveolar bone in the implant area affect various factors related to a successful implant restoration as the three-dimensional position of the implant, the primary stability, the soft tissue behavior (3). Even with the development of numerous techniques and augmentation materials, the reestablishment of an adequate bone anatomy, especially in vertical defects, still remains an ultimate challenge (2). Moreover, bone volume loss as a consequence of many systemic and periodontal diseases, trauma and tumors, may result in major difficulties to rehabilitate with endosseous dental implants (1).

One can say that severe bone loss and anatomical consequences of the bone defects determine not only the prognosis but augmentation treatment itself (1), especially in cases of long-lasting edentulism, where the residual bone volume is insufficient to place dental implants in a prosthetic driven way, as requested by the most recent rehabilitation guidelines (4).

Another important aspect relies on maxilla and mandible alveolar bone resorption patterns, since it jeopardizes the structural, functional, and esthetic outcomes of

implant treatment. After teeth loss, alveolar bone resorption takes place initially in a horizontal direction, proximally within the first 6 months, and then in a vertical direction (1). In case of the mandible, it is also primarily horizontal; in interforaminal regions and characterized by a centripetal resorption pattern; however, it is vertical and centrifugal in retroforaminal areas (5).

As found in the literature, teeth extractions are responsible for bone dimensional changes, occurring mostly within the first year. Overall, the crestal width reduction can be higher than 50%, with 2/3 of this horizontal resorption occurring during the first 3 months after tooth extraction (6)(7).

Other reports described bone loss after tooth loss to vary between 40% and 60% during the first 3 years, and then calculated to continuously increase in a range between 0.25% and 0.5% annually (7).

To achieve good long-term results in dental implantology, adequate bone quality and quantity are needed (8). In order to achieve this goal, a wide variety of strategies, from the alveolar preservation techniques to bone-grafting techniques by means of bone blocks (free vascularized autografts), Ridge Splitting, Sinus Lifting, Bone Distraction, and Guided Bone Regeneration (GBR), have been used to preserve bone or regain the lost bone and to allow implants to be fully integrated and maintained during mechanical loading, overcoming the limitations of an insufficient residual bone (1) (3)(6)(7)(9)(10)(11)(12)(13)(14)(15)(16)(17)

Even though these surgical therapies have been widely and long term studied, in the last three decades, the most adequate approach remains unclear, especially when effectiveness of these techniques are orientated for vertical clinical bone gain. In other words, there is inconclusive evidence to support the effectiveness of a surgical technique over another (11)(12).

One particular technique, Guided Bone Regeneration (GBR), was brought to our attention since it has been considered as one of the bone augmentation methods most applied (1)(18), demonstrating high success rates, less complications and long-term stability (17)(19).

Guided Bone Regeneration is a successful, well-documented, and widely used procedure in prosthetic rehabilitation that implicates some kind of bone augmentation, during or previously to implant placement (1).

According to the literature, it represents the gold standard of bone augmentation procedures and is the most documented bone augmentation technique (20)(21).

The concept of GBR, as usually referred to, was first introduced more than 50 years ago by Hurley et al (1959), by using cellulose acetate filters to regenerate nerves and tendons (14)(22)(23)(24). Next, cellulose acetate (MilliporeTM membrane filter) showed enhanced osseous healing of several different bone (rib, radial bone and femoral) defects. Later, a few animal studies demonstrated that GBR can predictably facilitate bone regeneration even in critical-sized osseous defects, as well as the healing of bone defects around dental implants by horizontal and vertical augmentation of atrophic alveolar ridges before implant placement (22)(24).

The basic principle of GBR involves the placement of mechanical barriers to protect blood clots and to separate the bone defect from the surrounding connective tissue, enabling bone-forming cells with access to an isolated area ment for bone regeneration (13)(14)(17)(22)(25)(26).

In other words, GBR prevents in a selective way that epithelial and connective tissue cells invade the bone defect area, by means of barrier membranes based on different migration rate of various cells, allowing osteoblasts preferentially enter the bone defect area to complete bone induction and regeneration. By using bone graft materials as scaffolds in the defect area, guiding will be provided to osteoblasts and osteocyte in order to form new bone (3).

Focused on Wang´s PASS Principle for a correct surgical approach (primary closure, angiogenesis, space maintenance and blood clot stability) (21), Guided Bone Regeneration is presumed to be achieved when bone precursor cells (osteoprogenitor) occupy the bone defect site and simultaneous avoided the entry of non-osteogenic tissues. It has been estimated at least 40% of osseointegrated implants require GBR as part of the patient’s rehabilitation. Several reports have

indicated that the survival rates of implants placed in regenerate areas by means of GBR are quite similar to those reported for implants placed in pristine bone. The survival rate of implants placed in augmented sites varied between 79% and 100%. Moreover, most of those reports indicated a survival rate of more than 90% at least 1 year after loading(1).

Like other alveolar ridge augmentation procedures, GBR is a sensitive technique that depends on the operator´s experience and skills. For this reason, new procedures and materials are frequently proposed in order to achieve more predictable results, with easier workflows (11)(12)(18)(25)(27). However, as mention before, it has been indicated that bone augmentation is still challenging in vertical bone defects and extreme horizontal atrophy (4)(11)(12)(27). This is primarily due to technique sensitivity and, consequently, some relatively frequent surgical complications (regardless of being intra or post-operatory). Vertical bone augmentation aims to achieve bone regeneration without osseous wall containment (in other words, without a bone envelope to support the stability of the clot and the bone graft). This is why it is a biologically demanding procedure, as angiogenesis must reach a certain distance from existing bone for new bone to be formed. In addition, the soft tissue must be mobilized to provide a closed healing environment for the increased dimensions of the alveolar ridge, demanding a correct flap design and tension-free closure of the wound (11).

Currently, different types of membranes (resorbable and non-resorbable, example figure 1.a and 1.b respectively) in conjunction with various bone substitutes (allogenic, xenogenic and alloplastic) materials can be used in GBR procedures, the choice of depends on numerous factors.

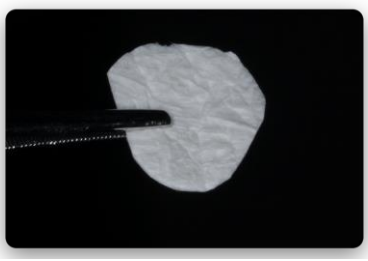

Figure 1.a: Collagen resorbable membrane.

Figure 1.b: d-PTFE non-resorbable membrane.

Clinical studies demonstrate that GBR is predictable and successful for horizontal defect augmentation, independently of the type of membrane used, either resorbable or non-resorbable (1).

Supporting this findings, recent investigations have proven GBR techniques to be the most reliable in terms of bone gain and absence of complications. As such, Urban and colleagues demonstrated vertical bone gain of 5.1 ± 1.8 mm and horizontal bone gain of 7.0 ± 1.5 mm by means of combination of heterologous and autogenous bone with barrier membranes (6).

However, even using autologous bone by itself (known as the gold standard filling material) one of the biggest challenges is to minimize the graft resorption. With this same purpose, some authors have presented augmentation procedures in conjunction with a non-resorbable barrier membrane, while others have choosen to use of bone blocks without membranes. Published data, comparing two techniques of bone augmentation with an onlay graft alone or associated with a membrane, showed that the membrane group presented significantly less resorption than the graft-alone group. Curiously, similar results were published by Roccuzzo et al in 2006, when comparing the results of vertical bone regeneration gains using autologous bone alone or covered with a titanium mesh (28).

Another important aspect of the use of a bone graft material is that it prevents membrane to collapse, while creating the necessary space for regeneration during a certain period of time. Moreover, micromovement of the resorbable membrane following surgery may disturb the blood clot, disrupt of the bone grafting material and cause soft tissue dehiscence (7).

Not only from a biological point of view but also from a mechanical perspective, membranes play a crucial role in GBR, acting as a barrier and space maintainer scaffold. Moreover, as medical devices they should be able to integrate the surrounding tissue, biocompatible, able to create and maintain space, cellocclusive and manageable by the operator (1)(22).

In other words, when considering non resorbable membranes (not only indicated for horizontal defects but specially for vertical defects), the ideal GBR membrane should be sufficiently rigid to sustain compression forces coming from the overlying soft tissue. It should also possess a degree of plasticity in order to be easily adapted to the shape of the defect. A balance between these mechanical properties will result in an adequate space-making capacity (1).

The most representative non resorbable membranes are titanium meshes and polytetrafluoroethylene (PTFE) expanded (e-PTFE, discontinued and no longer available, known as Gore-Tex) or high density (d-PTFE, also known as Teflon).

Titanium is a commonly used material in dentistry, craniomaxillofacial surgery, and orthopedics. Among its properties are biocompatibility, high strength and rigidity, low density and weight, the ability to withstand high temperatures, and resistance to corrosion. This is a highly reactive metal, and can be readily passivated to form a protective oxide layer, giving it a high corrosion resistance (29)(30)(31)(32)(33)(29)(34)(35).

The use of titanium for GBR was inspired from a successful outcome of using a titanium mesh for reconstruction of maxillofacial defects (1)(3)(22).

Back in 1969, Boyne et al. used a titanium mesh for the first time to reconstruct large bone defects (22), and then proposed it for osseous restoration of deficient

edentulous ridges (9), as showed by Boyne et al in 1985 and by Gongloff et al in 1986 (26)(36)(37).

The use of titanium meshes was once again highlighted by von Arx et al with the so called “the TIME technique”, characterized by the use of micro titanium augmentation mesh specifically designed for bone augmentation (38). Von Arx et al. showed good results when using the micro titanium meshes for ridge augmentation prior and simultaneously to implant placement (14).

Occlusive titanium (without pores) membranes have also been successfully introduced and used for ridge augmentation and surrounding implant defects. Several studies have shown that using a titanium mesh is an effective procedure for bone augmentation procedures prior or simultaneously with implant placement (1).

Again, titanium has excellent mechanical properties. Its rigidity prevents membrane collapse and provides space maintenance and on the other hand, its plasticity permits bending, contouring, and adaptation to the bone defect (figure 2). This mechanical strength responsible for space maintenance seems to be an important success criterion, and can be affected by the thickness and pore size properties (figure 3).

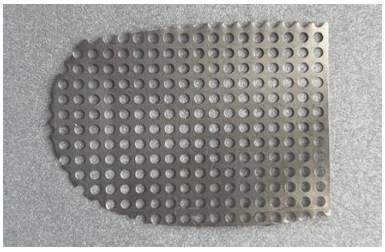

Figure 2: Example of a standard titanium mesh.

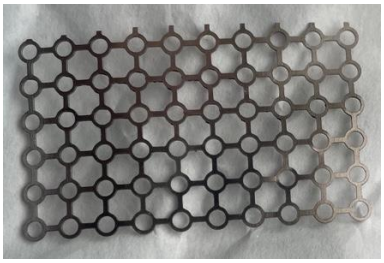

Figure 3: Example of another standard titanium mesh.

However, the stiffness and cut edges of titanium mesh sometimes cause mucosal irritation that may lead to exposure of the membrane and possibly infection. In addition, sharp edges, caused by cutting, trimming, and bending of titanium mesh, can be responsible for exposure of titanium barriers.

On the other hand, several studies demonstrated that titanium meshes maintains space with a high degree of predictably, even when involving large bony cavities. In addition, it is believed that the smooth surface of titanium mesh makes it less susceptible to bacterial contamination than resorbable materials (1)(3)(10)(22)(39)(40)(41)(42).

A particular aspect is that, in case of exposure, no infection of the graft is noticed, according to von Arx et al. This is no doubt an advantage when comparing with e-PTFE barriers, which many times result in infection when exposed and consequently loss of bone volume (22).

In a recent randomized clinical trial published by Cucchi et al, 2017, bone gain, surgical and healing complications in regenerated areas, using titanium meshes and d-PTFE membranes where compared. They concluded that both GBR approaches for the restoration of atrophic posterior mandible achieved similar results, on vertical bone gain and implant stability and presented same rate of complications (5).

According to the type of pores, two types of titanium meshes can be distinguish: micro porous and macro porous although their thickness can vary (3)(7).

The thickness and porosity of titanium meshes are the key elements that affect mechanical properties. It has been suggested that the thickness of titanium mesh may affect the total amount of new bone formation, while the pore size may affect the proportion of bone and soft tissue formation under titanium mesh (3).

The thickness of titanium meshes usually ranging between 0.1 and 0.6 mm is directly proportional to its mechanical properties. Titanium meshes with 0.2 mm can be suitable for most instances (3)(10).

Results published in 2018, by Bai et al, indicate that the titanium mesh with a thickness of 0.4 mm is more suitable for clinical use. Regarding the optimal pore size of the titanium mesh, the diameter of the pores had less influence on mesh mechanical properties (10).

A study showed that 0.1–0.2 mm is the ideal thickness of titanium mesh to use in several different clinical situations. Consistent with this result, Rakhmatia et al. compared bone augmentation achievements with titanium mesh at 20, 50, and 100 μm in an animal study and concluded that the 100 μm meshes can achieve more extensive bone regeneration effect. Basically, when it comes to mesh thickness, a balance between the strength for spatial stability and malleability for adapting to the adjacent bone contours must be found (3).

The occlusive pattern of a membrane is a property related to its porosity, with major influence on the potential for cell invasion. Literature that supports the role of pore size of barrier membranes in preventing excessive soft tissue ingrowth showed the formation of a layer of fibrous tissue of varying thickness adhering to newly regenerated bone (22)(23). In fact, there is no doubt that it should be considered at least as important as its space-maintaining properties when regenerating bone defects (22).

The architecture of the porous structures in general, and not the type of material used, has been suggested to influence the biological capacity of a material. Pores

facilitate the diffusion of fluids, oxygen, nutrients and bioactive substances essential for cell development, within a bone and soft tissue regeneration process. However, these pores must also be impermeable to soft tissue cells (epithelial cells or gingival fibroblasts) (22).

Due to this fact, the ideal pore size still remains unclear. A larger pore size will allow these faster-growing cells to invade the defect area, drastically reducing the activity of bone-forming cells. Moreover, some authors defend that larger pore size permit an easy pathway for bacterial contamination, when exposed, leading to premature removal of the membrane in extreme infection situation. On the other hand, if pores are too small, cell migration will be strongly diminished, which leads to enhanced collagen deposition, the formation of avascular tissue, and an absence of organized capillary blood supply. Also, pore size will affect the capacity of the material to support the tissue. A large pore size will inevitably decrease the resulting surface area of the material, which can be an important obstacle to the initial cell adhesion onto the membrane and subsequent decrease of blood vessel ingrowth. In other words, macroporosity promotes the attachment of soft tissues, which may stabilize and restrict the migration of soft tissue (22)(43).

However, this makes the material difficult to remove at the second surgery (22)(43).

Gutta et al published a study about the comparison of bone formation by means of microporous titanium meshes alone or combined with collagen membranes, and macroporous titanium meshes. Greater bone formation was found in those cases where microporous meshes without collagen membrane were used. In addition, there was a significant soft tissue ingrowth within the resorbable membrane, whereas the macroporous titanium mesh prevented soft tissue ingrowth better than the other two types of membranes.

However, other studies reported more complications and high percentages of graft loss associated with the use of titanium micromesh (7).

In conclusion, the relationship between the pore size of titanium mesh and bone formation is still under discussion (3).

At this point, exploring the incidence and possible consequences of mesh exposure is mandatory, in order to better understand the reliability of titanium meshes use in bone augmentation procedures.

Mesh exposure has been reported has the most common complication, with different rates ranging from 5% up to 50% (40)(44).

The mean exposure rate was found to be 20.7%. The average reported bone regeneration with commercially available titanium meshes was 4.91 mm (2.56–8.6 mm) vertically and 4.36 mm (3.75–5.65 mm) horizontally (40)(45)(46).

Since the most common complication with titanium meshes is exposure(46), there is no doubt that a correct management of soft tissue plays a significant role in order to avoid premature or even late exposure of the mesh and regenerated area. In fact, Briguglio et al concluded, in their systematic review published in 2019, that a careful surgical planning and proper soft tissue management make this type of regenerative therapy the gold standard (20).

There is still a controversy in the literature regarding the effect of titanium mesh exposure on bone regeneration volume outcome. While several authors have reported no consequences of graft exposure,23,36 others have reported bone losses when the mesh is exposed (13)(47)(38)(48).

However, when bone loss was noticed, the obtained bone volume was enough to place implants.

Aceves-Argemí et al published in 2021 a systematic review where a significant prevalence of mesh exposure (28%) was reported. Despite of soft tissue dehiscence and membrane exposure high risk, the optimal management of membrane exposition allows enough bone volume in order to achieve the expected treatment outcome. Those findings are in line with other systematic reviews published before. One curious aspect of this review was that the authors

included different types of titanium meshes: commercial standard foils, preshaped and custom-made (21).

Furthermore, the exposure rate of titanium meshes is lower than that of PTFE membranes, and if the exposure occurs, it is not necessary to remove the mesh immediately in the majority of the clinical situations. This is due to its pore structure, which allows a proper vascular supply to the underlying tissues without blood flow interruption. As mentioned before, there is also a low risk of infection in this situation (3)(20).

However, if a post-operation serious infection occurs, implant surfaces are exposed to a bacteria-rich environment and rapidly become colonized by oral bacteria, competing with epithelial and connective tissues and cells for binding to the implant surface, leading to a possible implant failure (49)(50).

In conclusion, probably the most important factor affecting the bone formation capability seems to be exposure of the mesh, especially in terms of the extent and timing, even if this complication apparently does not compromise the prosthetic result (18)(41)(45)(51).

The effect of the size of the exposure, the timing of the exposure after the initial ridge augmentation procedure, and the type of graft material on the final clinical outcome need further investigation (46).

The introduction of digital tools in dentistry were a game changer. The implementation of 3D computer-aided design/computer-aided manufacturing (CAD/CAM) was able to introduce a new concept of bone regeneration performance based on the patient specific needs, meaning a new stabilization concept that is specifically manufactured to fit into the individual defect morphology. The individualized 3D titanium mesh designed and produced based on virtual planning and design (figure 4) using computed tomography (CT) or cone beam computed tomography (CBCT) Dicom files (8).

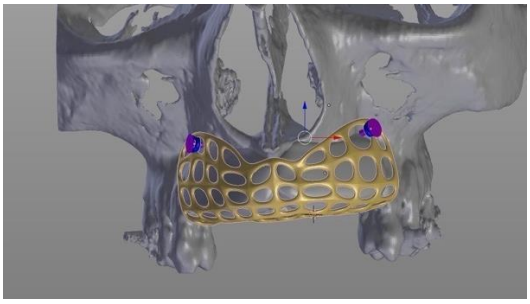

Figure 4: Example of a virtual planning and design of a titanium mesh.

Selective laser melting (SLM) is a rapid prototyping manufacture process that allows to build up customized titanium alloy scaffolds with highly defined shape (52)(53).

SLM is capable of producing complex structures layer by layer with high precision, using biocompatible materials like ceramics, polymers, titanium and its alloys (52)(53)(54). By using a very precise nanolaser beam of only 0.03mm diameter, this process is able to build up titanium alloy structures layer by layer with any desirable form, in steps of only 0.05mm along the z-axis (52).

This method has proven to be a suitable technique to produce with accuracy individualized titanium meshes with cell compatible surfaces and remains as first choice until today (53)(55)(56).

When combined with computer-assisted design (CAD) we are able to create three-dimensional individualized medical devices like scaffolds or meshes for bone augmentation (figure 5).

Figure 5: Example of an individualized titanium mesh.

Yet, there is still limited information on the effect of design and processing parameters of SLM on the quality and mechanical properties of this titanium scaffolds (33).

In 2011, Ciocca et al describes a protocol for the direct manufacturing of a customized titanium mesh using Computer Aid Design (CAD) and Computer aid Manufacture (CAM) to rapid prototype a titanium mesh for maxillary bone augmentation (57).

As far as we know, this was the first report on a new novel of GBR using custommade titanium meshes and represented an important landmark for the following 10 years of investigation on this subject.

At this point, no existing bone augmentation protocol considered an exact quantification of the volume needed to surgery to the minimum and, at the same time, enough for implant therapy. Also, no technique existed which considered planning bone augmentation in relation to implant length and position, as dictated by the final position of the prosthesis (57)(58), also known as reverse planning or prosthetically guided bone regeneration (15).

This enables the direct production of patient-specific titanium meshes, which allows aiming bone to regenerate towards the recreation of the lost anatomy.

Moreover, it eliminates the need to cut and pre-bend the mesh and offers better control over the bone regenerative procedure (59).

When compared to the conventional titanium meshes, custom-made meshes greatly reduce the intervention time and are more adjust to the alveolar bone. The individualized shape that entirely fits the alveolar ridge also allows to use less stabilization screws. The rounded blunt edges produced by 3D printing reduces the risk of mucosal rupture and titanium mesh exposure, making it more accurate and less invasive (3). That being said, a smaller rate exposure can indicate a more predictable result. Also, it can greatly reduce surgical time and potential errors in adapting the mesh intraorally, improve fitting and restore geometrically complex anatomical defects as showed in the literature (10)(42)(58)(60).

In conclusion, all the surgical and biological principles of Guided Bone Regeneration apply to this particular technique, especially those that guide the use of traditional titanium meshes. All the advantages previously mentioned, are confirmed in biomechanical, animal and human research published so far, stating that this kind of 3D printed titanium meshes can provide excellent biocompatibility, fitting ability, space creating capacity, adequate mechanical and physical properties. Moreover, when compared to traditional meshes, their use turns out into a lower risk of mesh exposure (0%-33%) (16)(19)(41)(56)(58)(61)(62)(63)(64)(2), shorter surgery and better post operation recovery. Up till now, the existing literature suggests that the use of individualized meshes can achieve clinical efficacy and long-term stability, with high GBR success rate and implant survival rate (19)(56).

Although exposures are, without any doubt, a common complication related to mesh placement, most of the time bone gains are not affected and the final treatment not compromised (61)(62)(63)(64)(65).

Nevertheless, exposure rates still remain a major concern when considering this particular surgical technique.

Independently of the production technique for any implantable devices, it is important to control the characteristics to optimize their biological performance.

Regardless the thickness of the material and pore dimensions, already addressed before, properties that influence cellular interactions like surface topography and chemical composition, results of surface treatments applied and play an important role (17).

The biocompatibility of materials can be analyzed according to corrosion resistance and cytotoxicity (3)(16)(66).

Titanium mesh has good biocompatibility and can be well tolerate by both hard and soft tissues. It's a reactive metal that forms, spontaneously, in the air, water or any other electrolyte, a thin and strongly bonded native oxide film, which is responsible for titanium biocompatibility. Also, because of its low electrical conductivity, titanium is able to perform electrochemical oxidation, creating a passive and inert oxide layer. This oxide layer can be retained under the pH of human body, resulting in strong corrosion resistance. Basically, this is why little amount of particles are released from titanium mesh, having no significant effect on human cells' relative growth rate. Surface properties play a critical role in the process of bone cells recognition and response (3)(16)(66)(67).

Regarding the biocompatibility of titanium, initial cell attachment and growth and bacterial response are closely related to surface properties such as roughness, topography, wettability and chemistry (29)(31)(50)(68).

The presence of different specific proteins at the cell-biomaterial interface may potentiate transduction signals, by the ECM-transmembrane-cytoskeleton and between the extracellular/intracellular network (69)(70).

Surface topography and roughness are aspects that can be easily developed by post-production surface treatments; they play a strategic role in the determination of cellular interactions, influencing adhesion, differentiation and also migration, in order to seal off the underlying defect from the oral flora (17)(43). On the other hand, the microstructure may also influence the behavior of osteoblasts, their attachment, spread, and activity with interference on the mineralization result of the regenerative area (62).

In the study published by Dellavia et al in 2020, evaluated meshes were biocompatible in all cases without signs of adverse reactions. The tissue surrounding the mesh was well organized, covered by mucosa and lining in direct contact with mineralized bone, characterized superiorly by mucosa and inferiorly by mineralized bone well in contact with the mesh (62).

Morphological and histomorphometric assessments, apparently indicate that the use of customized titanium meshes induces the regeneration of a well-structured and organized bone tissue, vital, and active in the remodeling and integration of the bone substitute material. This result was in line with previous studies (62)(71).

Attachment of cells to a barrier membrane involves a four-step sequence that includes adsorption of glycoproteins to the substrate surface, cell contact, attachment and spreading. Cell migration and proliferation can be watched after these events have happened (43).

In a reasonable way, it can be said that the most important aspect of a biomaterial is that it is biocompatible, being the degrees of compatibility or, in its case of toxicity, evaluated throughout test to analyze (72):

- The interaction between the material and the tissues; - The reaction resulting from the degradation of the material; - Mechanical factors (elasticity, toughness, etc.).

It is completely understood that the corrosion products formed as a result of metal-environment interactions have important consequences on the biocompatibility and long-term stability of the medical device. There must not be adverse reactions caused by the applied material and neither properties should be affected during function (34).

Literature shows that high degree of roughness presents a major risk for ionic release and increased bacterial colonization. On the other hand, smooth surfaces are capable of minimizing the biological reactions at the interface, keeping the titanium oxidized layer more stable for longer periods. An adequate micro and nano-roughness surface can stimulate osteoblast differentiation, proliferation and

maturation. Also, if there is an exposure during healing, it would be important to realize if chemical modifications of the exposed surface could affect the bone growth (17).

Titanium and its alloys are used for manufacturing dental implantable devices due to their favorable properties for in vivo use. Titanium ability to spontaneously and quickly form a passive oxide film leads to a bioinert layer. Even if the passive oxide is broken, it can be rapidly regenerated in the presence of oxygen, regaining the surface protection (32)(72)(73).

This passive layer is very stable during function even under demanding mechanical and chemical conditions (mastication, exposure to fluids in the oral cavity, etc.). Various studies pointed out to the effects of some of the environment factors on the corrosion resistance. Examples of the medium factors that affect the corrosion behavior of dental materials are saliva composition, microbiological and enzymatic characteristics, humidity, biofilm formation, contact with blood and its constituents, presence of fluorine and hydrogen peroxide, pH change in the buccal region, physical and chemical properties of foods, hypersensitivity reactions to titanium [15], contact with different organic compounds and different concentrations of proteins, presence or absence of oxygen. Berbel et al (2019) concluded that titanium's corrosion resistance can be reduced by intense inflammatory conditions, by simulating those conditions in vitro (reduced pO2, acidic environment, presence of Albumin similar to one found in body fluids and hydrogen peroxide) (34)(73).

In surface engineering of biomaterials, changing the properties of the material surface, such as charge and roughness, is mainly a good strategy for enhancing the interactions between the cell and the implantable material, in which extracellular matrix adhesion proteins can appropriately function (70).

The Different processes used to modify the physical and/or chemical properties of materials surfaces can be divided in two main categories, depending on whether a layer of new material is applied on the implant surface (additive) or if

the surface itself is changed by exposing it to physical or chemical agents, such as sand, gases, plasmas, or wet chemicals (subtractive) (74).

Cell differentiation and secretion are mediated by implant surface irregularities and roughness. The advantages of a particularly moderate rough surfaces are the wider contact area between implant and host environment, a firmer mechanical link and, above all, the enhanced and faster cell-mediated osteointegration process. Not only the depth, but the distribution of irregularities, cavity morphology, and the presence of contaminating elements derived from the treatment procedures, probably play an important role in cell behavior (29).

Osteoblast/titanium adhesion depends on the surface characteristics of titanium which may be described according to local mesoscale, microscale and nanoscale patterns of topography, roughness, charge distribution and chemistry (66).

Osteogenic cell differentiation is higher on surfaces with roughness in the range of 0.2–2 μm Ra (microscale roughness) (75).

Fibroblasts adhesion and spreading upon the biomaterial surface is also an important parameter. Their behavior is also correlated to surface characteristics like hydrophilicity, roughness, texture, chemical composition, charge and morphology, which strongly affect cellular responses (76).

Fibroblasts have higher adhesion on surfaces with roughness below 0.2 μm Ra and with regular patterns. The upper limit to roughness in order to positively stimulate fibroblast adhesion, could be around 0.1 μm (75).

In this context, fibroblasts and macrophages behavior are particularly relevant as macrophages react to an implant as it being a chronic inflammation or healing and fibroblasts establishing the initial granulation tissue to be remodeled and hopefully replaced by the local tissue type (75).

A strong correlation between surface roughness and cell proliferation has been demonstrated in a study published by Ponsonnet et al. In this study, the authors concluded that, despite the high number of parameters that influence cell adhesion and proliferation, surface free energy appears to be a dominant factor.

However, roughness can strongly interfere in the relationships between surface free energy and cell proliferation. When taking roughness into consideration, there might be a threshold between 0.08 – 1 μm over which the surface free energy can be altered, leading to a lower fibroblast proliferation (76).

When surface chemistry in concerned, it is reported that high hydrophilic surfaces are capable of inducing fast adhesion, spreading and organization of fibroblast´s cytoskeleton, as well as production of collagen fibers and formation of a connective tissue with good vascular network. Roughness on nanoscale (below 0.2 μm Ra) is also an advantage, not only because promote higher adhesion of fibroblasts but also when there is risk of infection. In order to avoid bacterial contamination, it is better not overcome the threshold of 0.2 μm Ra (75).

Moving towards, commercially pure titanium and the titanium alloys have recently been reviewed in their biocompatibility and tissue performance similarities/differences (1).

Both cp-Ti and Ti6Al4V have moderate wettable surfaces and are hydrophilic, with similar water contact angles. Both cp-Ti and Ti6Al4V Surface topography created by blasting, acid etching, or anodization show a reduced wetting similarity (32).

Commercially pure titanium implants are extensively used, however, there are disadvantages as low wear, shear resistance, and little deformability. For that reason, they are not indicated for load support since there is a risk of fracture. Therefore, titanium alloy implants are a first choice due to better general mechanical properties, which allow to meet the adequate requirements for load bearing medical devices (77)(78).

However, $\mathcal{B}$-Titanium Alloys, composed of chemical elements such as Nb, Ta, Zr, Mo, and Sn, seems to be a promising choice since do not present cytotoxic reactions when they are in contact with cells. This is mainly due to their better resistance to corrosion (77).

Nevertheless, there is still a lack of consensus on the best chemical composition of the Ti alloy for biomedical applications based on the possible release and effects of its ions in long term, in vivo studies (77).

Titanium meshes has been used with success with different graft materials (40) and, as in any regenerative process, a sequence of biochemical, cellular and tissue events must occur, which are more significantly dependent from the biological characteristics of the grafted tissue rather than from the surgical technique performed (79).

A key element for bone regeneration is the scaffold that serves as a template for cell interactions and formation of bone extracellular matrix to support to the newly formed tissue. These scaffolds must fulfill important criteria to perform their function, including mechanical properties similar to the native bone, biocompatibility and biodegradability. These templates must be osteoconductive and may serve as delivery vehicles for cytokines such as bone morphogenetic proteins (BMPs), insulin-like growth, factors (IGFs) and transforming growth factors (TGFs). These mediators are responsible for osteoinduction, attracting and transforming recruited undifferentiated precursor cells from the host into bone matrix producing cells. Osteogenesis occurs by complementing the scaffolds before implantation with osteoblasts and mesenchymal cells that have the potential to create new bone formation (80)(81).

By adding a favorable mechanical environment, we reach the four major elements that constitute Wang´s Diamond Concept for bone regeneration (82).

An ideal scaffold can be described by Hollister et al 4Fs rule: Form, function, Fixation and Formation. It should maintain, induce, and restore biological functions. At the same time, it must also have flexibility and strength, be cell binding and up taker, and biodegradable with non-immunogenicity (82).

In short, biomaterials or bone substitutes (figure 6) act themselves like scaffolds and ideally should fulfill a set of important characteristics (83):

1. Have high porosity, an interconnected pore network to allow cell migration and growth and vital movement of nutrients and metabolic waste;
2. Be biocompatible and bioresorbable with a desirable resorption rate, to match bone formation;
3. Suitable chemical surface for cell attachment, proliferation, and differentiation;
4. Have mechanical properties as close as possible to the tissues at the site of implantation;
5. Be able to be commercially available, safely sterilized without any compromising its properties.

Figure 6: Example of a bone substitute (DBBM).

Clinically, a bone substitute should be easy to use and cost effective. A feature also important, being easily recognized radiographically, allows to follow the rate of resorption/substitution.

Regarding the structure, materials particle size affects contact area while pore size, has major influence over the interaction of osteogenic cells with the

biomaterial surface. Biological integration requires pores that are greater than 100–150mm in diameter to provide a blood supply to the tissues.

Moreover, a material's resorption rate should match the formation rate of the new bone tissue (81).

Bone is a living tissue that serves for structural support and Calcium (Ca) metabolism. Bone matrix is organic and consists of a network of collagen protein fibers (mainly Type I collagen) impregnated with calcium phosphate (85%), calcium carbonate (10%), calcium and magnesium fluoride a (5%). The mineral compartment of bone is predominantly present in the form of calcium hydroxyapatites (Ca10[PO4]6[OH]2). Bone tissue also contains small amounts of non-collagen proteins, including bone morphogenetic proteins (BMPs) (80)(81)(82).

Calcium (Ca) plays a significant part in osteoconductivity by enhancing bone tissue integration by aggregating bone growth factors (BMPs) and osteoprogenitor cells that circulate (81).

Cells can sense the topography and scaffold elastic modulus and these properties can have an effect on progenitor cells whenever in contact with a scaffold(82). For example, osteoblasts perform greater migration, attachment and proliferation, in the presence of pores with a mean diameter of 200-400 μm, probably because the curvature of these pores provides adequate compression and tension on cell mechanoreceptors. pores greater than 300 μm are more suitable for the vascularization. In general, investigators indicate an open porosity above 50 vol% and pore sizes between 200–800 μm optimal for bone tissue growth (79).

Various bone substitutes, either synthetic (such as tricalcium phosphate, hydroxyapatite) or natural (such as coral, bovine or human bone) have been used as filling material. Autogenous bone is still considered to be the gold standard, due to the intrinsic osteogenic and osteoinductive properties. However, resorption can be expected and strategies must be implemented to avoid an unwanted loss of volume. When an extraoral site is involved as a donor, over contouring can be provided since there is enough autogenous bone available. On

the other hand, if intraoral harvesting is required, bone availability is limited. In order to overcome such limitations, deproteinized bovine bone (DBBM) as well has synthetic bone substitutes can be mixed with autogenous bone graft (14).

Scaffold properties, depend primarily on the nature of the biomaterial and the fabrication process and it has been the subject of extensive studies, including different materials such as metals, ceramics, glass, chemically synthesized polymers, natural polymers and combinations of these materials to form composites (80).

Since the 1980s, “first-generation” conventional porous calcium hydroxyapatite ceramics have been used in orthopedic, dental, and craniofacial surgery(82).

Biphasic Calcium Phosphates (BCP) have been described for the first time in 1985 at the 11th Annual Meeting of the Society for Biomaterials. They were used by Nery et al. in 1975 but the preparation was wrongly described as ‘tricalcium phosphate’ which was corrected by these authors in 1986 (84) and confirmed by LeGeros in 1988 (85).

Calcium phosphates (CaPs) biomaterials, which includes BCP, have proven efficacy in several clinical situations. Their specific physical and chemical properties (HA/TCP ratio, dual porosity and resultant architecture) regulate the progressive resorption and the simultaneous bone substitution process (86).

There are many synthetic bone graft materials available as alternatives to autogenous bone for repair, substitution or augmentation and include: metals; resorbable and non-resorbable polymers; inert ceramics (e.g., alumina, zirconia); bioactive glasses; calcium sulfates, calcium carbonates and calcium phosphates (86).

Synthetic calcium phosphates presently used as biomaterials are classified as calcium hydroxyapatite (HA), Ca10(PO4)6(OH)2; alpha- or beta-tricalcium phosphate (□- or □-TCP), Ca3(PO4)2; biphasic calcium phosphates (BCPs) as mixtures of HA and □-TCP (87).

Biphasic calcium phosphate (BCP) composed of hydroxyapatite (HA) and tricalcium phosphate (- TCP) is a bone graft substitute that resembles the inorganic phase of human bone tissue (figure 7). The insoluble HA retains its form and structure to maintain space, while the -TCP will stimulate new bone formation by dissolving into calcium and phosphate ions. The alteration of the HA/ -TCP ratio has been demonstrated to positively influence the substitution rate as well as the bioactivity of these materials (88).

Figure 7: Example of a BCP.

Calcium phosphate ceramics have been widely applied as bone substitutes, coatings, cements, drug delivery systems, and tissue engineering scaffolds due to their resemblance to the mineral portion of the bone tissue, relative ease in processing and good cell attachment. Its biocompatibility, safety, lower morbidity for the patient, predictability, unlimited availability, lower morbidity for the patient, and cost effectiveness are responsible for advantages over autografts and allografts and make them a good choice for reconstructive surgery, orthopedics, dentistry, maxillo and craniofacial surgeries, spinal arthrodesis, and neurosurgery (87).

Changes in the physico-chemical properties of bone substitute materials, i.e., porosity, shape, and size, are described as influencing the outcome of new bone formation and bone regeneration and even promoting osteoinductive properties

(87).

Moreover, materials based on calcium phosphate, β-tricalcium phosphate (βTCP; Ca3(PO4)2; Ca/P = 1.5) and hydroxyapatite (HA; Ca10(PO4)6(OH)2; Ca/P = 1.67) are considered the most adequate ceramic materials for bone augmentation, as studies demonstrate a good integration between the grafted biomaterial and the newly formed bone tissue, together with expression of osteonectin, a non-collagenous protein related to osteoblasts differentiation and metabolism (74). Other studies refer that a chemical dissolution of β-TCP particles is responsible for a local decrease of pH that favors bone tissue regeneration (89).

Hydroxyapatite (HA) is characterized for its good biocompatibility and bioactivity, osteoconductive and osteophilic properties. It can be of natural origin or it may be synthetically produced. It can be dense, microporous or macroporous HA, according to the porosity percentage, and can be presented in a crystalline or amorphous form (89).

Crystalline HA is more resistant to fracture than the amorphous form. The fact of not being able to resorb is an unfavorable point. Nevertheless, calcium phosphate (CaP) bioceramics, both of natural and synthetic origin, are among the biomaterials with higher bone replacement potential, especially biphasic calcium phosphates (HA + □−TCP) (89).

In such a complex biological and mechanical procedure like GBR, all the variables involved assume a vital role in the final outcome. The use of custommade titanium meshes with their biological and mechanical properties is, without a doubt, a major factor when applied in a bone augmentation technique. Since surface characteristics may influence the outcome and success of bone regeneration using custom-made titanium meshes, our work focused in some particular aspects of their physical and chemical characteristics, like roughness, corrosion resistance, cellular and bactericidal behavior.

Blibliography

1. Elgali I, Omar O, Dahlin C, Thomsen P. Guided bone regeneration: materials and biological mechanisms revisited. European Journal of Oral Sciences. 2017;125(5):315–37.

2. Cucchi A, Vignudelli E, Franceschi D, Randellini E, Lizio G, Fiorino A, et al. Vertical and horizontal ridge augmentation using customized CAD/CAM titanium mesh with versus without resorbable membranes. A randomized clinical trial. Clinical Oral Implants Research. 2021;32(12):1411–24.

3. Xie Y, Li S, Zhang T, Wang C, Cai X. Titanium mesh for bone augmentation in oral implantology: current application and progress. International Journal of Oral Science [Internet]. 2020;12(1):1–12. Available from: http://dx.doi.org/10.1038/s41368-020-00107-z

4. Rasia dal Polo M, Poli PP, Rancitelli D, Beretta M, Maiorana C. Alveolar ridge reconstruction with titanium meshes: A systematic review of the literature. Medicina Oral, Patologia Oral y Cirugia Bucal. 2014;19(6):e639–46.

5. Cucchi A, Vignudelli E, Napolitano A, Marchetti C, Corinaldesi G. Evaluation of complication rates and vertical bone gain after guided bone regeneration with non-resorbable membranes versus titanium meshes and resorbable membranes. A randomized clinical trial. Clinical Implant Dentistry and Related Research. 2017;19(5):821–32.

6. Elnayef B, Porta C, del Amo F, Mordini L, Gargallo-Albiol J, HernándezAlfaro F. The Fate of Lateral Ridge Augmentation: A Systematic Review and Meta-Analysis. The International Journal of Oral & Maxillofacial Implants. 2018;33(3):622–35.

7. Soldatos NK, Stylianou P, Koidou P, Angelov N, Yukna R, Romanos GE. Limitations and options using resorbable versus nonresorbable membranes for successful guided bone regeneration. Quintessence international (Hanover Park, IL). 2017;48(2):131–47.

8. Ghanaati S, Al-Maawi S, Conrad T, Lorenz J, Rössler R, Sader R. Biomaterial-based bone regeneration and soft tissue management of the individualized 3D-titanium mesh: An alternative concept to autologous transplantation and flap mobilization. Journal of Cranio-Maxillofacial Surgery [Internet]. 2019;47(10):1633–44. Available from: https://doi.org/10.1016/j.jcms.2019.07.020

9. Roccuzzo M, Ramieri G, Spada MC, Bianchi SD, Berrone S. Vertical alveolar ridge augmentation by means of a titanium mesh and autogenous bone grafts. Clinical Oral Implants Research. 2004;15(1):73–81.

10. Bai L, Ji P, Li X, Gao H, Li L, Wang C. Mechanical Characterization of 3DPrinted Individualized Ti-Mesh (Membrane) for Alveolar Bone Defects. Journal of Healthcare Engineering. 2019;2019.

11. Urban IA, Montero E, Monje A, Sanz-Sánchez I. Effectiveness of vertical ridge augmentation interventions: A systematic review and meta-analysis. Journal of Clinical Periodontology. 2019;46(S21):319–39.

12. Maiorana C, Fontana F, Polo MR dal, Pieroni S, Ferrantino L, Poli PP, et al. Dense Polytetrafluoroethylene Membrane versus Titanium Mesh in Vertical Ridge Augmentation: Clinical and Histological Results of a Splitmouth Prospective Study. Journal of Contemporary Dental Practice. 2021;22(5):465–72.

13. Her S, Kang T, Fien MJ. Titanium mesh as an alternative to a membrane for ridge augmentation. Journal of Oral and Maxillofacial Surgery [Internet]. 2012;70(4):803–10. Available from: http://dx.doi.org/10.1016/j.joms.2011.11.017

14. Poli PP, Beretta M, Cicciù M, Maiorana C. Alveolar Ridge Augmentation with Titanium Mesh. A Retrospective Clinical Study. The Open Dentistry Journal. 2014;8(1):148–58.

15. Ciocca L, Ragazzini S, Fantini M, Corinaldesi G, Scotti R. Work flow for the prosthetic rehabilitation of atrophic patients with a minimal-intervention CAD/CAM approach. Journal of Prosthetic Dentistry [Internet]. 2015;114(1):22–6. Available from: http://dx.doi.org/10.1016/j.prosdent.2014.11.014

16. Seiler M, Kämmerer PW, Peetz M, Hartmann AG. Customized Titanium Lattice Structure in Three-Dimensional Alveolar Defect: An Initial Case Letter. Journal of Oral Implantology. 2018;44(3):219–24.

17. de Angelis N, Solimei L, Pasquale C, Alvito L, Lagazzo A, Barberis F. Mechanical properties and corrosion resistance of tial6v4 alloy produced with slm technique and used for customized mesh in bone augmentations. Applied Sciences (Switzerland). 2021;11(12).

18. Andreasi Bassi M, Andrisani C, Lico S, Ormanier Z, Ottria L, Gargari M. Guided bone regeneration via a preformed titanium foil: Clinical, histological and histomorphometric outcome of a case series. ORAL and Implantology. 2016;9(4):164–74.

19. Li L, Wang C, Li X, Fu G, Chen D, Huang Y. Research on the dimensional accuracy of customized bone augmentation combined with 3D-printing individualized titanium mesh: A retrospective case series study. Clinical Implant Dentistry and Related Research. 2021;23(1):5–18.

20. Briguglio F, Falcomatà D, Marconcini S, Fiorillo L, Briguglio R, Farronato D. The Use of Titanium Mesh in Guided Bone Regeneration: A Systematic Review. International Journal of Dentistry. 2019;2019:1–8.

21. Aceves-Argemí R, Roca-Millan E, González-Navarro B, Marí-Roig A, Velasco-Ortega E, López-López J. Titanium meshes in guided bone regeneration: A systematic review. Coatings. 2021;11(3).

22. Rakhmatia YD, Ayukawa Y, Furuhashi A, Koyano K. Current barrier membranes: Titanium mesh and other membranes for guided bone regeneration in dental applications. Journal of Prosthodontic Research [Internet]. 2013;57(1):3–14. Available from: http://dx.doi.org/10.1016/j.jpor.2012.12.001

23. Gutta R, Baker RA, Bartolucci AA, Louis PJ. Barrier Membranes Used for Ridge Augmentation: Is There an Optimal Pore Size? Journal of Oral and Maxillofacial Surgery [Internet]. 2009;67(6):1218–25. Available from: http://dx.doi.org/10.1016/j.joms.2008.11.022

24. Scantlebury T v. 1982-1992: A Decade of Technology Development for Guided Tissue Regeneration. Journal of Periodontology [Internet]. 1993;64(11S):1129–37. Available from: https://aap.onlinelibrary.wiley.com/doi/abs/10.1902/jop.1993.64.11s.1129

25. Cucchi A, Vignudelli E, Sartori M, Parrilli A, Aldini NN, Corinaldesi G. A microcomputed tomography analysis of bone tissue after vertical ridge augmentation with non-resorbable membranes versus resorbable membranes and titanium mesh in humans. International Journal of Oral Implantology. 2021;14(1):25–38.

26. Ricci L, Perrotti V, Ravera L, Scarano A, Piattelli A, Iezzi G. Rehabilitation of Deficient Alveolar Ridges Using Titanium Grids Before and Simultaneously With Implant Placement: A Systematic Review. Journal of Periodontology. 2012;84(9):1234–42.

27. Torres J, Tamimi F, Alkhraisat MH, Manchón Á, Linares R, Prados-Frutos JC, et al. Platelet-rich plasma may prevent titanium-mesh exposure in alveolar ridge augmentation with anorganic bovine bone. Journal of Clinical Periodontology. 2010;37(10):943–51.

28. Roccuzzo M, Ramieri G, Bunino M, Berrone S. Autogenous bone graft alone or associated with titanium mesh for vertical alveolar ridge augmentation: A controlled clinical trial. Clinical Oral Implants Research.

2007;18(3):286–94.

29. Guizzardi S, Galli C, Martini D, Belletti S, Tinti A, Raspanti M, et al. Different Titanium Surface Treatment Influences Human Mandibular Osteoblast Response. Journal of Periodontology. 2004;75(2):273–82.

30. Lukaszewska-Kuska M, Wirstlein P, Majchrowski R, Dorocka-Bobkowska B. Osteoblastic cell behaviour on modified titanium surfaces. Micron. 2018;105(September 2017):55–63.

31. Markhoff J, Krogull M, Schulze C, Rotsch C, Hunger S, Bader R. Biocompatibility and inflammatory potential of titanium alloys cultivated with human osteoblasts, fibroblasts and macrophages. Materials. 2017;10(1):9–12.

32. Shah FA, Trobos M, Thomsen P, Palmquist A. Commercially pure titanium (cp-Ti) versus titanium alloy (Ti6Al4V) materials as bone anchored implants - Is one truly better than the other? Materials Science and Engineering C [Internet]. 2016;62:960–6. Available from: http://dx.doi.org/10.1016/j.msec.2016.01.032

33. Sing SL, Yeong WY, Wiria FE, Tay BY. Characterization of Titanium Lattice Structures Fabricated by Selective Laser Melting Using an Adapted Compressive Test Method. Experimental Mechanics [Internet]. 2016;56(5):735–48. Available from: http://dx.doi.org/10.1007/s11340-0150117-y

34. Bhola R, Bhola SM, Mishra B, Olson DL. Corrosion in titanium dental implants/prostheses - A review. Trends in Biomaterials and Artificial Organs. 2011;25(1):34–46.

35. El-Hajje A, Kolos EC, Wang JK, Maleksaeedi S, He Z, Wiria FE, et al. Physical and mechanical characterisation of 3D-printed porous titanium for biomedical applications. Journal of Materials Science: Materials in Medicine. 2014;25(11):2471–80.

36. Boyne PJ, Cole MD, Stringer D, Shafqat JP. A technique for osseous restoration of deficient edentulous maxillary ridges. Journal of Oral and Maxillofacial Surgery. 1985;43(2):87–91.

37. Gongloff RK, Cole M, Whitlow W, Boyne PJ. Titanium mesh and particulate cancellous bone and marrow grafts to augment the maxillary alveolar ridge. Int J Oral Maxillofac Surg. 1986;15(3):263–8.

38. T von A, Hardt N, Wallkamm B. The TIME technique: a new method for localized alveolar ridge augmentation prior to placement of dental implants. Implant Dentistry [Internet]. 1997;6(1). Available from: https://journals.lww.com/implantdent/Fulltext/1997/00610/The_TIME_technique__a_new_method_for_localized.41.aspx

39. Cucchi A, Giavatto MA, Giannatiempo J, Lizio G, Corinaldesi G. Custommade titanium mesh for maxillary bone augmentation with immediate implants and delayed loading. Journal of Oral Implantology. 2019;45(1):59–64.

40. Al-Ardah AJ, Alqahtani N, AlHelal A, Goodacre BJ, Swamidass R, Garbacea A, et al. Using Virtual Ridge Augmentation and 3-Dimensional Printing to Fabricate a Titanium Mesh Positioning Device: A Novel Technique Letter. Journal of Oral Implantology. 2018;44(4):293–9.

41. Chiapasco M, Casentini P, Tommasato G, Dellavia C, del Fabbro M. Customized CAD/CAM titanium meshes for the guided bone regeneration of severe alveolar ridge defects: Preliminary results of a retrospective clinical study in humans. Clinical Oral Implants Research. 2021;32(4):498–510.

42. Connors C, Liacouras P, Grant G. Custom Titanium Ridge Augmentation Matrix (CTRAM): A Case Report. The International Journal of Periodontics & Restorative Dentistry. 2016;707–14.

43. Rakhmatia YD, Ayukawa Y, Atsuta I, Furuhashi A, Koyano K. Fibroblast attachment onto novel titanium mesh membranes for guided bone regeneration. Odontology. 2015;103(2):218–26.

44. Ciocca L, Fantini M, de Crescenzio F, Corinaldesi G, Scotti R. CAD–CAM prosthetically guided bone regeneration using preformed titanium mesh for the reconstruction of atrophic maxillary arches. Computer Methods in Biomechanics and Biomedical Engineering. 2013;16(1):26–32.

45. Lizio G, Corinaldesi G, Marchetti C. Alveolar Ridge Reconstruction with Titanium Mesh: A Three-Dimensional Evaluation of Factors Affecting Bone Augmentation. The International Journal of Oral & Maxillofacial Implants. 2014;29(6):1354–63.

46. Al-Ardah AJ, AlHelal A, Proussaefs P, AlBader B, al humaidan AA, Lozada J. Managing Titanium Mesh Exposure With Partial Removal of the Exposed Site: A Case Series Study. Journal of Oral Implantology. 2017;43(6):482–90.

47. Proussaefs P, Lozada J. Use of titanium mesh for staged localized alveolar ridge augmentation: clinical and histologic-histomorphometric evaluation. Journal of Oral Implantology. 2006;32(5):237–47.

48. Pieri F, Corinaldesi G, Fini M, Aldini NN, Giardino R, Marchetti C. Alveolar Ridge Augmentation With Titanium Mesh and a Combination of Autogenous Bone and Anorganic Bovine Bone: A 2-Year Prospective Study. Journal of Periodontology. 2008;79(11):2093–103.

49. Liu P, Hao Y, Zhao Y, Yuan Z, Ding Y, Cai K. Surface modification of titanium substrates for enhanced osteogenetic and antibacterial properties. Colloids and Surfaces B: Biointerfaces [Internet]. 2017;160:110–6. Available from: https://doi.org/10.1016/j.colsurfb.2017.08.044

50. Miao X, Wang D, Xu L, Wang J, Zeng D, Lin S, et al. The response of human osteoblasts, epithelial cells, fibroblasts, macrophages and oral bacteria to nanostructured titanium surfaces: A systematic study.

International Journal of Nanomedicine. 2017;12:1415–30.

51. Cunha G, Carvalho PH de A, Quirino LC, Torres LHS, Filho VAP, Gabrielli MFR, et al. Titanium Mesh Exposure After Bone Grafting: Treatment Approaches—A Systematic Review. Craniomaxillofacial Trauma & Reconstruction. 2021;(September):194338752110461.

52. Warnke PH, Douglas T, Wollny P, Sherry E, Steiner M, Galonska S, et al. Rapid prototyping: Porous titanium alloy scaffolds produced by selective laser melting for bone tissue engineering. Tissue Engineering - Part C: Methods. 2009;15(2):115–24.

53. Kawase M, Hayashi T, Asakura M, Mieki A, Fuyamada H, Sassa M, et al. Cell Proliferation Ability of Mouse Fibroblast-Like Cells and Osteoblast-Like Cells on a Ti-6Al-4V Alloy Film Produced by Selective Laser Melting. Materials Sciences and Applications. 2014;05(07):475–83.

54. Variola F, Brunski J, Orsini G, Oliveira PT de, Nanci A. NIH Public Access. 2012;3(2):335–53.

55. Otawa N, Sumida T, Kitagaki H, Sasaki K, Fujibayashi S, Takemoto M, et al. Custom-made titanium devices as membranes for bone augmentation in implant treatment: Modeling accuracy of titanium products constructed with selective laser melting. Journal of Cranio-Maxillofacial Surgery [Internet]. 2015;43(7):1289–95. Available from: http://dx.doi.org/10.1016/j.jcms.2015.05.006

56. Sumida T, Otawa N, Kamata Y, Kamakura S, Mtsushita T, Kitagaki H, et al. Custom-made titanium devices as membranes for bone augmentation in implant treatment: Clinical application and the comparison with conventional titanium mesh. Journal of Cranio-Maxillofacial Surgery. 2015;43(10):2183–8.

57. Ciocca L, Fantini M, de Crescenzio F, Corinaldesi G, Scotti R. Direct metal laser sintering (DMLS) of a customized titanium mesh for prosthetically

guided bone regeneration of atrophic maxillary arches. Medical and Biological Engineering and Computing. 2011;49(11):1347–52.

58. Cucchi A, Bianchi A, Calamai P, Rinaldi L, Mangano F, Vignudelli E, et al. Clinical and volumetric outcomes after vertical ridge augmentation using computer-aided-design/computer-aided manufacturing (CAD/CAM) customized titanium meshes: a pilot study. BMC Oral Health. 2020;20(1):1–11.

59. Xu X, Lu Y, Li S, Guo S, He M, Luo K, et al. Copper-modified Ti6Al4V alloy fabricated by selective laser melting with pro-angiogenic and antiinflammatory properties for potential guided bone regeneration applications. Materials Science and Engineering C [Internet]. 2018;90:198–210. Available from: https://doi.org/10.1016/j.msec.2018.04.046

60. Inoue K, Nakajima Y, Omori M, Suwa Y, Kato-Kogoe N, Yamamoto K, et al. Reconstruction of the alveolar bone using bone augmentation with selective laser melting titanium mesh sheet: A report of 2 cases. Implant Dentistry. 2018;27(5):602–7.

61. Hartmann A, Seiler M. Minimizing risk of customized titanium mesh exposures - A retrospective analysis. BMC Oral Health. 2020;20(1):1–9.

62. Dellavia C, Canciani E, Pellegrini G, Tommasato G, Graziano D, Chiapasco M. Histological assessment of mandibular bone tissue after guided bone regeneration with customized computer-aided design/computer-assisted manufacture titanium mesh in humans: A cohort study. Clinical Implant Dentistry and Related Research. 2021;23(4):600–11.

63. Sagheb K, Schiegnitz E, Moergel M, Walter C, Al-Nawas B, Wagner W. Clinical outcome of alveolar ridge augmentation with individualized CADCAM-produced titanium mesh. International Journal of Implant Dentistry. 2017;3(1).

64. Seiler M, Peetz M, Hartmann A, Witkowski R. Individualized CAD-CAMproduced titanium scaffolds for alveolar bone augmentation: a retrospective analysis of dehiscence events in relation to demographic and surgical parameters. J Oral Science Rehabilitation. 2018;4(1):38–46.

65. Ciocca L, Lizio G, Baldissara P, Sambuco A, Scotti R, Corinaldesi G. Prosthetically CAD-CAM–guided bone augmentation of atrophic jaws using customized titanium mesh: Preliminary results of an open prospective study. Journal of Oral Implantology. 2018;44(2):131–7.

66. Gongadze E, Kabaso D, Bauer S, Slivnik T, Schmuki P, van Rienen U, et al. Adhesion of osteoblasts to a nanorough titanium implant surface. Int J Nanomedicine. 2011;6:1801–16.

67. Santiago AS, Soares GDA. Response of osteoblastic cells to titanium submitted to three different surface treatments Resposta de células osteoblásticas ao titânio submetido a três diferentes tratamentos de superfície. Brasilian Oral Reserch-Dental Materials. 2005;19(3):203–8.

68. Jayaraman M, Meyer U, Bühner M, Joos U, Wiesmann HP. Influence of titanium surfaces on attachment of osteoblast-like cells in vitro. Biomaterials. 2004;25(4):625–31.

69. Nune KC, Kumar A, Misra RDK, Li SJ, Hao YL, Yang R. Functional response of osteoblasts in functionally gradient titanium alloy mesh arrays processed by 3D additive manufacturing. Colloids and Surfaces B: Biointerfaces. 2017;150:78–88.

70. Chen S, Lee CY, Li RW, Smith PN, Qin QH. Modelling osteoblast adhesion on surface-engineered biomaterials: optimisation of nanophase grain size. Computer Methods in Biomechanics and Biomedical Engineering [Internet]. 2017;20(8):905–14. Available from: http://dx.doi.org/10.1080/10255842.2017.1314468

71. Cucchi A, Sartori M, Parrilli A, Aldini NN, Vignudelli E, Corinaldesi G. Histological and histomorphometric analysis of bone tissue after guided

bone regeneration with non-resorbable membranes vs resorbable membranes and titanium mesh. Clinical Implant Dentistry and Related Research. 2019;21(4):693–701.

72. Gil FJ, Planell Estany JA. Aplicaciones biomédicas del titanio v sus aleaciones. Biomecánica. 1993;1(1).

73. Berbel LO, Banczek E do P, Karousis IK, Kotsakis GA, Costa I. Determinants of corrosion resistance of Ti-6Al-4V alloy dental implants in an In Vitro model of peri-implant inflammation. PLoS ONE [Internet]. 2019;14(1):1–17. Available from: http://dx.doi.org/10.1371/journal.pone.0210530

74. Mandracci P, Mussano F, Rivolo P, Carossa S. Surface treatments and functional coatings for biocompatibility improvement and bacterial adhesion reduction in dental implantology. Coatings. 2016;6(1).

75. Barthes J, Cazzola M, Muller C, Dollinger C, Debry C, Ferraris S, et al. Controlling porous titanium/soft tissue interactions with an innovative surface chemical treatment: Responses of macrophages and fibroblasts. Materials Science and Engineering C [Internet]. 2020;112(December 2019):110845. Available from: https://doi.org/10.1016/j.msec.2020.110845

76. Ponsonnet L, Reybier K, Jaffrezic N, Comte V, Lagneau C, Lissac M, et al. Relationship between surface properties (roughness, wettability) of titanium and titanium alloys and cell behaviour. Materials Science and Engineering C. 2003;23(4):551–60.

77. Dias Corpa Tardelli J, Bolfarini C, Cândido dos Reis A. Comparative analysis of corrosion resistance between beta titanium and Ti-6Al-4V alloys: A systematic review. Journal of Trace Elements in Medicine and Biology. 2020;62(June).

78. Nune KC, Misra RDK, Li SJ, Hao YL, Zhang W. The functional response of bioactive titania-modified three-dimensional Ti-6Al-4V mesh structure

toward providing a favorable pathway for intercellular communication and osteoincorporation. Journal of Biomedical Materials Research - Part A. 2016;104(10):2488–501.

79. Zizzari VL, Zara S, Tetè G, Vinci R, Gherlone E, Cataldi A. Biologic and clinical aspects of integration of different bone substitutes in oral surgery: a literature review. Oral Surgery, Oral Medicine, Oral Pathology and Oral Radiology [Internet]. 2016;122(4):392–402. Available from: http://dx.doi.org/10.1016/j.oooo.2016.04.010

80. Karageorgiou V, Kaplan D. Porosity of 3D biomaterial scaffolds and osteogenesis. Biomaterials. 2005;26(27):5474–91.

81. Berberi A, Samarani A, Nader N, Noujeim Z, Dagher M, Kanj W, et al. Physicochemical characteristics of bone substitutes used in oral surgery in comparison to autogenous bone. BioMed Research International. 2014;2014.

82. Minami M, Takechi M, Ohta K, Ohta A, Ninomiya Y, Takamoto M, et al. Bone formation and osseointegration with titanium implant using granularand block-type porous hydroxyapatite ceramics (IP-CHA). Dental Materials Journal. 2013;32(5):753–60.

83. Giuliani A, Manescu A, Mohammadi S, Mazzoni S, Piattelli A, Mangano F, et al. Quantitative kinetics evaluation of blocks versus granules of biphasic calcium phosphate scaffolds (HA/β-TCP 30/70) by synchrotron radiation xray microtomography: A human study. Implant Dentistry. 2016;25(1):6–15.

84. Ellinger R. Histological assessment of periodontal osseous defects following implantation of hydroxyapatite and biphasic calcium phosphate ceramics: a case report. Int J Periodont Restor Dent. 1986;6:23–33.

85. Legeros RZ. Calcium Phosphate Materials in Restorative Dentistry: a Review. Advances in Dental Research [Internet]. 1988;2(1):164–80. Available from: https://doi.org/10.1177/08959374880020011101

86. Bouler JM, Pilet P, Gauthier O, Verron E. Biphasic calcium phosphate ceramics for bone reconstruction: A review of biological response. Acta Biomaterialia [Internet]. 2017;53:1–12. Available from: http://dx.doi.org/10.1016/j.actbio.2017.01.076

87. Maté Sánchez de Val JE, Calvo-Guirado JL, Gómez-Moreno G, PérezAlbacete Martínez C, Mazón P, de Aza PN. Influence of hydroxyapatite granule size, porosity, and crystallinity on tissue reaction in vivo. Part A: synthesis, characterization of the materials, and SEM analysis. Clinical Oral Implants Research. 2016;27(11):1331–8.

88. Nevins M, Nevins ML, Schupbach P, Kim SW, Lin Z, Kim DM. A prospective, randomized controlled preclinical trial to evaluate different formulations of biphasic calcium phosphate in combination with a hydroxyapatite collagen membrane to reconstruct deficient alveolar ridges. Journal of Oral Implantology. 2013;39(2):133–9.

89. Marques CF, Perera FH, Marote A, Ferreira S, Vieira SI, Olhero S, et al. Biphasic calcium phosphate scaffolds fabricated by direct write assembly: Mechanical, anti-microbial and osteoblastic properties. J Eur Ceram Soc [Internet]. 2017;37(1):359–68. Available from: http://dx.doi.org/10.1016/j.jeurceramsoc.2016.08.018

2. Hypothesis

The hypothesis of this doctoral thesis is that the surface topography of the meshes can affect the physical-chemical behavior and the biological and microbiological response. It is possible to modify the surface by chemical passivation techniques to improve the function on the oral cavity of the meshes studied.

3. Objectives

The objectives of our line of work can be divided in primary (specific objectives) and secondary (general objectives).

Our investigation started by focusing in the secondary objectives:

1. To compare the surface characteristics of three commercially available individualized titanium meshes between them and according to the manufacturer's specifications.
2. To determine the contamination of the meshes due to the manufacture procedures.

These objectives are expressed in our first published article

Then we proceed towards our primary objectives:

1. To study an alternative passivation method using the so-called Piranha solution.
2. To analyze the effects of Piranha solution treatment on surface physical-chemical properties, chemical degradation (corrosion and release of ions) and antimicrobial activity against Gram-positive and Gram-negative bacteria.
3. To optimize the roughness of the meshes to obtain a good biological seal while maintaining a behavior that does not favor bacterial colonization
4. To study the sintered meshes as an alternative to standard titanium meshes

These objectives are expressed in our second and third published articles.

4. Materials and Methods

4.1. Surface Comparison of Three Different Commercial Custom-Made Titanium Meshes Produced by SLM for Dental Applications

The implantable devices used for this study were custom-made titanium meshes, produced in order to fit perfectly to each patient's specific needs. The acquired meshes analyzed were Mesh4U (Fig.8a) from BoneEasy (Arada, Ovar, Portugal), Yxoss CBR® mesh (Fig.8b) from ReOss® (Filderstadt, Esslingen, Germany) and 3D-MESH (Fig.8c) from BTK (Dueville, Vicenza, Italy), selected as they were the ones available in the European market with more expressive presence.

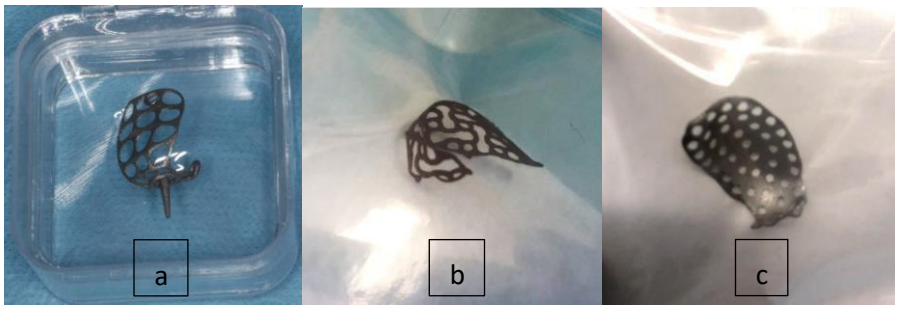

Figure 8. Custom made titanium meshes samples.

To evaluate the main design features of each mesh, the dimensions were determined by measuring in triplicates using a digital caliper.

To evaluate the material's structure and composition, XRD analyses were carried out resorting to the Bruker D8 Discover equipment (Bruker, Billerica,

Massachusetts, USA). The XRD acquisition was performed in the 5°–80° 2θ degree range with a 0.04° step size and an acquisition time corresponding to 1 s per step.

The meshes' superficial morphology was analyzed trough scanning electron microscopy. The samples were attached to aluminum supports using carbon tape and the analysis was performed resorting to the Quanta 400 FEG ESEM/EDAX Genesis X4M (Thermo Fisher Scientific, Hillsboro, Oregon, USA): a high resolution (Schottky) environmental scanning electron microscope with X-ray microanalysis and electron backscattered diffraction analysis (Thermo Fisher Scientific, Hillsboro, Oregon, USA). Furthermore, resorting to the same system, the samples were characterized using energydispersive X-ray spectroscopy.

The surface's profile was analyzed in triplicate, through a contact profilometry measurement, using the Hommel Werk LV-50 equipped with a 5μm radius TK pointer (Hommelwerke Co, Villingen-Schwenningen, Schwarzwald-Baar, Germany). The data acquired were processed by the application of a Gaussian filter in order to isolate roughness from the waviness and shapes of the samples.

4.2. Relevant Aspects of Piranha Passivation in Ti6Al4V Alloy Dental Meshes.

4.2.1. Samples

One hundred twenty Grade 5 titanium alloy (Ti6Al4V) meshes (BoneEasy, Arada, Portugal) were used. Figure 9 shows the mesh and its application as a membrane with calcium phosphate.

Figure 9. Grade 5 titanium mesh used in this study.

We worked with 3 groups of samples:

- Control: as-received material.
- HCl passivation: The meshes were immersed in a solution of hydrochloric acid (HCl) 20% (v) for 40 s at room temperature (HCl group). This is the gold-standard passivation treatment for dental implants and prosthesis.
- Piranha passivation: The meshes were immersed in a solution of Piranha, which is a mixture of sulfuric acid 96% (v) and a 50:50 ratio of hydrochloric acid (HCl) 20% (v) and hydrogen peroxide 30% (v) for 2 h.

Piranha solutions are a mixture of concentrated sulfuric acid with hydrogen peroxide, usually in a ratio of 3:1 to 7:1. They are used to remove trace amounts of organic residues, such as photoresist, from substrates. The mixing procedure is an exothermic reaction that can reach temperatures of 100 °C or higher. The reaction of hydrogen peroxide on concentrated sulfuric acid produces highly activated and oxidizing peroxymonosulfuric acid (H2SO5), also called Caro's acid. However, there are many different mixture ratios that are commonly used, and all are called Piranha. The addition of NH4OH in order to accelerate the decomposition of H2O2 or the addition of HCl, as in this research, favors cleanness and increases the oxide stabilization. Piranha solution must be prepared with great care. It is highly corrosive and an extremely powerful oxidizer. Surfaces must be reasonably clean and completely free of organic solvents from previous washing steps before coming into contact with the solution. Piranha

solution cleans by decomposing organic contaminants, and a large amount of contaminant will cause violent bubbling and a release of gas that can cause an explosion.

After treatment, all samples were cleaned a sequence of 3 ultrasonic baths (3 min each): two consecutives with distilled water, followed by one with ethanol.

4.2.2. Surface Characterization

Roughness for all groups was determined using an Olympus LEXT OLS3100 confocal microscope (Olympus, Tokyo, Japan). Three samples per group were tested and 3 measurements per sample were taken at x1000 magnification. The parameters Ra and Rz were determined. Ra corresponds to the arithmetic mean of the absolute values of the deviations of the profiles of a given length of the sample. Rz corresponds to the sum of the maximum peak height and the maximum valley depth within the sampling length.

The water sessile drop technique was used for the measurement of the contact angle, θ, formed between the water drop and the surface. The greater the contact angle, the lower the wettability and vice versa. For angles less than 10°, the surface is considered superhydrophilic, for angles between 10° and 90° surfaces are hydrophilic and for angles greater than 90°, surfaces are considered hydrophobic. A droplet generation system equipped with a 500 µL Hamilton syringe with micrometric displacement control was used to control the volume (3 µL) and to deposit the droplet. The analysis was performed using a gonyometer with drop profile image capture (Contact Angle System OCA15plus, DataPhysics, Filderstadt, Germany) and analyzed with SCA20 software (DataPhysics, Filderstadt, Germany).

To calculate the surface free energy, the contact angle was measured with two different liquids, water and diiodomethane. The contact angle measurements of diiodomethane were obtained following the same procedure used to measure

water contact angles. The surface free energy and its polar (γp) and dispersive (γd) components were then calculated using the Owens and Wendt equation:

$$\gamma_L (1+\cos\theta) = 2 (\sqrt{\gamma_{dL}\gamma_{Sd}} + \sqrt{\gamma_{Lp}\gamma_{Sp}}) \quad (1)$$

Surface morphology of the samples was analyzed with a focused ion beam Zeiss Neon40 FE-SEM (Carl Zeiss NTS GmbH, Oberkochen, Germany). Images of uncoated samples were taken at a working distance of 7 mm and an accelerating voltage of 5 kV. An EDS detector (INCA PentaFETx3 system, Oxford Instruments, Abingdon, UK) was used to detect silver presence on the surface of the samples. This microscope has a resolving power of 3 nm and allows the observation of the nanotextures produced by the reaction of the Piranha solution with the Ti6Al4V alloy.

4.2.3. Corrosion Behavior

A total of 60 samples, (n = 20) for each group of samples, were used for the corrosion tests. The test area for each sample was 19.6 mm2. The electrolyte for all tests was Hank's solution (Table 1), which is a saline fluid that closely captures the ion composition of the human serum environment.

Chemical Product	Composition (mM)
K2HPO4	0.44
KCl	5.4
CaCl2	1.3
Na2HPO4	0.25
NaCl	137
NaHCO3	4.2
MgSO4	1.0
C6H12O6	5.5

Table 1. Composition of Hank’s solution.

The electrochemical cell used was a polypropylene (PP) container with a capacity of 185 mL and a methacrylate lid with 6 holes for the introduction of the sample, the reference electrode and the counter electrode (Figure 10). For both the open circuit potential measurement tests and the potentiodynamic tests, the reference electrode used was a calomel electrode (saturated KCl), with a potential of 0.241 V compared to the standard hydrogen electrode. All tests were performed at room temperature and in a Faraday cage to avoid the interaction of external electric fields.

For the open circuit potential measurement tests, only the sample and the reference electrode were placed in the electrochemical cell. Tests were carried out for 5 hours for all the samples, taking measurements every 10 s. The potential was considered to be stabilized when the variation of the potential is less than 2 mV over a period of 30 min as indicated in the ASTM G31 standard. This test assesses which materials are more noble (higher potential) and thus, less susceptible to corrode. The data and the E-t curves were obtained using the PowerSuite software (Schneieder Electric, Ruil-Malmaison, France) with the PowerCorr-Open circuit (Schneieder Electric, Ruil-Malmaison, France).

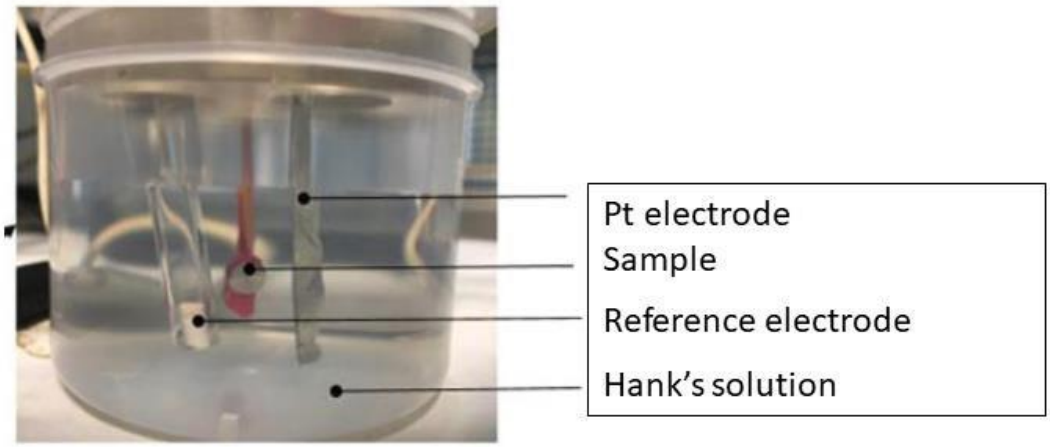

Figure 10. Experimental set up used for assessing corrosion resistance.

Cyclic potentiodynamic polarization curves were obtained for the 3 study groups following the ASTM G5 standard. In this test, a variable electrical potential is imposed by the potentiostat between the sample and the reference electrode, causing a current to flow between the sample and the counter electrode. The counter electrode used was platinum. Before starting the test, the system was allowed to stabilize by means of an open circuit test for 1 h. After stabilization, the potentiodynamic test was launched, performing a cyclic sweep from −0.8 mV to 1.7 mV at a speed of 2 mV/s. These parameters were entered into the PowerSuite program using the PowerCorr-Cyclic Polarization function to obtain the curves. The parameters studied were:

- icorr (μA/cm2)—corrosion current density;
- Ecorr (mV)—corrosion potential: value at which the current density changes from cathodic to anodic;
- Erep (mV)—repassivation potential: potential at which the passive layer regenerates;
- Ep (mV)—pitting potential: value at which pitting corrosion may occur;
- ip (μA/cm2)—passivation current density;
- ip (μA/cm2)—repassivation current density.

The Ecorr and icorr parameters are obtained by extrapolating the Taffel slopes.

The Taffel slopes are also used to obtain the Taffel coefficients: anodic (βa) and cathodic (βc). These coefficients represent the slopes of the anodic and cathodic branch, respectively. In accordance with the ASTM G102-89 standard, these values are then used to calculate the polarization resistance (Rp) using the Stern–Geary expression and the corrosion rate (CR in mm/year).

$$Rp = \frac{\beta_a \beta_c}{2{,}303 (\beta_a + \beta_c) i_{corr}}$$

The polarization resistance indicates the resistance of the sample to corrosion when subjected to small variations in potential. A total of 30 potentiodynamic tests were carried out, obtaining at least 10 curves per group.

$$CR = K_1 \cdot \frac{i_{corr} \cdot EW}{\rho}$$

4.2.4. Ion Release

Five samples from each group were used for the metal ion recovery test. After weighing the samples (m = 0.206 g) and following the ISO 10993-12 standard [26], a weight adjustment was made at the rate of 1 mL of Hank's solution for each 0.2 g of sample, as indicated in the standard. The 5 samples of each group were placed in the same Eppendorf with 5 mL of Hank's solution and stored at 37 °C. Hank's solution should be extracted and stored in the refrigerator after 1, 3, 7, 14, and 21 days. After each extraction, 5 mL of fresh Hank's solution has been replenished into the Eppendorf containing the samples. All Eppendorf tubes should be cleaned with 2% Nitric Acid and dried before use.

After 21 days, the concentration of released titanium ions was measured, at the test times indicated above, by inductively coupled plasma mass spectrometry (ICP-MS) with the Agilent Technologies 7800 ICP-MS (figure 11).

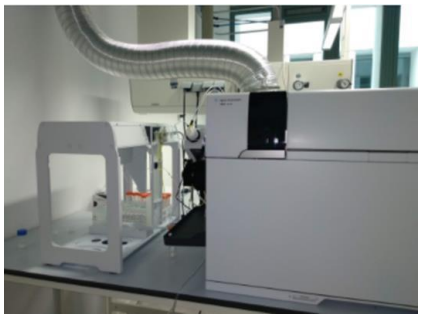

Figure 11: ICP-MS equipment

4.2.5. Bacteria Analysis

Two types of bacteria, P. aeruginosa (Colección española de cultivos tipo, CECT 110, Valencia, Spain) and S. sanguinis (Culture Collection University of Gothenburg, CCUG 15915, Gothenburg, Sweden), a Gram-negative and a Gram-positive strain, respectively, were used for the bacterial adhesion test.
Three samples per group and bacterial strain were tested.

The culture media and material (PBS) were previously sterilized by autoclaving at 121 °C for 30 min. Prior to the adhesion test, the samples were also sterilized. For this purpose, three 5 min ethanol washes were carried out in sterile culture plates. After removing the ethanol, the samples were exposed to ultraviolet light for another 30 min [29-30].

The agar plates were cultured at 37 °C for 24 h. From this culture, the liquid inoculum was prepared by suspending the bacteria in 5 mL of BHI (Brain Heart Infusion) and incubated for 24 h at 37 °C. The medium was then diluted to an optical density of 0.1 at a wavelength of 600 nm (OD600 = 0.1). For bacterial adhesion, enough solution with a concentration equivalent to OD600 = 0.1 to cover the surfaces (500 µl/sample) was introduced into the well of the culture plate of each sample and incubated at 37 °C for 1 h.

After this time, the samples were rinsed with PBS for 5 min twice and the bacteria were fixed with a 2.5% glutaraldehyde solution in PBS (30 min in the refrigerator). The glutaraldehyde solution was then removed and the samples were rinsed with PBS 3 times for 5 min. For viability analysis by confocal microscopy, the LIVE/DEAD BacLight bacterial viability kit (Thermo Fisher, Madrid, Spain) was used. A solution was prepared with 1.5 µL of propidium in 1 mL of PBS. Using a micropipette, a drop of this solution (approximately 50 µL/sample) was deposited on the study surface and after incubation at room temperature in the dark for 15 min, the samples were rinsed 3 times with PBS for 5 min. The surfaces were then observed under a confocal microscope. Three images per sample were taken at 630x magnification (x63 objective). Wavelengths of 488 and 561 nm were used to detect bacteria with non-compromised membranes (LIVE) and compromised membranes (DEAD), respectively.

Prior to the observation of the samples by scanning electron microscopy (SEM), the samples were dehydrated. For the dehydration process and the critical point drying, 10 min washes were carried out with ethanol solutions of gradual concentrations of 30, 50, 70, 80, 90, 95 and 100%. They were then left to dry for 24 h at room temperature. Then, samples were coated with platinum for 5 s before observation under the microscope. Ten images of each sample were taken at 20000x magnifications for bacterial quantification on each surface.

4.2.6. Statistical Analysis

All results were expressed as mean and standard deviation except for the bacterial adhesion test results which were expressed as median and standard error. The comparative T.TEST (with the Excel software) was carried out between the different groups at 95%, which means that for values of $p < 0.05$, there are significant differences.

4.3. Optimization of Titanium Dental Mesh Surfaces for Biological Sealing and Prevention of Bacterial Colonization

4.3.1. Materials

120 grade 5 titanium alloy (Ti6Al4V) meshes (BoneEasy, Arada, Portugal) were used. In Figure 12 shows the mesh design used.

Figure 12: Ti6Al4V mesh used in this study

Cylindrical shape samples (5 mm diameter, 2 mm width) were cut and six different surfaces were evaluated:

- (Mesh): as-received lathe cut titanium samples (control samples). Mesh samples used in the study correspond to the same material, roughness and mesh conditions. The samples are extracted from the same material with the same mesh conditions.
- (Smooth): samples were treated with 220 to 4000 grit SiC paper in water medium, deburred, and after polished by SiO_2 suspension.

Sand-blasted: the surfaces were sand-blasted (figure 13) at a pressure of 2.5 MPa with:

- (Al2): Al_2O_3 small size particles (212-300 µm)
- (Al6): Al_2O_3 medium size particles (425-600 µm)
- (Al9): Al_2O_3 big size particles (1000-1400 µm)
- (Sinter): Ti6Al4V spheres sintered from 10-50 µm of diameter.

Figure 13: Sand-blasting machine

After treatment, all samples were cleaned with deionized water, ethanol and acetone, dried at 25ºC and sterilized by autoclave at 120 °C for half an hour.

4.3.2. Characterization of the surfaces

Roughness parameters were obtained by means of a white light interferometer microscope (Wyko NT1100, Veeco Instruments Inc., USA), figure 14, and proprietary software (Vison32, Veeco Instruments Inc., USA).

Figure 14: Interferometer microscope

The measurements were realized in 10 samples to determine the average roughness (Ra), which represents the mean height of the peaks indicated by the arithmetic average of the absolute values of all points of the profile, and the real surface area (Ar), larger than the nominal area (70.7 mm^2) due to the surface roughness.

Hydrophilic and hydrophobic characters were measured using a contact angle video-based system (Contact Angle System OCA15plus, Dataphysics, Germany) and analyzed with proprietary software (SCA20, Dataphysics, Germany). The analysis was performed under conditions of 100% relative humidity and controlled temperature.

The topography of the samples was observed by scanning the electron microscopy (SEM) using the Phenom XL Desktop SEM microscope (PhenomWorld, Eindhoven, The Netherland) using a voltage of 20 keV to accelerate the electrons and to achieve a good resolution (7 nm). This

microscope has an EDX microanalysis in order to atomic chemical analysis with a sensitivity around 0.1% (figure 15).

Figure 15: Scanning Electron Microscope (SEM)

4.3.3. Cell culture and cell seeding

Primary human foreskin fibroblast cells (Millipore, Billerica, MA, USA) were cultured in Dulbecco's minimal essential medium (DMEM; Invitrogen, Carlsbad, CA, USA) and the addition of 10 % fetal bovine serum (FBS), L-glutamine (2 mM) and penicillin/streptomycin (50 U/ml and 50 g/ml, respectively) at 37 °C in a humidified incubator at 5% CO_2. The culture medium was changed every 48 hours. Subconfluent fibroblasts were trypsinised, centrifuged and seeded with 6 x 10^3 cells/disc with DMEM without serum and phenol red in the different Ti6Al4V samples placed in a 48-well microplate. An agarose film was introduced (in order to inhibit fibroblast adhesion) in order to have a negative control and can determine the adhesion behavior. Tissue culture polystyrene (TCPS) and polished Ti6Al4V (Smooth) were used as reference substrates. Fibroblast analyses were carried out at 4 hours, 24 hours and 72 hours.

4.3.4. Cell morphology

Field Emission Scanning Electron Microscopy (FESEM), (JSM-7001F JEOL Ltd., Tokyo, Japan) was used to characterized the cellular morphologies. For this objective, the discs cultured were cleaned by means of 0.1M phosphate buffer (PB) and fixed with 2.5% glutaraldehyde solution in PB, 4 hours at 4ºC. The samples were immersed 2 hours at room temperature in a 1% solution of osmium tetroxide in order to improve the observation. Fixed samples were then dehydrated in 50, 70, 90, 96 and 100% ethanol series three times followed by a hexamethyldisilazane (HDMS) drying procedure.

4.3.5. Cell proliferation – WST-1

HFF fibroblasts were cultured on the different surfaces studied, analyzing adhesion and proliferation using WST-1 (Roche Applied Science, Penzberg, Germany). This colorimetric determination quantifies cell activity by formazan staining. The mechanism is that mitochondrial dehydrogenases in living cells cause the separation of tetrazole salts and the colour of the soluble formazan is measured spectrophotometrically. The absorbance increases and can be correlated with increasing cell number. For the determination of cell viability, cell viability was determined at the different specified culture times by incubating for 2 h with WST-1 1:10 in DMEM without serum and phenol red. The optical density (OD) at 440 nm of the cell supernatant was measured with the ELx800 universal microplate reader (Bio-Tek Instruments, Inc., Winooski, VT, USA). Three different samples were studied for each surface type and two different experiments were performed in parallel. The optical density (OD) at 440 nm of the cell supernatant was determined with the ELx800 universal microplate reader (Bio-Tek Instruments, Inc., Winooski, VT, USA). Three samples were studied for each

surface type and two tests were performed. A curve was obtained using different number of cells from 3 x 10^3 to 50 x 10^3.

4.3.6. Cell viability – LDH

Lactate dehydrogenase (LDH) enzyme release at culture times was the methodology used for quantification of non-viable cells.The supernatant liquid was extracted from the cell-free culture. This broth was centrifuged at 250 x g for 5 minutes and subsequently detected by the Cytotoxicity Kit LDH (Roche Applied Science). The decrease of tetrazolium compounds in formazan staining by LDH activity was determined spectrophotometrically using 490 nm (figure 16). TCPS was used as a minimum control and lysed cells (maximum LDH activity) as a maximum control. Two experiments were realized in order to evaluate the cytotoxicity of three samples of each series.

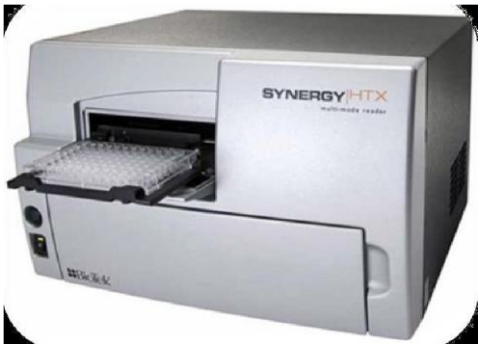

Figure 16: Cytotoxicity spectrophotometer equipment

4.3.7. Microbiological behavior

The bacteria strain *Streptococcus sanguinis* (CECT 480) and *Lacobacillus salivarius* (CECT 4063) (Colección Española de Cultivos Tipo, Valencia, Spain) were tested in this research. Strains were cultured in Todd-Hewitt broth at 37 ºC in a 5 % CO_2-enriched atmosphere (figure 17).

Figure 17: Culture chamber

Microbial Adhesion to Solvents (MATS) assay was followed to determine bacterial adhesion in physiological medium is the MATS test based on the electronic exchange of bacteria (donor/acceptor).

Bacteria were collected when proliferation was in exponential growth function. Bacteria were collected after centrifugation at 4500 g for 15 minutes at a temperature of 4 ºC. Once obtained, the bacteria were washed with Phosphate Buffer Solution (PBS) at 0.15 M. The bacteria were then suspended in PBS and their optical density was determined at a wavelength of 550 nm (A_0). The MATS test was performed in hexane, chloroform and diethyl ether. 3 ml of bacteria dissolution was extracted into 9 tubes and 400 µl of solvent (3 samples for each solvent) were added. The different suspensions were incubated at 20 °C for 10

minutes and mixed in a vortex shaker for 1 minute. Phase separation was performed after 15 minutes by measuring the optical density of the aqueous phase at the same wavelength (A_1). The resulting bacterial adhesion was determined according to the formula: $(1-A_1/A_0) \times 100$.

Ti6Al4V samples of 5 mm diameter and 2 mm thickness were tested. These were cleaned in 70 % ethyl alcohol, acetone and distilled water, dried at room temperature and autoclaved. These discs were seeded with two bacterial strains frequently present the oral cavity: *Streptococcus sanguinis* (CECT 480) and *Lactobacillus salivarius* (CECT 4063). The bacteria were incubated on the discs for 2 hours at 37 °C and 5 % CO_2. Subsequently, they were washed with PBS and detached in Ringers' solution. Bacterial seedings from the suspension (MRS for *Lactobacillus salivarius* and Todd-Hewitt for *Streptococcus sanguinis*) were incubated at 37 ºC for 2 days. Subsequently, the number of colonies was analysed. The variation of acidity during bacterial growth was also determined.

The discs were cleaned with phosphate buffer (PB, pH 7.2–7.4) for 5 min and then fixed with a 2.5% solution of glutaraldehyde in 0.1 M PB for 30 min at 4 °C. This washing process was repeated twice. After washing for 5 min with PB thrice, the discs were stored at 4 °C prepared for further treatment according to the MATS.

The samples were dehydrated by 10 min exposure to a graded sequence of aqueous ethanol (30–100%) and finally dried overnight at 25ºC. Then, discs were treated by sputtering in order to coat with a carbon (Emitech k950x, Kent, UK) and can be observed by SEM.

4.3.8. Statistical analysis

Data were expressed as the mean ± standard deviation. Statistical analysis was performed using MINITAB® (version 18, Minitab Inc.). We used nonparametric test because although the normal distribution of each data population was

confirmed by Anderson-Darling normality test, homocedasticity was ruled out (Barlett and Levene's test for homogeneity of variances). Therefore, we used Kruskal-Wallis test for multiple comparisons and U Mann-Whitney test for individual (one-to-one) comparisons. Statistical significance was set at $p<0,01$.

5. Results

Guided Bone Regeneration is an extremely complex biological and mechanical procedure and, according to the literature, needed in at least half of the clinical procedures that involve oral rehabilitation with dental implants. Multiple local and systemic factors are part of the process in order to provide an adequate environment for different cells with different biological behaviours to attach, grow and mature. Acknowledging this reality, our work focused in the surface characteristics of custom-made titanium meshes and how influence the bone regeneration outcome.

Starting out by comparing and analyzing individualized meshes produced by different companies allowed not only to characterize the surface of titanium meshes produced by SLM, but also how could they benefit of a surface treatment with Piranha Solution. On the other hand, it is also of great importance to avoid or minimize bacterial colonization, usually responsible for graft infection and loss. This led us to further investigate how could we treat the surface of those custommade meshes in order to increase fibroblast adhesion (for a biological sealing without drawbacks) and, at the same time, reduce bacteria colonization.

In our first published work, particular interest was given to the roughness studies.

The results from the scanning electron microscopy, energy-dispersive X-ray spectroscopy, X-ray diffraction and the contact profilometry measurements were analyzed and cross-checked.

The BoneEasy's mesh was the one that presented the lowest Ra value and was the mesh that got the closest to the reported optimal roughness degree that enhances the osteoblasts' affinity to the surface, reported as 0.5 μm. The reported differences between the surfaces were due to the divergent postproduction superficial treatments applied. Mesh4U endured an electropolishing treatment of high quality that was able to deliver flawless smooth

surfaces, as it delivers the mesh with the lowest Ra value, 0.61 ± 0.14 µm. Contrastingly, the

BTK produced mesh also withstood the same polishing process but its surface displayed countless non-polished pits, exposing the less perfect treatment application. In addition, evidences of stainless-steel contamination were found on this mesh surface. The Yxoss CBR® mesh suffered a sandblasting treatment that, apart from introducing alumina and silicon impurities onto the surface, was responsible for the very high roughness values that were reported (Ra of 6.59 ± 0.76 µm).

In our following work, results showed that the passivation of titanium meshes with Piranha solution improved their hydrophilicity and conferred a notably higher bactericidal activity in comparison with the meshes passivated with HCl. This unique response can be attributed to differences in the obtained nanotextures of the TiO_2 layer. However, Piranha solution treatment decreased electrochemical stability and increased ion release as a result of the porous coating formed on the treated surfaces, which can compromise their corrosion resistance.

Finally, in our third published work, the results showed that the samples treated with alumina particles by sandblasting at 200 micrometres were the ones that performed best with fibroblasts, in order to achieve a good biological sealing, and also with the number of bacterial colonies in both strains.

Microbiological studies have determined that the roughness generated by these particles presents a behavior very similar to the polished samples with minimal bacterial colonies on their surface. It has been shown that increased roughness leads to increased contact angles by studying wettability and thus makes the surfaces more hydrophobic.

Furthermore, this treatment shows a low bacterial adhesion (*Streptococcus sanguinis* and *Lactobacillus salivarius*) comparable to polished surfaces.

5.1. Surface Comparison of Three Different Commercial Custom-Made Titanium Meshes Produced by SLM for Dental Applications

Published in

Journal	Materials
DOI	**https://doi.org/10.3390/ma13092177**
Website link	https://www.mdpi.com/711294
Publishing year	2020
Impact Factor	3.623 (2020) ; 5-Year Impact Factor: 3.920 (2020) JCR - Q1 (*Metallurgy & Metallurgical Engineering*) / CiteScore - Q2 (*Condensed Matter Physics*)

References

1. Saini, M.; Singh, Y.; Arora, P.; Arora, V.; Jain, K. Implant biomaterials: A comprehensive review. *World J. Clin. Cases* 2015, 3, 52–57.
2. Toledano-Serrabona, J.; Sánchez-Garcés, M.; Sánchez-Torres, A.; Gay-Escoda, C. Alveolar distraction osteogenesis for dental implant treatments of the vertical bone atrophy: A systematic review. Med. Oral Patología Oral Cir. Bucal 2018, 24, 70–75.
3. Bai, L.; Ji, P.; Li, X.; Gao, H.; Li, L.; Wang, C. Mechanical Characterization of 3D-Printed Individualized Ti-Mesh (Membrane) for Alveolar Bone Defects. J. Healthc. Eng. 2019, 2019, 1–13.
4. Donos, N.; Lang, N.; Karoussis, I.; Bosshardt, D.; Tonetti, M.; Kostopoulos, L. Effect of GBR in combination with deproteinised bovine bone minerals/or enamel matrix proteins on healing of critical size defects. Clin. Oral Implant. Res. 2004, 15, 101–111.
5. Donos, N.; Kostopoulos, L.; Karring, T. Alveolar ridge augmentation using a resorbable copolymer membrane and autogenous bone grafts. Exp. Study Rat Clin. Oral Implant. Res. 2002, 13, 203–13.
6. Levine, R.; McAllister, B. Implant Site Development Using Ti-Mesh and Cellular Allograft in the Esthetic Zone for Restorative-Driven Implant Placement: A Case Report. Int. J. Periodontics Restor. Dent. 2016, 36, 373–381.

7. Boyne, P.J.; Cole, M.D.; Stringer, D.; Shafqat, J.P. A technique for osseous restoration of deficient edentulous maxillary ridges. J. Oral Maxillofac. Surg. 1985, 43, 87–91.

8. Her, S.; Kang, T.; Fien, M. Titanium Mesh as an Alternative to a Membrane for Ridge Augmentation. J. Oral Maxillofac. Surg. 2012, 70, 803–810.

9. Rakhmatia, Y.; Ayukawa, Y.; Furuhashi, A.; Koyano, K. Current barrier membranes: Titanium mesh and other membranes for guided bone regeneration in dental applications. J. Prosthodont. Res. 2013, 57, 3–14.

10. Becker, W.; Becker, B.; Mellonig, J.; Caffesse, R.; Warrer, K.; Caton, J.; Moore, T. A Prospective Multi-Center Study Evaluating Periodontal Regeneration for Class II Furcation Invasions and Intrabony Defects After Treatment with a Bioabsorbable Barrier Membrane: 1-Year Results. J. Periodontol. 1996, 67, 641–649.

11. Ciocca, L.; Ragazzini, S.; Fantini, M.; Corinaldesi, G.; Scotti, R. Work flow for the prosthetic rehabilitation of atrophic patients with a minimal-intervention CAD/CAM approach. J. Prosthet. Dent. 2015, 114, 22–26.

12. Ngo, T.D.; Kashani, A.; Imbalzano, G.; Nguyen, K.T.Q.; Hui, D. Additive manufacturing (3D printing): A review of materials, methods, applications and challenges. Compos. Part. B Eng. 2018, 143, 172–196.

13. Tack, P.; Victor, J.; Gemmel, P.; Annemans, L. 3D-printing techniques in a medical setting: A systematic literature review. Biomed. Eng. OnLine 2016, 15, 115.

14. Sidambe, A.T. Biocompatibility of Advanced Manufactured Titanium Implants-A Review. Materials 2014, 7, 8168–8188.

15. Pegueroles, M.; Tonda-Turo, C.; Planell, J.A.; Gil, F.-J.; Aparicio, C. Adsorption of Fibronectin, Fibrinogen, and Albumin on TiO2: Time-Resolved Kinetics, Structural Changes, and Competition Study. Biointerphases 2012, 7, 48.

16. Prasad, S.; Ehrensberger, M.; Gibson, M.; Kim, H.; Monaco, E. Biomaterial properties of titanium in dentistry. J. Oral Biosci. 2015, 57, 192–199.

17. Ponsonnet, L.; Reybier, K.; Jaffrezic-Renault, N.; Comte, V.; Lagneau, C.; Lissac, M.; Martelet, C. Relationship between surface properties (roughness, wettability) of titanium and titanium alloys and cell behaviour. Mater. Sci. Eng. C 2003, 23, 551–560.

18. Al-Radha, A.; Dymock, D.; Younes, C.; O'Sullivan, D. Surface properties of titanium and zirconia dental implant materials and their effect on bacterial adhesion. J. Dent. 2011, 40, 146–153.

19. Elias, C.; Oshida, Y.; Lima, J.; Müller, C. Relationship between surface properties (roughness, wettability and morphology) of titanium and dental implant removal torque. J. Mech. Behav. Biomed. Mater. 2008, 1, 234–242.

20. Le Guehennec, L.; Soueidan, A.; Layrolle, P.; Amouriq, Y. Surface treatments of titanium dental implants for rapid osseointegration. Dent. Mater. 2007, 23, 844–854.

21. Dank, A.; Aartman, I.; Wismeijer, D.; Tahmaseb, A. Effect of dental implant surface roughness in patients with a history of periodontal disease: A systematic review and meta-analysis. Int. J. Implant. Dent. 2019, 5, 12.

22. Rosales-Leal, J.I.; Rodríguez-Valverde, M.A.; Mazzaglia, G.; Ramón-Torregrosa, P.J.; Diaz Rodriguez, L.; García-Martínez, O.; Vallecillo-Capilla, M.; Ruiz, C.; Cabrerizo-Vílchez, M.A. Effect of roughness, wettability and morphology of engineered titanium surfaces on osteoblast-like cell adhesion. Colloids Surf. A Physicochem. Eng. Asp. 2010, 365, 222–229.

23. Boyan, B.D.; Schwartz, Z. Modulation of osteogenesis via implant surface design. Bone Eng. 2000, 232–239.

24. Jemat, A.; Ghazali, M.J.; Razali, M.; Otsuka, Y. Surface Modifications and Their Effects on Titanium Dental Implants. BioMed Res. Int. 2015, 2015, 1–11.

25. Tajima, K.; Hironaka, M.; Chen, K.-K.; Nagamatsu, Y.; Kakigawa, H.; Kozono, Y. Electropolishing of CP Titanium and Its Alloys in an Alcoholic Solution-based Electrolyte. Dent. Mater. J. 2008, 27, 258–265.

26. Yang, G.; Wang, B.; Tawfiq, K.; Wei, H.; Zhou, S.; Chen, G. Electropolishing of surfaces: Theory and applications. Surf. Eng. 2016, 33, 1–18.

27. Yan, C.; Hussein, A.; Young, P. Ti–6Al–4V triply periodic minimal surface structures for bone implants fabricated via selective laser melting. J. Mech. Behav. Biomed. Mater. 2015, 51, 61–73.

28. Mandracci, P.; Mussano, F.; Rivolo, P.; Carossa, S. Surface Treatments and Functional Coatings for Biocompatibility Improvement and Bacterial Adhesion Reduction in Dental Implantology. Coatings 2016, 6, 7.

29. Shah, F.; Trobos, M.; Thomsen, P.; Palmquist, A. Commercially pure titanium (cp-Ti) versus titanium alloy (Ti6Al4V) materials as bone anchored implants—is one truly better than the other? — review. Mater. Sci. Eng. C 2016, 62, 960–966.

30. Scarano, A.; Piattelli, A.; Quaranta, A.; Lorusso, F. Bone Response to Two Dental Implants with Different Sandblasted/Acid-Etched Implant Surfaces: A Histological and Histomorphometrical Study in Rabbits. BioMed Res. Int. 2017, 2017, 1–8.

31. Piattelli, A.; Degidi, M.; Paolantonio, M.; Mangano, C.; Scarano, A. Residual aluminum oxide on the surface of titanium implants has no effect on osseointegration. Biomaterials 2003, 24, 4081– 4089.

32. Scardi, P.; Leoni, M.; Tesi, B.; Gianoglio, C.; Bacci, T. Structural refinement of α-β polymorphs in Ti-6Al-4V alloy. Surf. Eng. 1998, 14, 513–518.

33. Mengason, M.; Ritchie, N. Overcoming Peak Overlaps in Titanium- and Vanadium-Bearing Materials with Multiple Linear Least Squares Fitting. Microsc. Microanal. 2017, 23, 1–10.

34. Oh, J.-M.; Lee, B.-J.; Cho, S.; Lee, S.-W.; Good-Sun, C.; Jae Won, L. Oxygen Effects on the Mechanical Properties and Lattice Strain of Ti and Ti-6Al-4V. Met. Mater. Int. 2011, 17, 733–736.

35. Sudipto, M. Texture and Microstructure in Two-Phase Titanium Alloys. Ph.D. Thesis, Carnegie Mellon University, Pittsburgh, PA, USA, 2017.

36. Oom, A. How Surface Roughness and Wettability Affects Biocompatibility. Available online: https://blog.biolinscientific.com/how-surface-roughness-and-wettability-affects-biocompatibility-0 (accessed on 21 March 2020).

37. Anselme, K. Osteoblast adhesion on biomaterials. Biomaterials 2000, 21, 667–681.

38. Alla, R.K.; Ginjupalli, K.; Upadhya, N.; Mohammed, S.; Sekar, R.; Ravi, R. Surface Roughness of Implants: A Review. Trends Biomater. Artif. Organs 2011, 25, 112–118.

39. Coelho, P.; Bonfante, E.; Pessoa, R.; Marin, C.; Granato, R.; Giro, G.; Witek, L.; Suzuki, M. Characterization of Five Different Implant Surfaces and Their Effect on Osseointegration: A Study in Dogs. J. Periodontol. 2010, 82, 742–750.

40. Major, S.; Cyrus, P.; Hubálovská, M. The Influence of Surface Roughness on Biocompatibility and Fatigue Life of Titanium Based Alloys. IOP Conf. Ser. Mater. Sci. Eng. 2017, 175, 012053.

41. Albrektsson, T.; Wennerberg, A. Oral implant surfaces: Part 1. Int. J. Prosthodont. 2004, 17, 536–543.

42. Mummery, L. Parameters. In Surface Texture Analysis: The Handbook; Hommelwerke GmbH: Villingen-Schwenningen, Germany, 1992; pp. 23–59.

43. Gadelmawla, E.S.; Koura, M.; Maksoud, T.; Elewa, I.; Soliman, H. Roughness parameters. J. Mater. Process. Technol. 2002, 123, 133–145.

44. Keller, J.; Schneider, G.; Stanford, C.; Kellogg, B. Effects of Implant Microtopography on Osteoblast Cell Attachment. Implant. Dent. 2003, 12, 175–181.

45. Silva, T.; Cantarelli Machado, D.; Viezzer, C.; Júnior, A.; Oliveira, M. Effect of titanium surface roughness on human bone marrow cell proliferation and differentiation. Exp. Study Acta Cirúrgica Bras. 2009, 24, 200–205.

46. Aparicio, C.; Rodríguez, D.; Gil, F.J. Variation of roughness and adhesion strength of deposited apatite layers on titanium dental implants. Mater. Sci. Eng. C 2011, 31, 320–324.

47. Gil, F.J.; Planell, J.A.; Padrós, A.; Aparicio, C. The effect of shot blasting and heat treatment on the fatigue behavior of titanium for dental implant applications. Dent. Mater. Off. Publ. Acad. Dent. Mater. 2007, 23, 486–491.

48. Guo, C.; Matinlinna, J.; Tsoi, J.; Tang, A. Residual Contaminations of Silicon-Based Glass, Alumina and Aluminum Grits on a Titanium Surface After Sandblasting. Silicon 2019, 11, 2313–2320.

49. Perkins, G.S.; Pawlik, E.V.; Philips, W.M. Sandblasting Nozzle. U.S. Patent 4252768A, 24 February 1981.

50. Lucchetti, M.C.; Fratto, G.; Valeriani, F.; De Vittori, E.; Giampaoli, S.; Papetti, P.; Romano Spica, V.; Manzon, L. Cobalt-chromium alloys in dentistry: An evaluation of metal ion release. J. Prosthet. Dent. 2015, 114, 602–608.

51. ECHA. Comments and Response to Comments on CLH: Proposal and Justification. Available online: https://echa.europa.eu/documents/10162/39a20032-2e9b-d383-7050-e052d38a5e14 (accessed on 26 March 2020).

Surface Comparison of Three Different Commercial Custom-Made Titanium Meshes Produced by SLM for Dental Applications

Nuno Cruz [1], Maria Inês Martins [2], José Domingos Santos [3] Javier Gil Mur [1] and João Paulo Tondela [4]

[1] Faculty of Dentistry.Universitat Internacional de Catalunya, 08017 Barcelona, Spain; nuno.cruz@orismed.pt

[2] Faculty of Engineering. University of Porto (FEUP), 4200-465 Porto, Portugal; up201305982@fe.up.pt

[3] REQUIMTE-LAQV, Department of Metallurgical Engineering and Materials, Faculty of Engineering. University of Porto (FEUP), 4200-465 Porto; jdsantos@fe.up.pt

[4] Bioengineering Institute of Technology, Faculty of Dentistry. Universitat Internacional de Catalunya, 08017 Barcelona, Spain; xavier.gil@uic.cat

[5] CIROS from the Faculty of Medicine. University of Coimbra, 3004-504 Coimbra, Portugal; jtondela@fmed.uc.pt

Abstract: The use of individualized titanium meshes has been referred to in scientific literature since 2011. There are many advantages to its use, however, the main complications are related to early or late exposures. As some aspects such as its surface properties have been pointed out to influence the soft tissue response, this study was designed to compare the surface characteristics of three commercially available individualized titanium meshes between them and according to the manufacturer's specifications. The results from the scanning electron microscopy, energydispersive X-ray spectroscopy, X-ray diffraction and the contact profilometry measurements were analyzed and cross-checked. It was discovered that, the BoneEasy's post-processing superficial treatment was more refined, as it delivers the mesh with the lowest Ra value, 0.61 ± 0.14 µm, due to the applied electropolishing. On the other hand, the Yxoss CBR® mesh from ReOss® was sandblasted, presenting an extremely rough surface with a Ra of 6.59 ± 0.76 µm.

Keywords: biomaterial; bone regeneration; titanium mesh; 3D printing; surface properties; roughness

1. Introduction

Oral and maxillofacial reconstructive attempts are traceable back to as early as the Egyptian and South-Central American cultures. Obviously, over the centuries and with the development of material, biological and medical sciences, techniques that fulfill both the functional and esthetical requirements of dental implants have arose [1].

Currently, fixed prosthetics solutions sustained by dental implants for oral rehabilitation no longer consist in their simple placement following the existing bone anatomy. Instead, the current trend demands for individualized solutions and treatment plans that start way before and go far beyond the simple computed tomography (CT)/cone beam computed tomography (CBCT) bone defect scan analysis.

Many patients suffer from horizontal or vertical bone deficiency, especially in cases of longlasting edentulous ridges and bone defects, which are frequently caused by trauma or bone pathology. Thus, for prosthetic-driven procedures, the existent resorbed alveolar bone is often not enough for dental implant placement and even when possible, it frequently jeopardizes the successful outcome of an optimized implant placement. In order to prevent such complications and to achieve an appropriate positioning of dental implants, several augmentation strategies have been developed with the purpose of favoring the new bone's growth. Some of these techniques include alveolar distraction osteogenesis, block bone graft and guided bone regeneration [2,3].

One of the most familiar and most commonly used strategies, guided bone regeneration (GBR), resorts to a barrier membrane to isolate the growth of soft tissue while promoting the bone tissue growth as a priority [4]. However, especially for large bone defects, the desired bone shape and volume are hard to maintain throughout the entire GBR healing period. Furthermore, graft material displacement and compression during the post-operative period have been cited as relevant phenomena [5].

Since its introduction in 1969, the titanium mesh has received profound attention and has been extensively used for the reconstruction of oral and maxillofacial bone defects; its intensive use is due to its favorable characteristics [6,7]. The titanium mesh is rigid enough, being able to control bone shape and volume, a basic prerequisite for any bone regeneration process, and its pores play an important role both in enabling the vascular supply from the overlaying periosteum to the grafted defect and in improving tissue integrity [8].

However, despite the tremendous potential of the titanium mesh, obviously some limitations were also recorded; for the application of the conventional mesh, manual shaping through cutting, bending and trimming is required. These processes are very manually challenging, timeconsuming and highly influence the overall regenerative outcome [9]. Furthermore, the corners and edges of the bended and cut meshes can cause severe gingiva damage and expose the mesh's site [10].

Fortunately, in recent years, the development of personalized rapid prototyping medical devices based on the digital imaging and communications in medicine (DICOM) files provided by CT/CBCT scans, has deeply intensified [11]. Based on the patient's bone defect and resorting to computer aided design (CAD) software, it is possible to design medical devices with the intent of recreating the lost tridimensional bone anatomy. Furthermore, the virtual design can be physically produced by a recurring tridimensional (3D) printing technique.

Without a doubt, individualized titanium meshes for bone regeneration are an excellent example of a medical device whose quality has greatly benefited from these technological advances. In fact, resorting to selective laser melting (SLM) and a powder bed fusion 3D printing process [12], custom made meshes are already being produced worldwide. The personalized manufacture of titanium meshes through the digital modelling and 3D printing integration enables the accurate reconstruction of the bone's volume and position, promoting an optimal fit between the mesh and the anatomical shape as well as grants the opportunity for the procedure to be planned in advance. In addition, by avoiding manual shaping and the pruning of the implantable device in the moment of application, the procedure's duration can be greatly shortened [3] and the medical outcome of the surgery can be notably enhanced [13].

Titanium is a well-established choice as a material for use in biomedical applications. Its remarkable biocompatibility properties are due to the existence of a superficial passive oxide layer that is formed by the electromechanical oxidation of the material and delivers the titanium's excellent resistance to corrosion in combination with its excellent chemical inertness [14]. In vitro studies have implied that the negatively charged and hydrophilic TiO_2 layer is, in fact, the key

factor for the overall biocompatibility as it regulates the protein adsorption [15]. For the particular case of the dentistry, countless studies have already been conducted in order to guarantee the implantation safety. Usually, no inflammatory response signs are found in the oral tissue adjacent to titanium implants, however, it is important to note that for some patients, hypersensitivity can be induced [16].

Regardless of the production technique, either by conventional methods or by rapid prototyping, as for all implantable devices, it is important to control the meshes' characteristics to optimize its biological performance [1]. The inherent stiffness of titanium meshes can be responsible for causing irritation to the soft tissue, and properties such as mechanical strength, that deeply influence the meshes' use success, are affected by the thickness of the material and pore characteristics, size and number. More specifically, the surface properties of the biomaterial highly direct the interactions at the implant–cell interface [17]. These properties that range from physical to chemical features, including surface topography and chemical composition, are usually dictated by the superficial treatments applied whose current importance is well established [18]. Physicians favor the use of implantable devices that have undergone surface treatments that improve the success rate, accelerating the osseointegration mechanism [18,19]. Furthermore, it has already been reported that dental implants without surface treatments are associated with higher healing times when compared with the treated ones [19]. Surface topography and roughness are some of the aspects that can be easily manipulated by resorting to post-production surface treatments and that play an important role in the determination of cellular response, influencing adhesion, adsorption and differentiation [17,19]. High roughness degrees represent a major risk as the ionic leakage from the material can increase [20] and the bacterial adhesion is facilitated, intensifying the possibility of implant failure [21]. Smooth surfaces are able to slow down the biological processes at the interface, keeping the titanium oxidized layer properties unaffected for longer time periods [19]; the associated correct micro- and nanoroughness level can stimulate osteoblast differentiation, proliferation and production of both matrix and local growth factors [22]. Furthermore, changes in roughness correlate with selective protein adsorption, collagen synthesis and the maturation of chondrocytes, which all significantly influence the implant's osseointegration [23].

Some of the frequently used treatment techniques include sandblasting, acid etching and electropolishing; each one imprinting unique topographic features on the treated surfaces [19]. By projecting pressurized particles, the sandblasting treatment delivers titanium surfaces with roughness values highly superior relative to the ones in a controlled polishing technique, and is responsible for the introduction of contaminants into the surface. Regarding the acid etching, the treatment with strong acids cleans the metal substrate and delivers homogeneous roughness attributes throughout the entire surface [24]. In turn, electropolishing is a electrochemical process that delivers titanium surfaces with a bright, clean and smooth appearance, through the removal of a thin top layer of the material [25,26]. For the particular case of the SLM-based production of titanium constructs, post-production processes are fundamental and consist in both a thermal treatment and surface treatments, required to remove the raw metal particles that remain bonded to the manufactured piece. These particles, that stick to the structure due to the thermal diffusion associated to the temperature difference between the solidified material and the loose powder, must be removed as after implantation, as they can be released into the surrounding biological environment, possibly leading to inflammation, and are related to the loss of adequate mechanical properties such as fatigue resistance [27].

Even though the meshes characteristics should be deeply tailored and controlled in order to deliver the best possible clinical outcome, it is important to note that the biological progress associated to its use also greatly depends on the correct diagnosis and clinical indication as well as on the host characteristics themselves, such as medical history, the location and dimension of the bone defect and the type of residual bone, among others.

The present study intended to study the surface properties of three different commercially available individualized titanium meshes produced by SLM. The samples' morphological surface analysis was carried out by scanning electron microscopy (SEM) and the elemental analysis for chemical characterization was fulfilled resorting to an energy-dispersive X-ray spectroscopy (EDS). X-ray diffraction (XRD) was used to discern detailed information about the chemical structure of the materials and a contact profilometry measurement took place to evaluate the meshes' roughness.

2. Materials and Methods

The implantable devices used for this study were custom-made titanium meshes, produced in order to fit perfectly to each patient's specific needs. The acquired meshes analyzed were Mesh4U from BoneEasy (Arada, Ovar, Portugal), Yxoss CBR® mesh from ReOss® (Filderstadt, Esslingen, Germany) and 3D-MESH from BTK (Dueville, Vicenza, Italy), selected as they were the ones available in the European market with more expressive presence.

To evaluate the main design features of each mesh, the dimensions were determined by measuring in triplicates using a digital caliper.

To evaluate the material's structure and composition, XRD analyses were carried out resorting to the Bruker D8 Discover equipment (Bruker, Billerica, Massachusetts, USA). The XRD acquisition was performed in the 5°–80° 2θ degree range with a 0.04° step size and an acquisition time corresponding to 1 s per step.

The meshes' superficial morphology was analyzed trough scanning electron microscopy. The samples were attached to aluminum supports using carbon tape and the analysis was performed resorting to the Quanta 400 FEG ESEM/EDAX Genesis X4M (Thermo Fisher
Scientific, Hillsboro, Oregon, USA): a high resolution (Schottky) environmental scanning electron microscope with X-ray microanalysis and electron backscattered diffraction analysis (Thermo Fisher Scientific, Hillsboro, Oregon, USA). Furthermore, resorting to the same system, the samples were characterized using energy-dispersive X-ray spectroscopy.

The surface's profile was analyzed in triplicate, through a contact profilometry measurement, using the Hommel Werk LV-50 equipped with a 5µm radius TK pointer (Hommelwerke Co, Villingen-Schwenningen, Schwarzwald-Baar, Germany). The data acquired were processed by the application of a Gaussian filter in order to isolate roughness from the waviness and shapes of the samples.

3. Results

Foremostly, a simple morphological evaluation took place as all the samples displayed themselves with unique identities. The BoneEasy (Figure 1a) and the BTK (Figure 1c) meshes shared similarities as they closely resemble dense plates where circular apertures were planted. In this way, the main feature to evaluate corresponded to the pore diameter. On the other hand, the Yxoss CBR® mesh from ReOss® (Figure 1b) presented a maze-like shaped surface, composed of two distinct coordinating elements that together formed a repetitive pattern: regular circular pores intercalated with longer apertures with a peanut-like shape.

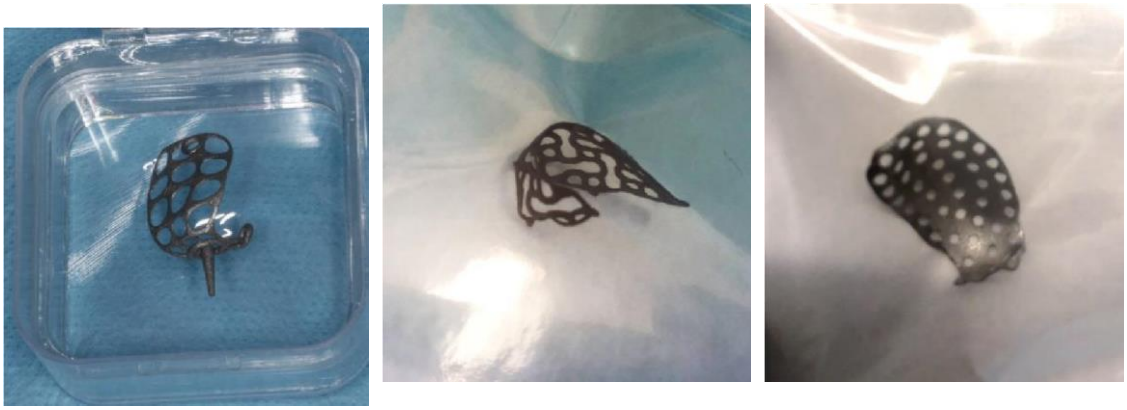

(a) **(b)** **(c)**

Figure 1. Acquired meshes as received from the manufacturers: (**a**) Mesh4U from BoneEasy; (**b**) Yxoss CBR® mesh from ReOss®; (**c**) 3DMESH from BTK.

The acquired results of the major design features of each mesh, including both the regular pores' diameter and the bigger structures' lengths, are represented in Table 1 by the calculated arithmetic mean of three measurements.

Table 1. Dimensions of the different samples' surface features.

Sample	Pore Diameter	Peanut-Shape Length
BoneEasy	1.93 ± 0.11 mm	n/a
ReOss®	1.38 ± 0.03 mm	5.47 ± 0.10 mm
BTK	1.23 ± 0.04 mm	n/a

To study the material composition of each individual mesh, a superficial X-ray diffraction analysis and an energy-dispersive X-ray spectroscopy was carried out. The experimentally obtained results are presented in Figures 2 and 3, respectively.

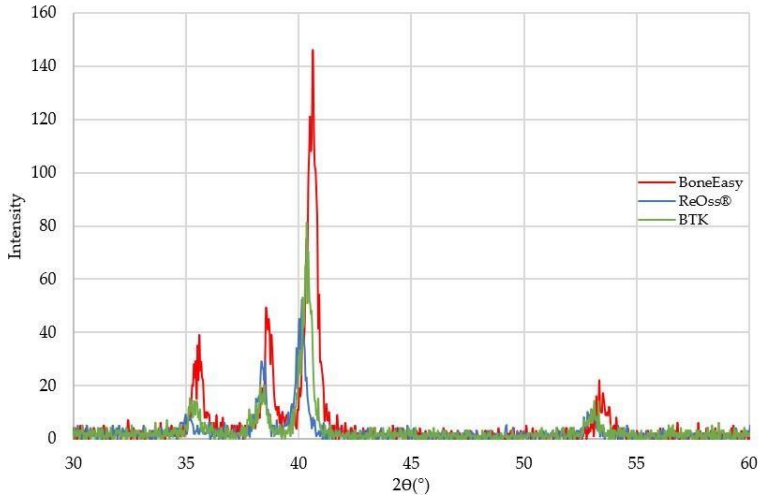

Figure 2. Combined diffractogram of the three meshes analyzed through XRD.

A first preliminary analysis revealed that all the implantable meshes displayed a very similar XRD diffraction pattern, suggesting that their structural composition was identical (see Figure 2).

When inspecting the EDS attainments (Figure 3), the same overall chemical identity also seemed to be shared as the presented spectra displayed, in a generalized way, the same emission lines. It appears evident that the major chemical dominance was granted by the titanium presence.

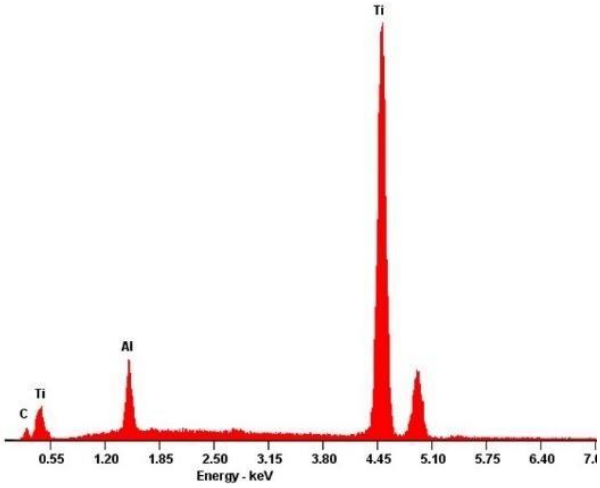

(**a**)

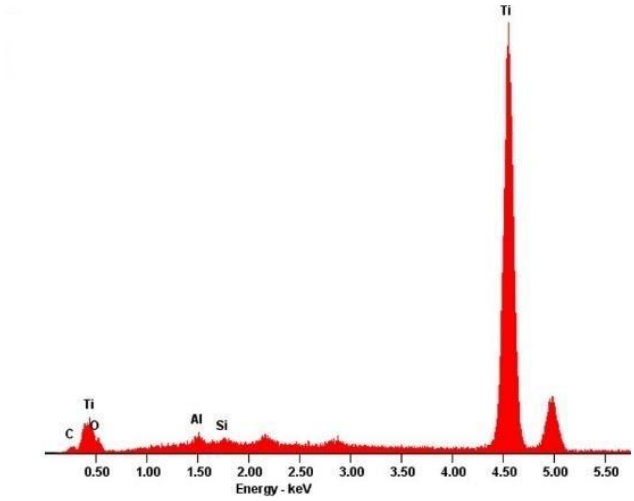

(**b**)

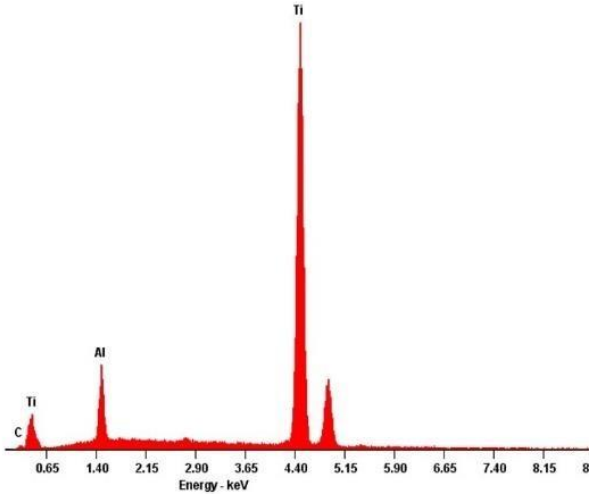

(**c**)

Figure 3. Energy dispersive X-ray spectroscopy results for the different samples' defects: (**a**) Mesh4U from BoneEasy; (**b**) Yxoss CBR® mesh from ReOss®; (**c**) 3D-MESH from BTK.

As for the topographical assessment of the meshes' surfaces, both a morphological analysis resorting to electronic microscopy and a roughness investigation based in the contact profilometry results were carried out.

The scanning electron microscopy images of the implants' surfaces are presented in Figure 4.

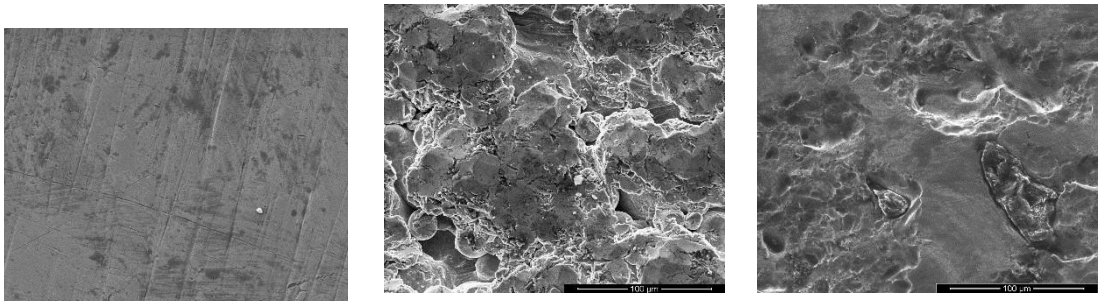

(**a**) (**b**) (**c**)

Figure 4. Scanning electron microscopy images for the morphology assessment of the different meshes' surfaces with 1000x magnification and in secondary electron mode: (**a**) Mesh4U from BoneEasy; (**b**) Yxoss CBR® mesh from ReOss®; (**c**) 3D-MESH from BTK.

For the surface texture analysis, high magnifications levels were adopted. The microscopic findings revealed that, from all the analyzed meshes, Mesh4U (Figure 4a) was the one that presented an overall more polished appearance with a homogenous and smooth presentation. However, long patterned surface sulci were easily identified throughout the sample's surface.

In contrast, the Yxoss CBR® mesh (Figure 4b) was without a doubt the sample that presented the most irregular surface. Smooth areas could not be identified as the totality of the surface consisted in very irregular sharp projections and depressions.

Finally, being neither the toughest nor the smoothest, the BTK mesh's surface (Figure 4c) displayed a binary topographic expression; both the flat areas and rough cavities could easily be found on the analyzed sample surface.

Surprisingly, while inspecting the overall topographical features of the meshes, some defects were identified. For both the ReOss®'s and BTK's samples, it was possible to pinpoint unexpected randomly dispersed irregular structures that appeared to be embedded in the surfaces. Closeups on these details are presented in Figure 5. It was noted that in the Mesh4U sample, no such defects were identified.

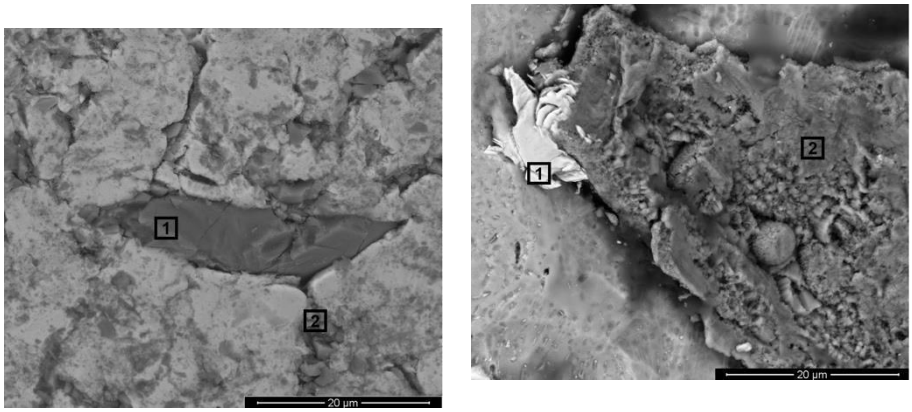

(**a**) (**b**)

Figure 5. Scanning electron microscopy images with 5000x magnification and in back scattering electron mode for the morphology evaluation of the identified surface defects. Interest areas for further analysis are signalized: (**a**) Yxoss CBR® from ReOss®; (**b**) 3D-MESH from BTK.

In order to inspect these features' compositions, energy-dispersive X-ray spectroscopy assessments were conducted targeting the specific areas of interest which are also highlighted in Figure 4. The corresponding EDS results are presented in Figures 6 and 7.

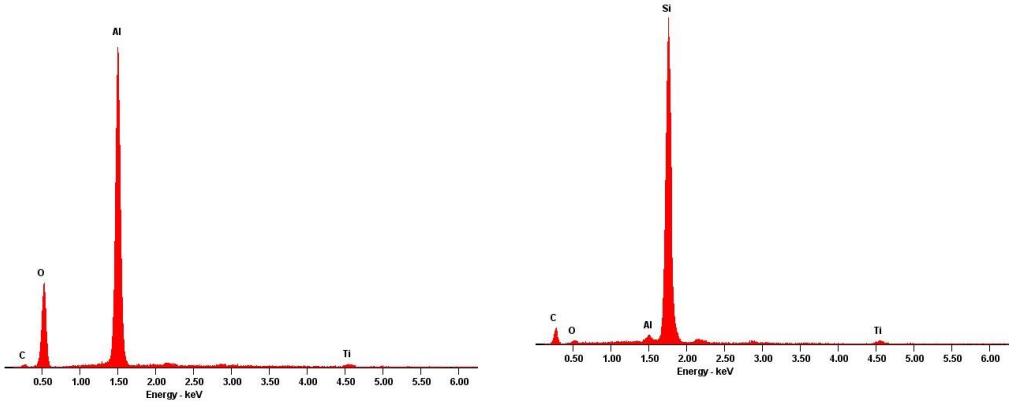

(**a**) (**b**)

Figure 6. Energy dispersive X-ray spectroscopy results for the identified ReOss® defect: (**a**) area of interest 1; (**b**) area of interest 2.

The first point to note was that, apart from the morphological divergence, the chemical composition of the defects was very diverse, either when comparing the different structures within the same sample or when considering different samples.

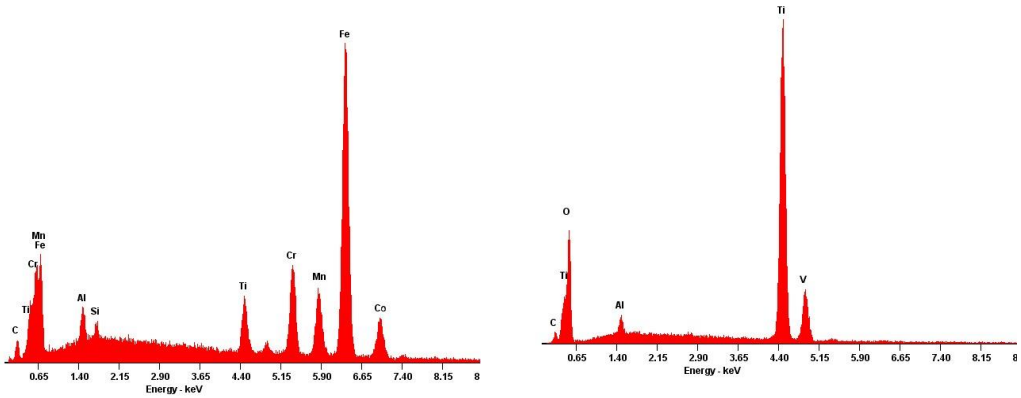

(**a**) (**b**)

Figure 7. Energy dispersive X-ray spectroscopy results for the identified BTK defect: (**a**) area of interest 1; (**b**) area of interest 2.

Considering the Yxoss CBR® defect (Figure 5a), two distinct types of infiltrations could be found. The features like the one marked as interest area 1 possessed bigger dimensions and their composition was mainly granted by the presence of aluminum and oxygen (Figure 6a). These artifacts were surrounded by multiple cracks where the smaller contaminations, in interest area 2, were built-in, presenting a granular form. The EDS results (Figure 6b) revealed that these masses were composed, essentially, of silicon.

As for the BTK mesh (Figure 5b), two different phases could also be found when analyzing the surface defect. The first one, area of interest 1, was easily identified throughout the acquired microscopic images due to its whitish and shiny appearance. Even though its presence was very obvious, its dimensions were diminished and the EDS results, presented in Figure 7a, revealed the presence of some metallic elements such as chromium, iron and manganese. Finally, the BTK interest area 2 could be described as large structures with irregular limits and their chemical identity, disclosed by the EDS analysis (Figure 7b), only registered a small deviation from the expected base composition due to the existence of carbon and oxygen peaks.

Returning to the lined up topographical evaluation and, although the microscopic analyses allowed a superficial qualitative assessment of the overall surface roughness of the meshes, for a more quantitative interpretation, contact profilometry measurements were performed. Figure 8 displays, for each surface, the results of the roughness profile monitoring in triplicate, for a 1200 µm sampling length.

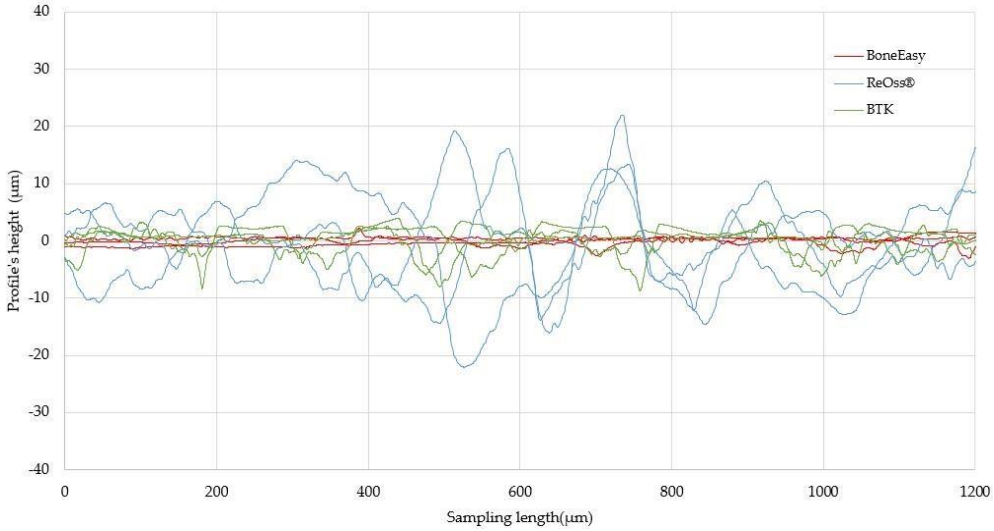

Figure 8. Plotted roughness profiles plotted from the profilometry analysis. In red, the BoneEasy's triplicates' profiles. In blue, the ReOss®'s triplicates' profiles. In green, the BTK's triplicates' profiles.

A simple plot evaluation corroborated with the already achieved inference that the different meshes presented considerably distinct topographies. In fact, while the BoneEasy's mesh presented a very regular surface with minimal variation in the profile's height, the surface of the Yxoss CBR® mesh from ReOss® displayed extremely profound profile variations, as substantially high and low peaks were registered. Considering the BTK 3D-MESH, it was possible to predicate that, even though the surface was not so uniform as the Mesh4U, it came closer to it than to the extremely irregular Yxoss CBR® mesh.

Obviously, the number of surface parameters one can evaluate is very large and their wide range allows a full characterization of each particular surface feature. In the present study, the topographic assessment rested only on amplitude parameters, namely, the average roughness (Ra) and the root mean square deviation (Rq or RMS). The acquired Ra and Rq values, resulting from each triplicates' average, are presented in Table 2 among with the respective squared deviations, to double check the information presented in the roughness profiles.

Table 2. Roughness parameters for the different samples' surfaces.

Sample	Ra	Rq
BoneEasy	0.61 ± 0.14 µm	0.73 ± 0.13 µm
ReOss®	6.59 ± 0.76 µm	8.39 ± 0.97 µm
BTK	1.63 ± 0.19 µm	2.08 ± 0.20 µm

Thus, the BoneEasy's mesh was the one that exhibited the lowest roughness values when analyzing either the Ra, 0.61 µm and the Rq value, 0.73 µm. Significant attention should fall on the ReOss® mesh which presented extremely high values of Ra and Rq, 6.59 µm and 8.39 µm respectively. Once again, as an intermediate between the other two meshes but much closer to the Mesh4U surface characteristics, the Ra parameter of the BTK mesh was 1.63 µm while the Rq was 2.08 µm.

4. Discussion

The overall success of a reconstructive dental procedure, encompassing an individual mesh introduction, relies profoundly on the physical-chemical properties of the implant's surface [19].

Thus, the first question that should be clarified is the composition of each mesh. Presently, without a doubt, commercially pure titanium and titanium–aluminum–vanadium (Ti–Al–V) alloys have established themselves as the prime choice materials for implants in dental applications [28,29] due to their remarkable biocompatibility, which is associated to the formation of a stable oxide layer on their surfaces and their favorable mechanical properties [1]. In fact, the surface oxide layer has been described as one of the main features that controls the titanium implant's integration in bone [30] since it regulates cellular attachment, highly influencing cell shape and function [31]. Even though the link between the contaminations' presence and the overall failure of the implant has not been fully explained, the lack of clinical success is often linked to the changes in the biocompatibility properties of this surface that may occur due to the presence of contaminations during the autoclaving process and to the contaminations' release from the surface, enhancing the inflammatory response [30]. This superficial passive oxide layer is responsible for delivering the titanium's distinctive corrosion resistance [14] and for that reason, alterations on its chemical identity could cause the dissolution of the implant [31], compromising its mechanical properties [14].

Titanium and titanium-based materials are usually composed by a combination of two distinct crystallographic phases: a hexagonal close packed alpha (α) phase and a body-centered cubic beta (β) phase. However, the two phases coexist in a balance that is determined by the thermal experience of the material or the presence of alloying elements [1,32]. For the case of biomedical applications, the most commonly used alloying elements are aluminum and vanadium, used in the exact proportions that give rise to the well known Ti–6Al–4V alloy [1]; these elements are responsible for stabilizing the titanium's α and β phases, respectively [32].

The analyzed meshes are no exception as their composition, qualitatively revealed by the EDS results, determined that in fact these meshes' raw material fell under the above described categories. However, the distinction between the two possible metal substrates, pure titanium (medical grade 4) or a Ti–Al–V alloy (medical grade 5) is extremely difficult; the titanium element displays two major emission lines, of which the secondary one, being around 5 keV, overlaps with the vanadium one [33]. Thus, for a clearer discrimination it is necessary to resort to another characterization technique.

In fact, the XRD outcome suggested that the chemical identities of all three meshes might be the same as the different diffractograms appeared to coincide. While commercially pure titanium consists entirely of the alpha crystallographic phase, the Ti–6Al–4V alloy's structure comprises both the alpha and beta phase [29]. In this way, the XRD identification of the β phase should allow the distinction between pure titanium and titanium alloy samples. However, since the Bragg reflections relative to the β phase were weaker than the α phase's ones, they were easily overlapped [32]. Thus, the X-ray diffraction results were also not reliable for crystallographic phase identification and a more adequate technique, such as a metallographic analysis, should be minded for further inquiry in order to provide a clear distinction between pure titanium and titanium alloy samples. However, it is clear that the collected spectra matched, indeed, either to pure titanium or to a Ti–6Al–4V alloy material as the identified main diffraction peaks, at 35°, 38°and 40°, matched to the ones reported for this type of material [34,35].

While the choice of material is extremely important when designing an implantable medical device, the final surface properties also play a key role in the success of the overall process, determining its interactions with the surrounding host tissue [36,37]. In fact, the superficial finishes highly affect the cell adhesion, spreading and differentiation that, in turn, are directly involved in the osseointegration mechanism [19,36].

Roughness is without a doubt one of the main aspects to mind since the implant's texture highly influences the tissue response [38]. In the past, smooth dental implant surfaces were desired [39], however, with the current awareness that completely smooth surfaces do not allow tissue adhesion, possibly leading to body fluid accumulation and inflammation [40], the prevailing trend points towards the use of moderately rough implant surfaces [39].

With this in mind, the meshes' surface profiles were examined; the microtopographic features of the implant surface (peaks, valleys and protrusions) are an essential factor in the biological response and the configuration of the bone–implant interface [41]. The Ra parameter, the roughness average, corresponds to the average distance from the profile to the mean line over the length of sampling and is not susceptible to the difference of peaks and valleys. In turn, the Rq value, the root mean square deviation, is the square root of the square of the deviation of the profile from the mean line and in this way, is more sensitive to peaks and valleys. Being associated with measuring instruments that grant higher repeatability and that have been more commonly adopted in monitoring production processes, Ra is more relevant for further discussion [42,43]. It has already been recorded that osteoblasts display greater affinity for the implant surface when it presents a microroughness degree associated to a Ra value of 0.5 µm [44,45]. In this way, it is possible to conclude that the BoneEasy's mesh was the one that had a surface associated Ra value closer to the recorded target and that the one from ReOss® was the one that diverged the most both from the reported desired roughness characteristics and also from the other analyzed meshes' superficial profiles.

Having the contact profilometry results analyzed, it is important to match them with the visual assessment from the SEM results. Regarding the Mesh4U sample, one could easily accept the low Ra value obtained since the mesh's surface without a doubt presented a highly smooth finish. On the other hand, for the higher Ra surface on the Yxoss CBR® mesh from ReOss®, delivered microscopic images indeed confirmed the rougher nature of the surface; the irregular clusters from a recognizable distinct nature, along with some cracks and projections, justified the higher variations of the profile distance to a mean line that reflected on the obtained Ra value. However, the major discussion topic arose when evaluating the results from the BTK 3D-MESH. Even though the Ra and Rq values of this surface were slightly higher than the ones of the BoneEasy sample, the registered deviation seemed to not corroborate with the evident topographical differences between the samples; such an irregularity degree of the BTK surface would translate into higher Ra and Rq when comparing to the BoneEasy's one. A possible explanation rests on the contact profilometry acquisition method. While the first two samples, Mesh4U and Yxoss CBR®, were analyzed by a 4.8 mm sampling length and then processed with a 0.8 mm Gaussian filter, due the intricate design and lack of continuous superficial area on the BTK's mesh, only a short and inadequate 1.5 mm length was covered and the acquired data were refined with a 0.25 mm Gaussian filter. In this way, the results may not be reliable and should not be straightforwardly compared with the ones of the other studied meshes. For a more solid evaluation, additional testing and resorting to alternative analysis methods that would not be compromised by the meshes' complex shape should be executed.

Proceeding with the morphological assessment, the smooth finish of the BoneEasy's mesh's surface was a strong indicator of the electropolishing technique applied to eliminate sharp edges, cracks and pits. The electropolishing process delivers pieces with a very intense natural metallic shine, as recognizable trough a preliminary unaided eye evaluation of the mesh, with higher corrosion resistance and clean from imperfections [26]. It is possible to hypothesize that the long imprints on the BoneEasy's mesh's surface corresponded to residual polishing contours.

Regarding the artefacts found on the surface of the Yxoss CBR® sample, due to the existence of the deep cracks that surrounded them, it was conjectured that these features must have been incorporated after the first production steps of the mesh. The EDS analysis revealed that the

embedded residues with bigger dimensions were primarily constituted of aluminum and oxygen. It was presumed that these alterations in the surface were induced by the post-production alumina (Al_2O_3) sandblasting process, used to improve the surface's texture. Even though this surface treatment is widely used, it is also known that it may introduce impurities originating from the blasting grits which, in turn, being extremely difficult to remove, may negatively affect the biocompatibility and bone formation beneath it. Furthermore, these alumina contaminations are known to be able to, when in a physiological environment, weaken the implant's corrosion resistance, compromising the mechanical properties [46-48], and may be responsible for debilitating bone formation, constraining regular bone deposition and mineralization [30]. An alternative that could be explored consists of the use of TiO_2 blasting particles that would not introduce foreign elements to the surface chemistry [30]. Moreover, the presence of the small silicon structures embedded into the alumina surrounding the cracks could be associated with the same sandblasting process; it is usual to resort to silicon for the production of sandblasters nozzles, with the absorption and shock protection intent in mind. However, due to the high aggressiveness of the used blast media, it is possible for the material to start cracking or even shatter with use [49]. In this way, one can speculate that, during the sandblasting process of the Yxoss CBR® mesh, essential for the post-production procedure, a silicon nozzle already over its predicted lifespan or possessing some deficiency was used, causing the release of some of its fragments that, in turn, lodged in the sandblasted surface.

The BTK 3D-MESH did also present signs of an electropolishing finish, with areas of clear lower roughness and polishing traces. However, the process must have been flawed since the surface was also rich in non-polished pits. Concerning the detected contaminations, the most relevant one was perhaps the one marked as interest area 1. These small metallic structures were easily found all over the mesh's surface and the EDS results suggested that these contaminations were, in fact, evidences that another production raw material, more specifically a stainless steel powder, was already being used in the equipment associated to the current production process. In fact, it was conjectured that the present material was a cobalt–chromium (Cr–Co) alloy, extensively used for medical applications, more particularly of great importance in the dental implant field due to the Cr presence; it is believed to deliver favorable biological and mechanical characteristics [50]. Furthermore, Cr–Co alloys are easily processed and sterilized and present high corrosion resistance [1,50]. Even though implants having these alloys as a chemical foundation have been successfully used over the years for clinical dentistry restorations, they have turned obsolete and gradually been replaced by titanium and titanium-based materials [1,50]. Additionally, these materials have recently lost their trustworthiness and their use is now non-advisable, as many reports have been published, including by the European Chemicals Agency, exposing cobalt's inherent toxicity when released in the biological environment during corrosion [50,51]. Thus, even though the relative amount of this contamination is doubtlessly very reduced, it is still important to emphasize its presence as it reveals some weaknesses in the production process of the BTK mesh.

5. Conclusions

There are many commercially available titanium bone regeneration meshes that, due to their personalized production methods resorting to modelling and 3D printing, perfectly fit to the patient's defect, greatly improving the reconstructive process outcome. In this work, three of these medical devices were analyzed, more specifically at the superficial properties level which is known for highly influencing the surrounding cellular response.

Particular interest was given to the roughness studies. The BoneEasy's mesh was the one that presented the lowest Ra value and was the mesh that got the closest to the reported optimal roughness degree that enhances the osteoblasts' affinity to the surface, reported as 0.5 µm. The reported differences between the surfaces were due to the divergent post-production superficial treatments applied. Mesh4U endured an electropolishing treatment of high quality that was able

to deliver flawless smooth surfaces. Contrastingly, the BTK produced mesh also withstood the same polishing process but its surface displayed countless non-polished pits, exposing the less perfect treatment application. In addition, evidences of stainless steel contamination were found on this mesh surface. The Yxoss CBR® mesh suffered a sandblasting treatment that, apart from introducing alumina and silicon impurities onto the surface, was responsible for the very high roughness values that were reported.

5.2. Relevant Aspects of Piranha Passivation in Ti6Al4V Alloy Dental Meshes.

Published in

Journal	Coatings
DOI	**https://doi.org/10.3390/coatings12020154**
Website link	https://www.mdpi.com/1470668
Publishing year	2022
Impact Factor	2.881 (2020) ; 5-Year Impact Factor: 3.038 (2020) JCR - Q2 (*Materials Science, Coatings & Films*) / CiteScore - Q2 (*Materials Chemistry*)

References

1. Toledano-Serrabona, J.; Sanchez-Garces, M.; Sánchez-Torres, A.; Escoda C.G. Alveolar distraction osteogenesis for dental implant treatments of the vertical bone atrophy: A systematic review. *Med. Oral. Patol. Oral. Cir. Bucal.* **2018**, *24*, 70–75, doi: 10.4317/medoral.22750.

2. Saini, M.; Singh, Y.; Arora, P.; Arora, V.; Jain, K. Implant biomaterials: A comprehensive review. *World J. Clin. Cases* **2015**, *3*, 52–57.

3. Lang, N.P.; Tonetti, M.S.; Suvan, J.E.; Bernard, J.P.; Botticelli, D.; Fourmousis, I.; Hallund, M.; Jung, R.; Laurell, L.; Salvi, G.E.; et al. Immediate implant placement with transmucosal healing in areas of aesthetic priority: A multicentre randomizedcontrolled clinical trial I. Surgical outcomes. *Clin. Oral Imp. Res.* **2007**, *18*, 188–196, doi: 10.1111/j.1600-0501.2006.01371.x.

4. Sanz-Sánchez, I.; Ortiz-Vigón, A.; Martín, I.S.; Figuero, E.; Sanz, M. Effectiveness of Lateral Bone Augmentation on the Alveolar Crest Dimension. *J. Dent. Res.* **2015**, *94*, 128–142, doi: 10.1177/0022034515594780.

5. De Angelis, N.; Solimei, L.; Pasquale, C.; Alvito, L.; Lagazzo, A.; Barberis, F. Mechanical Properties and Corrosion Resistance of TiAl6V4 Alloy Produced with SLM Technique and Used for Customized Mesh in Bone Augmentations. *Appl. Sci.* **2021**, *11*, 5622, doi: 10.3390/app11125622

6. Wang, H.; Boyapati, L. "PASS" Principles for Predictable Bone Regeneration. *Implant. Dent* **2006**; *15*, 8–17. doi: 10.1097/01.id.0000204762.39826.0f.

7. Levine, R.; McAllister, B. Implant Site Development Using Ti-Mesh and Cellular Allograft in the Esthetic Zone for Restorative-Driven Implant Placement: A Case Report. *Int J Periodontics Restorative Dent* **2016**, *36*, 373–81. doi: 10.11607/prd.2581.

8. Tan, X.; Tan, Y.J.; Chow, C.; Tor, S.B.; Yeong, W.Y. Metallic powder-bed based 3D printing of cellular scaffolds for orthopaedic implants: A state-of-the-art review on manufacturing, topological design, mechanical properties and biocompatibility. *Mater. Sci. Eng. C* **2017**, *76*, 1328–1343. doi: 10.1016/j.msec.2017.02.094.

9. Cruz, N.; Martins, M.I.; Santos, J.D.; Gil Mur, J.; Tondela, J.P. Surface Comparison of Three Different Commercial Custom-Made Titanium Meshes Produced by SLM for Dental Applications. *Materials* **2020**, *13*, 2177. doi: 10.3390/ma13092177.

10. Nicolas-Silvente, A.I.; Velasco-Ortega, E.; Ortiz-Garcia, I.; Monsalve-Guil, L.; Gil, J.; Jimenez-Guerra, A. Influence of the Titanium Implant Surface Treatment on the Surface Roughness and Chemical Composition. *Materials* **2020**, *13*, 314. doi: 10.3390/ma13020314

11. Rodrigues, D.; Valderrama, P.; Wilson, T.; Palmer, K.; Thomas, A.; Sridhar, S.; Sadhwani, C. Titanium Corrosion Mechanisms in the Oral Environment: A Retrieval Study. *Materials* **2013**, *6*, 5258–5274.

12. Godoy-Gallardo, M.; Manzanares-Céspedes, M. C.; Sevilla, P.; Nart, J.; Manzanares, N.; Manero, J. M.; Gil, F. J.; Boyd, S. K.; Rodríguez, D., Evaluation of bone loss in antibacterial coated dental implants: An experimental study in dogs. *Mater. Sci. Eng. C* **2016**, *69*, 538–45.

13. Gil, F.J.; Rodriguez, A.; Espinar, E.; Llamas, J.M.; Padulles, E.; Juarez, A. Effect of the oral bacteria on the mechanical behavior of titanium dental implants. *Int. J. Oral. Maxillofac. Implants* **2012**, *27*, 64–68.

14. Mombelli, A.; van Oosten, M.A.; Schurch, E.; Land, N.P. The microbiota associated with successful or failing osseointegrated titanium implants. *Oral Microbiol. Immunol*. **1987**, *2*, 145–151.

15. Punset, M.; Villarrasa, J.; Nart, J.; Manero, J.M.; Bosch, B.; Padrós, R.; Perez, R.A.; Gil, F.J. Citric Acid Passivation of Titanium Dental Implants for Minimizing Bacterial Colonization Impact. *Coatings* **2021**, *11*, 214. doi: 10.3390/ coatings11020214.

16. Duncan, W.J.; Lee, M.H.; Bae, T.S.; Lee, S.J.; Gay, J.; Loch, C. Anodisation increases integration of unloaded titanium implants in sheep mandible. *Biomed. Res. Int.* **2015**, *15*, 1–8.

17. Kasemo, B.; Gold, J. Implant Surfaces and Interface Processes. *Adv. Dent. Res.* **1999**, *13*, 8–20.

18. Variola, F.; Lauria, A.; Nanci, A.; Rosei, F. Influence of Treatment Conditions on the Chemical Oxidative Activity of H2SO4/H2O2Mixtures for Modulating the Topography of Titanium. *Adv. Eng. Mater.* **2009**, *11*, 227–234.

19. Variola, F.; Francis-Zalzal, S.; Leduc, A.; Barbeau, J.; Nanci, A. Oxidative nanopatterning of titanium generates mesoporous surfaces with antimicrobial properties. *Int. J. Nanomed.*, **2014**; *9*, 2319–2325.

20. Brunette, D.M.; Chehroudi, B. The effects of the surface topography of micromachined titanium substrata on cell behavior in vitro and in vivo. *J. Biomech. Eng.* **1999**, *121*, 49–57.

21. Jones, C.W. Applications of Hydrogen Peroxide and Derivatives, RSC Clean Technology, Monographs, Royal Society of Chemistry, Cambridge, 1999.

22. Bagno, A.; Di Bello, C. Surface treatments and roughness properties of Ti-based biomaterials. *J. Mater. Sci. Mater. Med*. **2004,** *15*, 939–945.

23. Liu, Y.; Zhao, Q. Influence of surface energy of modified surfaces on bacterial adhesion *Biophys. Chem.* **2005**; *117,* 39–46.

24. *ASTM-E3-11*; Standard guide for preparation of metallographic specimens; ASTM International: West Conshohocken, PA, USA, 2017.

25. *ASTM G5-14e1*; Standard reference test method for making potentiostatic and potentiodynamic anodic polarization measurements; ASTM International: West Conshohocken, PA, USA, 2014.

26. *ISO 10993-5:2009*; Biological evaluation of medical devices. Part 5: Tests for in vitro cytotoxicity. International Organization for Standardization: Geneve, Switzerland, 2009.

27. *ASTM G-102-89;* Standard practice for calculation of corrosion rates and related information from electrochemical measurements. ASTM International: West Conshohocken, PA, USA, 2010.

28. Gil, F.J.; Rodríguez, D.; Planell, J.A.; Cortada, M.; Giner, L.; Costa, S. Galvanic corrosion behaviour of Titanium implants coupled to dental alloys. *J. Mat. Sci. Mat. Med.* **2000**, *11*, 287–293.

29. Gil, F.J.; Sánchez, L.A.; Espias, A.; Planell, J.A. In vitro corrosion behaviour and metallic ion release of different prosthodontic alloys. *Int. Dent. J.* **1999**, *49*, 347–351.

30. Al-Hity, R.R.; Kappert, H.F.; Viennot, S.; Dalard, F.; Grosgogeat, B. Corrosion resistance measurements of dental alloys, are they correlated? *Dent. Mater*. **2007,** *23* ,679–687.

31. Socransky, S. S.; Haffajee, A. D.; Cugini, M. A.; Smith, C.; Kent, R. L., Microbial complexes in subgingival plaque. *J. Clin. Periodontol.* **1998**, *25*, 134–44.

32. Gil, F.J.; Rodriguez, A.; Espinar, E.; Llamas, J.M.; Padulles, E.; Juarez, A. Effect of the oral bacteria on the mechanical behavior of titanium dental implants. *Int. J. Oral Maxillofac. Impl.* **2012**, *27*, 64–68.

33. Godoy-Gallardo, M.; Wang, Z.; Shen, Y.; Manero, J. M.; Gil, F. J.; Rodriguez, D.; Haapasalo, M., Antibacterial coatings on titanium surfaces: a comparison study between in vitro single-species and multispecies biofilm. *ACS Appl. Mater. Interfaces* **2015**, *7*, 599–601.

34. Yi, J.-H.; Bernard, C.; Variola, F.; Zalzal, S. F.; Wuest, J. D.; Rosei, F.; Nanci, A. Characterization of a bioactive nanotextured surface created by controlled chemical oxidation of titanium. *Surf. Sci.*, **2006**, *600*, 4613–4621.

35. Castner, D. G., & Ratner, B. D. Biomedical surface science: Foundations to frontiers. *Surf. Sci. **2002**, 500*, 28–60.

36. Wheelis S.E.; Gindri, I.M.; Valderrama, P.; Wilson, T.G.; Jr. Huang, J.; Rodrigues, D.C. Effects of decontamination solutions on the surface of titanium: investigation of surface morphology, composition, and roughness. *Clin. Oral Implants Res.* **2015**, 27, 329–340.

37. Heitz-Mayfield, L. J.; Lang, N. P., Comparative biology of chronic and aggressive periodontitis vs. peri-implantitis. *Periodontol 2000* **2010**, *53*1, 67.

38. Michiardi, A.; Aparicio, C.; Ratner, B.D.; Planell, J.A.; Gil, J. The influence of surface energy on competitive protein adsorption on oxidized NiTi surfaces. *Biomaterials* **2007;** *28*, 586–594. doi: 10.1016/j.biomaterials.2006.09.040.

39. Variola, F.; Yi, J.H.; Richert, L.; Wuest, J.D.; Rosei, F.; Nanci, A. Tailoring the surface properties of Ti6Al4V by controlled chemical oxidation. *Biomaterials* **2008**; *29*, 1285–1298.

40. Muhonen, V.; Heikkinen, R.; Danilov, A.; Jamsa, T.; Tuukkanen, J. The effects of oxide thickness on osteoblast attachment and survival on NiTi alloy*. J. Mater. Sci. Mater. Med.* **2007**; *18*, 959–67.

41. Amor, S.B.; Baud, G.; Besse, J.P.; Jacquet, M. Structural and optical properties of sputtered titania films. *Mater Sci Eng B* **1997**; *47*, 110–118.

42. Velten, D.; Biehl, V.; Aubertin, F.; Valeske, B.; Possart, W.; Breme, J. Preparation of TiO2 layers on cp-Ti and Ti6Al4V by thermal and anodic oxidation and by sol-gel coating techniques and their characterization*. J. Biomed. Mater. Res.* **2002**; *59*, 18–28.

43. Amor, S.B.; Guedri, L.; Baud, G.; Jacquet, M.; Ghedira, M. Influence of the temperature on the properties of sputtered titanium oxide films. *Mater Chem Phys* **2002**, *77*, 903–911.

44. McCafferty, E.; Wightman, J.P. An X-ray photoelectron spectroscopy sputter profile study of the native air-formed oxide film on titanium. *Appl Surf Sci* **1999**; *143*, 92–100.

45. Arys, A.; Philippart, C.; Dourov, N.; He, Y.; Le, Q.T.; Pireaux, J.J. Analysis of titanium dental implants after failure of osseointegration: combined histological, electron microscopy, and X-ray photoelectron spectroscopy approach. *J. Biomed. Mater. Res.* **1998**, *43*, 300–312.

46. Lee, T.M.; Chang, E.; Yang, C.Y. Surface characteristics of Ti6Al4V alloy: effect of materials, passivation and autoclaving. *J. Mater. Sci. Mater. Med.* **1998**, *9*, 439–448.

47. Pouilleau, J.; Devilliers, D.; Garrido, F.; Durand-Vidal, S.; Mahe, E. Structure and composition of passive titanium oxide films. *Mater. Sci. Eng. B* **1997**, *47*, 235–243.

48. Lisowski, W.; van den Berg. A.H.J.; Smithers, M. Characterization of titanium hydride film after long-term air interaction: SEM, ARXPS and AES depth profile studies. *Surf. Interface Anal.* **1998**, *26*, 213–219.

49. Pegueroles, M.; Aparicio, C.; Bosio, M.; Engel, E.; Gil, F.J.; Planell, J.A.; Altankov, G. Spatial organization of osteoblast fibronectin matrix on titanium surfaces: effects of roughness, chemical heterogeneity and surface energy. *Acta Biomater.* **2010**, *6*, 291–301. doi: 10.1016/j.actbio.2009.07.030.

50. Mukaddam, K.; Astasov-Frauenhoffer, M.; Fasler-Kan, E.; Marot, L.; Kisiel, M.; Meyer, E.; Köser, J.; Waser, M.; Bornstein, M.M.; Kühl, S. Effect of a Nanostructured Titanium Surface on Gingival Cell Adhesion, Viability and Properties against P. gingivalis. *Materials* **2021**, *14*, 7686. doi: 10.3390/ ma14247686.

51. Ivanova, E.P.; Hasan, J.; Webb, H.K.; Truong, V.K.; Watson, G.S.; Watson, J.A.; Baulin, V.A.; Pogodin, S.; Wang, J.Y.; Tobin, M.J.; et al. Natural Bactericidal Surfaces: Mechanical Rupture of Pseudomonas Aeruginosa Cells by Cicada Wings. *Small.* **2012**, *8*, 2489–2494.

52. Ivanova, E.P.; Hasan, J.; Webb, H.K.; Gervinskas, G.; Juodkazis, S.; Truong, V.K.; Wu, A.H.F.; Lamb, R.N.; Baulin, V.A.; Watson, G.S.; et al. Bactericidal Activity of Black Silicon. *Nat. Commun*. **2013**, *4*, 2838.

53. Serrano, C.; García-Fernández, L.; Fernández-Blázquez, J.P.; Barbeck, M.; Ghanaati, S.; Unger, R.; Kirkpatrick, J.; Arzt, E.; Funk, L.; Turón, P.; et al. Nanostructured Medical Sutures with Antibacterial Properties. *Biomaterials* **2015**, *52*, 291–300.

54. Jenkins, J.; Mantell, J.; Neal, C.; Gholinia, A.; Verkade, P.; Nobbs, A.H.; Su, B. Antibacterial Effects of Nanopillar Surfaces Are Mediated by Cell Impedance, Penetration and Induction of Oxidative Stress. *Nat. Commun.* **2020**, *11*, 1626.

55. Xu, Z.; He, Y.; Zeng, X.; Zeng, X.; Huang, J.; Lin, X.; Chen, J. Enhanced Human Gingival Fibroblast Response and Reduced Porphyromonas Gingivalis Adhesion with Titania Nanotubes. *Biomed. Res. Int.* **2020**, *2020,* 5651780.

56. Kiran, A.S.; Kumar, T.S.; Perumal, G.; Sanghavi, R.; Doble, M.; Ramakrishna, S. Dual nanofibrous bioactive coating and antimicrobial surface treatment for infection resistant titanium implants. Progress in Organic *Coatings* **2018**, *121*, 112–119.

57. Seddiki, O.; Harnagea, C.; Levesque, L.; Mantovani, D.; Rosei, F. Evidence of antibacterial activity on titaniumsurfaces through nanotextures. *Appl. Surf. Sci*. **2014**, *308*, 275–284.

58. Skindersoe, M.E.; Krogfelt, K.A.; Blom, A.; Jiang, G.; Prestwich, G.D.; Mansell, J.P. (2015) Dual Action of Lysophosphatidate-Functionalised Titanium:Interactions with Human (MG63) Osteoblasts and Methicillin Resistant Staphylococcus aureus. *PLOS ONE* **2015**, *10*, 1–17. doi: 10.1371/journal.pone.0143509.

59. Vermeulen, N.; Werden J.; Keeler, W.J.; Nandakumar, K.; Leung, K.T. The Bactericidal Effect of Ultraviolet and Visible Light on Escherichia Coli. *Biotechnol. Bioeng.* **2008**, *99*, 550–556.

Relevant Aspects of Piranha Passivation in Ti6Al4V Alloy Dental Meshes.

Nuno Cruz [1], Javier Gil [1,2,*], Miquel Punset [3,1,2,3], José María Manero [3,4,6], João Paulo Tondela [4,*], Pablo Verdeguer [1], Conrado Aparicio [2] and Elisa Rúperez [3,4,6]

[1] Bioengineering Institute of Technology, International University of Catalonia (UIC), 08195 Barcelona, Spain; nuno.cruz@orismed.pt (N.C.); pabloverdeguerm@gmail.com (P.V.)

[2] School of Dentistry, International University of Catalonia (UIC), 08195 Barcelona, Spain; cjaparicio@uic.es.

[3] Biomaterials, Biomechanics and Tissue Engineering group (BBT), Department of Materials Science and Engineering, Technical University of Catalonia (UPC),

---

[1] Barcelona Research Centre in Multiscale Science and Engineering, Technical University of Catalonia (UPC), 08019 Barcelona, Spain

[2] Innovation and Technology Center (CIT), Polytechnic University of Catalonia (UPC), 08034 Barcelona, Spain

[3] Sant Joan de Déu Research Institute (IRSJD), 08034, Barcelona, Spain

[4] CIROS from the Faculty of Medicine, University of Coimbra, FMUC, 3004-531 Coimbra, Portugal

08019 Barcelona, Spain; miquel.punset@upc.edu (M.P.); jose.maria.manero@upc.edu (J.M.M.); elisa.ruperez@upc.edu (E.R.) * Correspondence: xavier.gil@uic.es (J.G.); jtondela@fmed.uc.pt (J.P.T.)

Abstract: Passivation of titanium alloy dental meshes cleans their surface and forms a thin layer of protective oxide (TiO_2) on the surface of the material to improve resistance to corrosion and prevent release of ions to the physiological environment. The most common chemical agent for the passivation process of titanium meshes is hydrochloric acid (HCl). In this work, we introduce the use of Piranha solution (H_2SO_4 and H_2O_2) as a passivating and bactericidal agent for metallic dental meshes. Meshes of grade 5 titanium alloy (Ti6Al4V) were tested after different treatments: as-received control (Ctr), passivated by HCl, and passivated by Piranha solution. Physical-chemical characterization of all treated surfaces was carried out by scanning electron microscopy (SEM), confocal microscopy and sessile drop goniometry to assess meshes' topography, elemental composition, roughness, wettability and surface free energy, that is, relevant properties with potential effects for the biological response of the material. Moreover, open circuit potential and potentiodynamic tests were carried out to evaluate the corrosion behavior of the differently-treated meshes under physiological conditions. Ion release tests were conducted using Inductively Coupled Plasma mass spectrometry(ICP-MS). The antibacterial activity by prevention of bacterial adhesion tests on the meshes was performed for two different bacterial strains, *Pseudomonas aeruginosa* (Gram-) and *Streptococcus sanguinis* (Gram+). Additionally, a bacterial viability study was performed with the LIVE/DEAD test. We complemented the antibacterial study by counting cells attached to the surface of the meshes visualized by SEM. Our results showed that the passivation of titanium meshes with Piranha solution improved their hydrophilicity and conferred a notably higher bactericidal activity in comparison with the meshes passivated with HCl. This unique response can be attributed to differences in the obtained nanotextures of the TiO_2 layer. However, Piranha

solution treatment decreased electrochemical stability and increased ion release as a result of the porous coating formed on the treated surfaces, which can compromise their corrosion resistance. Framed by the limitations of this work, we conclude that using Piranha solution is a viable alternative method for passivating titanium dental meshes with beneficial antibacterial properties that merits further validation for its translation as a treatment applied to clinically-used meshes.

Keywords: titanium; dental meshes; passivation; piranha; corrosion resistance; ion release; bacterial adhesion

1. Introduction

The amount of bone is paramount to predictably achieve success and long-term survival of implant-supported rehabilitations. Actually, implant dentistry has evolved to a prosthetically driven implant placement concept, meaning that biology, biomechanics, function and esthetics of the implant supported rehabilitation should be considered for the adequate implant position in bone. Although proper amount of bone is needed to go along with the esthetical and functional prosthetic design, variable discrepancies in the available bone are seldom found. This may occur because of prolonged tooth loss, trauma, injury or bone disease and resection, conducting to a horizontal, vertical or combined bone defect (Siebert). Hence, several techniques and materials for bone augmentation have been used concomitant with implant placement or as a staged approach [1–4].

Following the biological principles of selective cell exclusion for regenerative wound healing and guided tissue regeneration, these were later proven to be applicable to guided bone regeneration also. Techniques involve placing a

mechanical barrier to protect the blood clot and to isolate the bony defect from the surrounding connective and epithelial tissue invasion. This space is needed to allow the osteoblasts to access the space intended for bone regeneration [5,6].

Titanium rigid scaffolds were successfully used for bone augmentation, even outside of the bone envelope. Presently, one mainstream direction for 3D printing is biomedical applications, specifically in creating scaffolds for medical implants such as individualized titanium meshes for bone regeneration [7-9]. In recent years, the development of personalized rapid prototyping medical devices based on the digital imaging and communications in medicine (DICOM) files provided by computerized tomography/cone beam computerized tomography (CT/CBCT) scans has deeply intensified [10]. Based on the patient's bone defect and resorting to computer aided design (CAD) software, it is possible to design medical devices with the intent of recreating the lost tridimensional bone anatomy.

Regardless of the production technique for any implantable devices, it is mandatory to control the characteristics such as permeability, surface topography and roughness, and optimize their biological performance [11-16]. High degrees of roughness represent a major risk for ionic leakage from the material [17] and the bacterial adhesion can be increased, with the consequence of implant failures [10]. Smooth surfaces are able to slow down the biological processes at the interface, keeping the titanium oxidized layer properties unaffected for longer time periods [9]. The associated correct micro- and nano-roughness level can stimulate osteoblast differentiation, proliferation and production of both matrix and local growth factors [10]. Furthermore, changes in roughness correlate with selective protein adsorption, collagen synthesis and the maturation of chondrocytes, which all significantly influence the implant's osseointegration [10].

It is well known that the implant–living tissues interactions depend on the surface properties, such as roughness, wettability, surface energy and chemical composition, among others. Biomaterials research should optimize, at different scales, the surface characteristics in order to improve different functions: bioactivity, osseointegration or bactericide behavior. In addition, titanium meshes are susceptible to corrosion due to the presence of metals of different chemical nature in the mouth, as well as the release of titanium ions into the environment which must be taken into account [11–13]. It has been long recognized that the corrosion products formed as a result of metal–environment interactions have a significant bearing on the biocompatibility and long-term stability of the prostheses/implant. The material used must not cause any biological adverse reaction and must retain its form and properties [11,12] during function. Human stomatognathus is subjected to varying changes in pH and temperature owing to differences in local, systemic, environmental, economic and social conditions for each individual. Corrosion can result from the presence of a number of corrosive species such as hydrogen ion (H+), sulfide compounds (S2-), dissolved oxygen, free radicals (O2-, O-), and chloride ion (Cl-) resulting in the metal surface breakdown and a consequent adverse tissue reaction [13]. In addition, the effect of bacteria can lead to the appearance of bacterial plaque which will affect bone regeneration and cause inflammation in the patient [14–16].

Passivation is, in general, an oxidation reaction obtained by chemical or electrochemical process which promotes the formation and increasing of the thickness of protective layers [10–13]. The effect of passivation and oxidative agents and the role of titanium oxide as the physico-chemical characteristics of the surface are poorly studied and understood [17–20].

In vitro studies have implied that the negatively charged and hydrophilic TiO2 layer is, in fact, the key factor for the overall biocompatibility as it regulates the protein adsorption [9]. For the particular case of the dentistry, countless studies

have already been conducted in order to guarantee the implantation safety. Usually, no inflammatory response signs are found in the oral tissue adjacent to titanium implants; however, it is important to note that for some patients, hypersensitivity can be induced [9].

In this work, the aim was to study an alternative passivation method using the socalled Piranha solution. The Piranha solution is a mixture of sulfuric acid and hydrogen peroxide. We studied the effects of Piranha solution treatment on surface physical-chemical properties, chemical degradation (corrosion and release of ions) and antimicrobial activity against Gram-positive and Gramnegative bacteria.

2. Materials and Methods

2.1. Samples

One hundred twenty Grade 5 titanium alloy (Ti6Al4V) meshes (BoneEasy, Arada, Portugal) were used. Figure 1 shows the mesh and its application as a membrane with calcium phosphate.

We worked with 3 groups of samples:

- Control: as-received material.
- HCl passivation: The meshes were immersed in a solution of hydrochloric acid (HCl) 20% (v) for 40 s at room temperature (HCl group). This is the gold-standard passivation treatment for dental implants and prosthesis.
- Piranha passivation: The meshes were immersed in a solution of Piranha, which is a mixture of sulfuric acid 96% (v) and a 50:50 ratio of hydrochloric acid (HCl) 20% (v) and hydrogen peroxide 30% (v) for 2 h.

Piranha solutions are a mixture of concentrated sulfuric acid with hydrogen peroxide, usually in a ratio of 3:1 to 7:1. They are used to remove trace amounts of organic residues, such as photoresist, from substrates. The mixing procedure is an exothermic reaction that can reach temperatures of 100 °C or higher. The reaction of hydrogen peroxide on concentrated sulfuric acid produces highly activated and oxidizing peroxymonosulfuric acid (H_2SO_5), also called Caro's acid [1]. However, there are many different mixture ratios that are commonly used, and all are called Piranha. The addition of NH_4OH in order to accelerate the decomposition of H_2O_2 or the addition of HCl, as in this research, favors cleanness and increases the oxide stabilization. Piranha solution must be prepared with great care. It is highly corrosive and an extremely powerful oxidizer. Surfaces must be reasonably clean and completely free of organic solvents from previous washing steps before coming into contact with the solution. Piranha solution cleans by decomposing organic contaminants, and a large amount of contaminant will cause violent bubbling and a release of gas that can cause an explosion [21].

After treatment, all samples were cleaned a sequence of 3 ultrasonic baths (3 min each): two consecutive with distilled water, followed by one with ethanol.

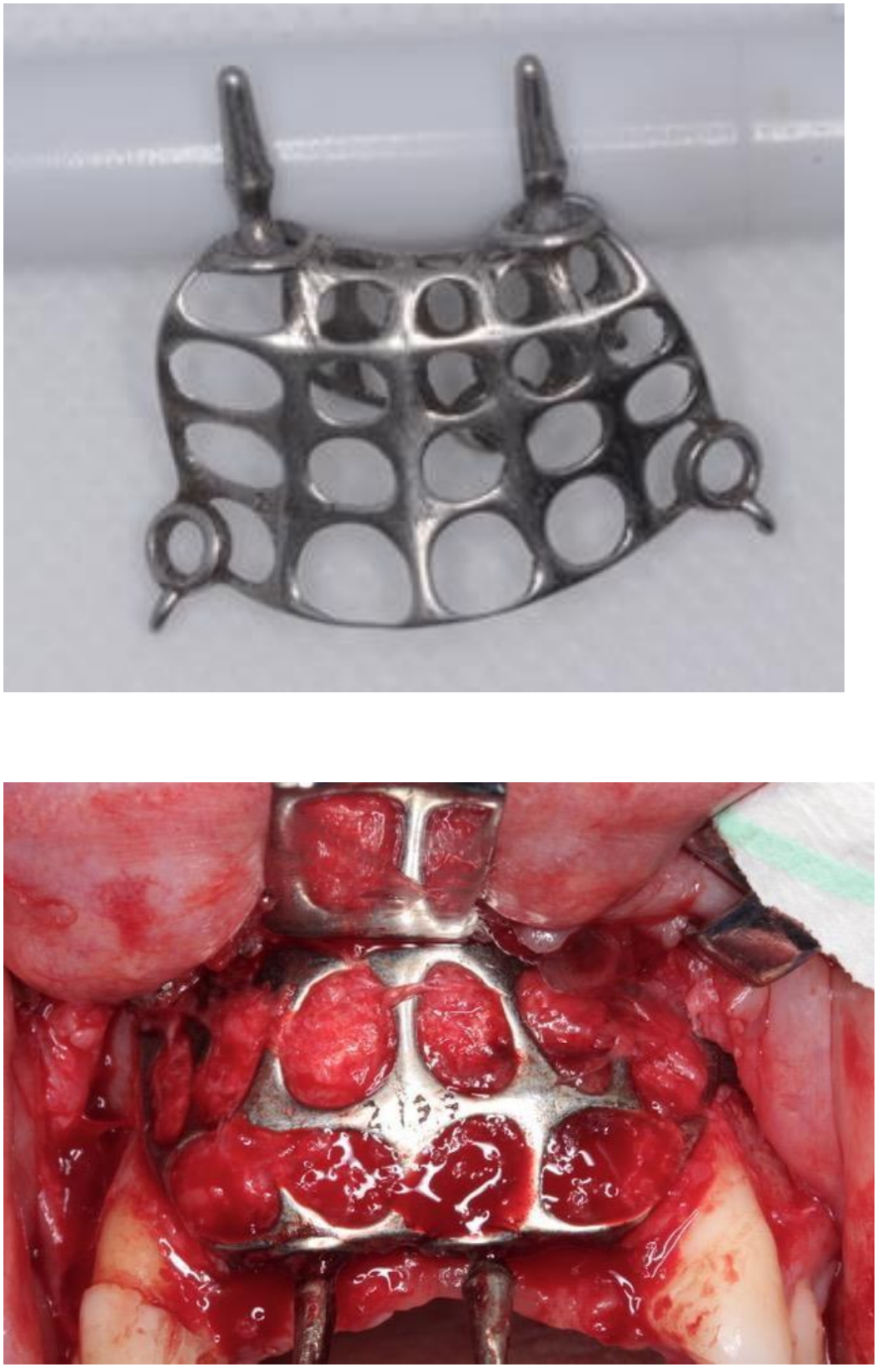

Figure 1. Grade 5 titanium mesh used in this study.

2.2. Surface Characterization

Roughness for all groups was determined using an Olympus LEXT OLS3100 confocal microscope (Olympus, Tokyo, Japan). Three samples per group were tested and 3 measurements per sample were taken at x1000 magnification. The parameters Ra and Rz were determined. Ra corresponds to the arithmetic mean of the absolute values of the deviations of the profiles of a given length of the sample. Rz corresponds to the sum of the maximum peak height and the maximum valley depth within the sampling length. [21].

The water sessile drop technique was used for the measurement of the contact angle, θ, formed between the water drop and the surface. The greater the contact angle, the lower the wettability and vice versa. For angles less than 10°, the surface is considered superhydrophilic, for angles between 10° and 90° surfaces are hydrophilic and for angles greater than 90°, surfaces are considered hydrophobic. A droplet generation system equipped with a 500 µL Hamilton syringe with micrometric displacement control was used to control the volume (3 µL) and to deposit the droplet. The analysis was performed using a gonyometer with drop profile image capture (Contact Angle System OCA15plus, DataPhysics, Filderstadt, Germany) and analyzed with SCA20 software (DataPhysics, Filderstadt, Germany) [22,23].

To calculate the surface free energy, the contact angle was measured with two different liquids, water and diiodomethane. The contact angle measurements of diiodomethane were obtained following the same procedure used to measure water contact angles [22]. The surface free energy and its polar (γp) and

dispersive (γd) components were then calculated using the Owens and Wendt equation [17]:

$$\gamma_L(1+\cos\theta)=2((\gamma_{dL}\gamma_{Sd})^{1/2}+(\gamma_{pL}\gamma_{Sp})^{1/2}) \quad (2)$$

Surface morphology of the samples was analyzed with a focused ion beam Zeiss Neon40 FE-SEM (Carl Zeiss NTS GmbH, Oberkochen, Germany). Images of uncoated samples were taken at a working distance of 7 mm and an accelerating voltage of 5 kV. An EDS detector (INCA PentaFETx3 system, Oxford Instruments, Abingdon, UK) was used to detect silver presence on the surface of the samples. This microscope has a resolving power of 3 nm and allows the observation of the nanotextures produced by the reaction of the Piranha solution with the Ti6Al4V alloy.

2.3. Corrosion Behavior

A total of 60 samples, (n = 20) for each group of samples, were used for the corrosion tests. The test area for each sample was 19.6 mm2. The electrolyte for all tests was Hank's solution (Table 1), which is a saline fluid that closely captures the ion composition of the human serum environment.

Table 1. Composition of Hank’s solution.

Chemical Product	Composition (mM)
K2HPO4	0.44
KCl	5.4
CaCl2	1.3
Na2HPO4	0.25
NaCl	137
NaHCO3	4.2
MgSO4	1.0
C6H12O6	5.5

The electrochemical cell used was a polypropylene (PP) container with a capacity of 185 mL and a methacrylate lid with 6 holes for the introduction of the sample, the reference electrode and the counter electrode (Figure 2). For both the open circuit potential measurement tests and the potentiodynamic tests, the reference electrode used was a calomel electrode (saturated KCl), with a potential of 0.241 V compared to the standard hydrogen electrode. All tests were performed at room

temperature and in a Faraday cage to avoid the interaction of external electric fields.

For the open circuit potential measurement tests, only the sample and the reference electrode were placed in the electrochemical cell. Tests were carried out for 5 hours for all the samples, taking measurements every 10 s. The potential was considered to be stabilized when the variation of the potential is less than 2 mV over a period of 30 min as indicated in the ASTM G31 standard [23]. This test assesses which materials are more noble (higher potential) and thus, less susceptible to corrode. The data and the E-t curves were obtained using the PowerSuite software (Schneieder Electric, Ruil-Malmaison, France) with the PowerCorr-Open circuit (Schneieder Electric, Ruil-Malmaison, France).

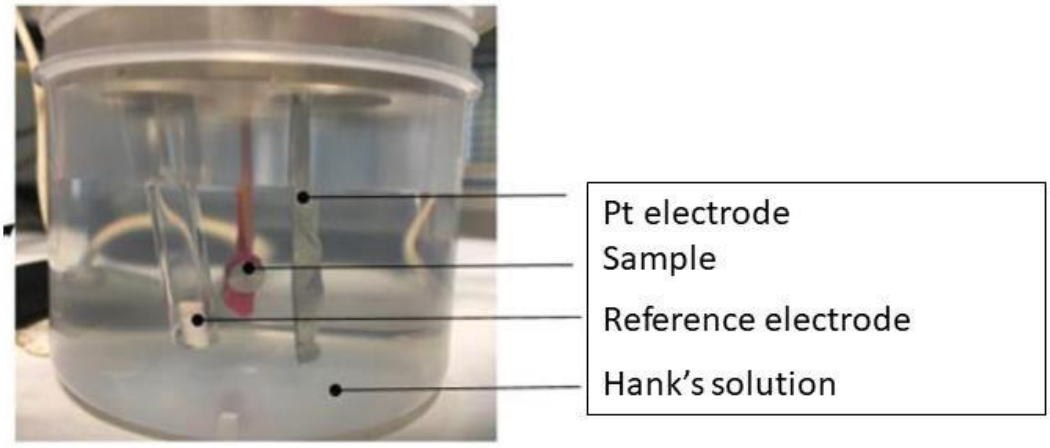

Figure 2. Experimental set up used for assessing corrosion resistance.

Cyclic potentiodynamic polarization curves were obtained for the 3 study groups following the ASTM G5 standard. In this test, a variable electrical potential is imposed by the potentiostat between the sample and the reference electrode, causing a current to flow between the sample and the counter electrode. The counter electrode used was platinum [17, 24–25]. Before starting the test, the

system was allowed to stabilize by means of an open circuit test for 1 h. After stabilization, the potentiodynamic test was launched, performing a cyclic sweep from −0.8 mV to 1.7 mV at a speed of 2 mV/s. These parameters were entered into the PowerSuite program using the PowerCorr-Cyclic Polarization function to obtain the curves. The parameters studied were:

- icorr (µA/cm2)—corrosion current density;
- Ecorr (mV)—corrosion potential: value at which the current density changes from cathodic to anodic;
- Erep (mV)—repassivation potential: potential at which the passive layer regenerates;
- Ep (mV)—pitting potential: value at which pitting corrosion may occur;
- ip (µA/cm2)—passivation current density;
- ip (µA/cm2)—repassivation current density.

The Ecorr and icorr parameters are obtained by extrapolating the Taffel slopes.

The Taffel slopes are also used to obtain the Taffel coefficients: anodic (βa) and cathodic (βc). These coefficients represent the slopes of the anodic and cathodic branch, respectively. In accordance with the ASTM G102-89 standard [23–26], these values are then used to calculate the polarization resistance (Rp) using the Stern–Geary expression and the corrosion rate (CR in mm/year) [24–28].

$$Rp = \frac{\square\square^{a}\square\ ^{c}}{2{,}303\ (\square\ \square\ \square a + c\ i)\square_{corr}} \quad (3)$$

The polarization resistance indicates the resistance of the sample to corrosion when subjected to small variations in potential. A total of 30 potentiodynamic tests were carried out, obtaining at least 10 curves per group.

$$CR = K_1 \cdot i_{corr} \cdot EW \quad (4)$$

2.4. Ion Release

Five samples from each group were used for the metal ion recovery test. After weighing the samples (m = 0.206 g) and following the ISO 10993-12 standard [26], a weight adjustment was made at the rate of 1 mL of Hank's solution for each 0.2 g of sample, as indicated in the standard. The 5 samples of each group were placed in the same Eppendorf with 5 mL of Hank's solution and stored at 37 °C. Hank's solution should be extracted and stored in the refrigerator after 1, 3, 7, 14, and 21 days. After each extraction, 5 mL of fresh Hank's solution has been replenished into the Eppendorf containing the samples. All Eppendorf tubes should be cleaned with 2% Nitric Acid and dried before use.

After 21 days, the concentration of released titanium ions was measured, at the test times indicated above, by inductively coupled plasma mass spectrometry (ICP-MS) with the Agilent Technologies 7800 ICP-MS.

2.5. Bacteria Analysis

Two types of bacteria, P. aeruginosa (Colección española de cultivos tipo, CECT 110, Valencia, Spain) and S. sanguinis (Culture Collection University of Gothenburg, CCUG 15915, Gothenburg, Sweden), a Gram-negative and a Gram-positive strain, respectively, were used for the bacterial adhesion test.

Three samples per group and bacterial strain were tested.

The culture media and material (PBS) were previously sterilized by autoclaving at 121 °C for 30 min. Prior to the adhesion test, the samples were also sterilized. For this purpose, three 5 min ethanol washes were carried out in sterile culture plates. After removing the ethanol, the samples were exposed to ultraviolet light for another 30 min [29-30].

The agar plates were cultured at 37 °C for 24 h. From this culture, the liquid inoculum was prepared by suspending the bacteria in 5 mL of BHI (Brain Heart Infusion) and incubated for 24 h at 37 °C. The medium was then diluted to an optical density of 0.1 at a wavelength of 600 nm (OD600 = 0.1). For bacterial adhesion, enough solution with a concentration equivalent to OD600 = 0.1 to cover the surfaces (500 µl/sample) was introduced into the well of the culture plate of each sample and incubated at 37 °C for 1 h.

After this time, the samples were rinsed with PBS for 5 min twice and the bacteria were fixed with a 2.5% glutaraldehyde solution in PBS (30 min in the refrigerator). The glutaraldehyde solution was then removed and the samples were rinsed with PBS 3 times for 5 min. For viability analysis by confocal microscopy, the LIVE/DEAD BacLight bacterial viability kit (Thermo Fisher, Madrid, Spain) was used [14, 32]. A solution was prepared with 1.5 µL of propidium in 1 mL of PBS. Using a micropipette, a drop of this solution (approximately 50 µL/sample) was deposited on the study surface and after incubation at room temperature in the dark for 15 min, the samples were rinsed 3 times with PBS for 5 min. The surfaces were then observed under a confocal microscope. Three images per sample were taken at 630x magnification (x63 objective). Wavelengths of 488 and 561 nm were used to detect bacteria with non-compromised membranes (LIVE) and compromised membranes (DEAD), respectively.

Prior to the observation of the samples by scanning electron microscopy (SEM), the samples were dehydrated. For the dehydration process and the critical point drying, 10 min washes were carried out with ethanol solutions of gradual concentrations of 30, 50, 70, 80, 90, 95 and 100%. They were then left to dry for 24 h at room temperature. Then, samples were coated with platinum for 5 s before observation under the microscope. Ten images of each sample were taken at 20000x magnifications for bacterial quantification on each surface.

2.6. Statistical Analysis

All results were expressed as mean and standard deviation except for the bacterial adhesion test results which were expressed as median and standard error. The comparative T.TEST (with the Excel software) was carried out between the different groups at 95%, which means that for values of $p < 0.05$, there are significant differences.

3. Results

Figure 3 shows SEM images of the surfaces of the titanium alloy after passivation treatments. No significant variations between the control and HCl treatment were detected and both types of surfaces clearly showed machining marks. Machining marks in HCl-passivated surfaces were lighter than in as-machined surfaces, probably due to the effect of the higher concentration of the acid. However, on the surface of the samples subjected to the Piranha passivation treatment, the acid attack almost completely removed the machining marks and, notably, produced a homogenously-distributed and commonly-obtained surface nanotexture in the form of nanocavities (Figure 4) [15].

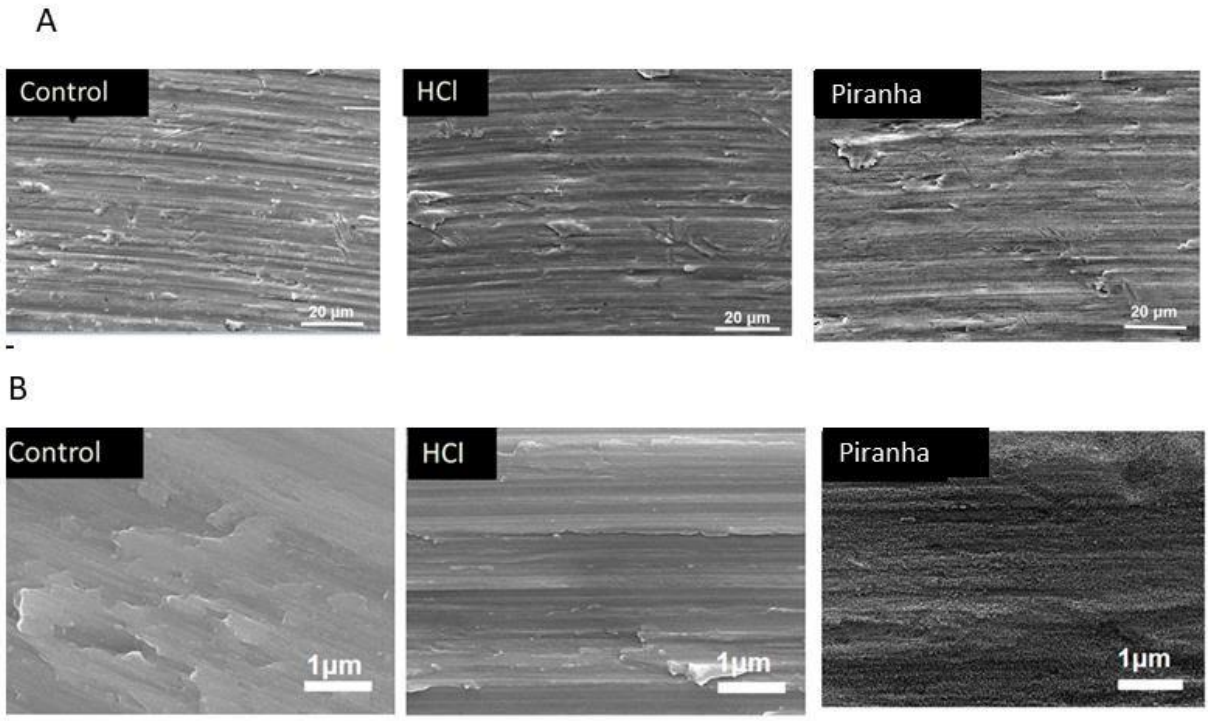

Figure 3. (**a**) Surfaces of grade 5 Ti alloy treated with different passivation methods; (**b**) at higher magnifications.

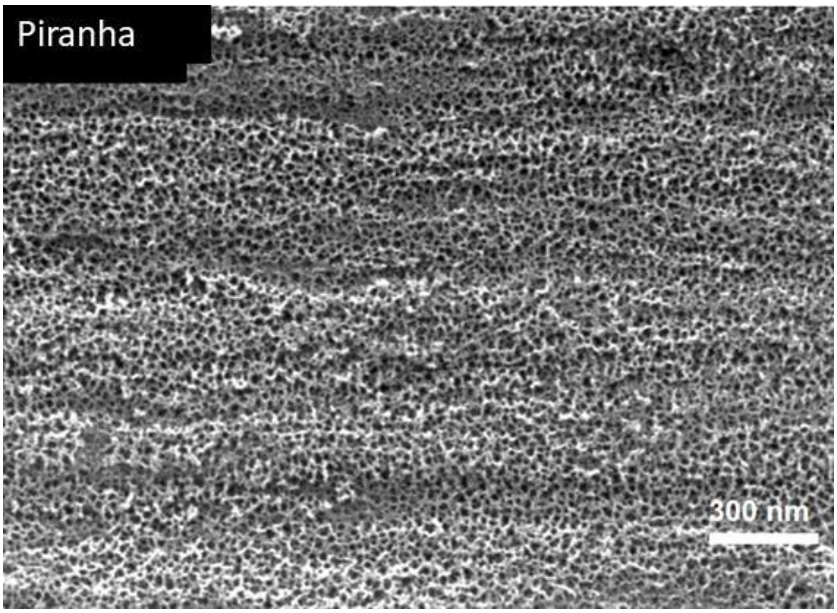

Figure 4. Nanotexture of titanium alloy after Piranha passivation treatment observed by high-resolution scanning electron microscopy.

The different passivation treatments on the titanium alloy meshes, either with HCl or Piranha solution, did not alter the average roughness (Ra), as no statistically significant differences were observed with respect to the control group (Table 2). However, the Piranha treatment showed statistically significant lower Rz values with respect to the other groups. These results suggest that the Piranha solution treatment attacked the titanium, reducing machining failures and creating an oxide layer that reduces the differences between valleys and peaks. The large difference between the Ra and Rz values shows that we have two types of texture (Figure 5), one associated with the turning marks responsible for the high Rz values and the other the nanotexture associated with the passivation treatment.

Table 2. Roughness values, Ra and Rz, for titanium alloy surfaces with different passivation treatments. Different letters in the same column denote statistically significant differences ($p < 0.05$) between groups.

Mesh	Ra (μm)	Rz (μm)
Control	0.12 ± 0.03 (a)	4.95 ± 0.76 (A)
HCl	0.14 ± 0.08 (a)	4.87 ± 0.90 (A)
Piranha	0.12 ± 0.05 (a)	1.90 ± 0.73 (B)

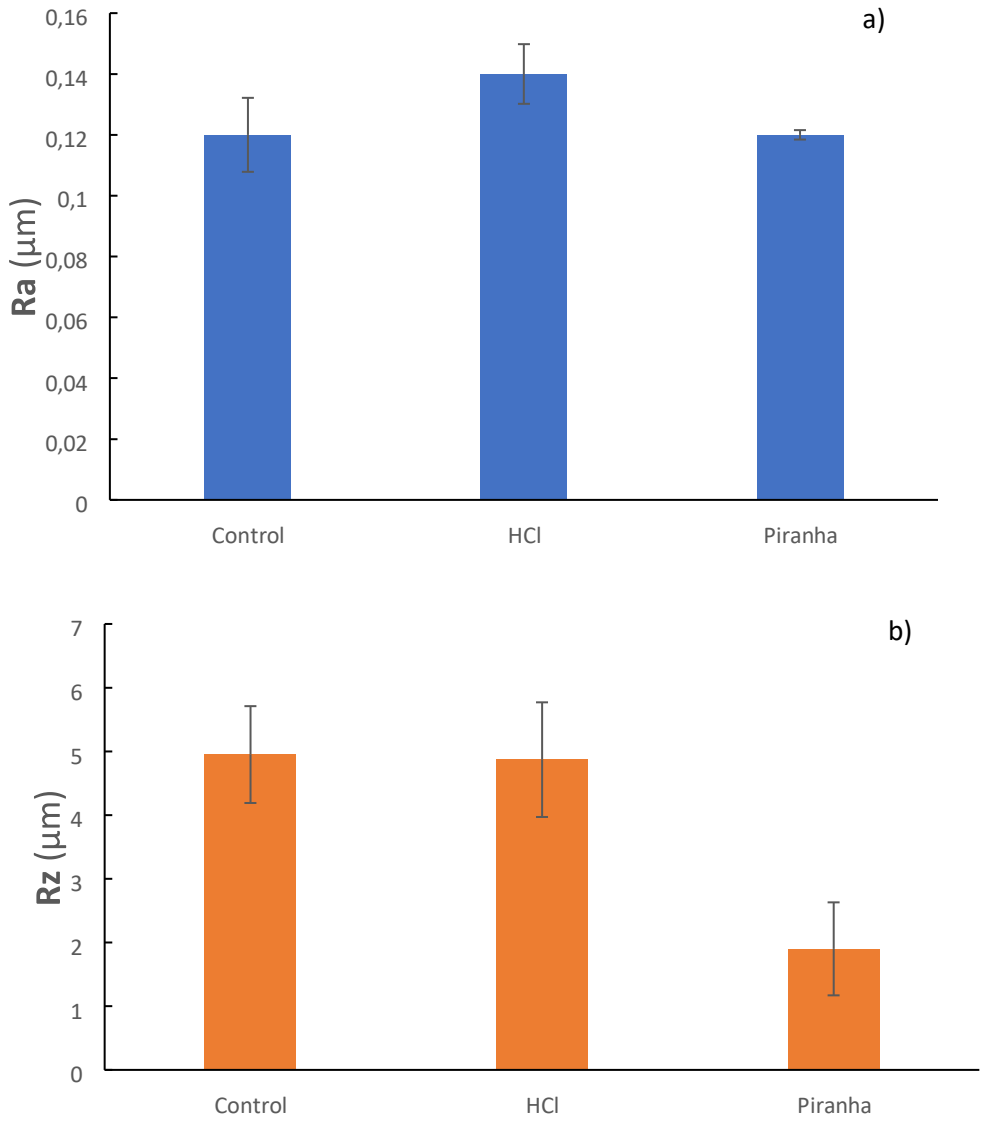

Figure 5. Roughness parameters quantified with different passivation conditions: (a) Ra and (b) Rz.

Wettability, i.e., hydrophilic/hydrophobic character of the tested surfaces, was determined measuring the water contact angle with the sessile drop technique (Table 3). Firstly, as-received control surfaces were hydrophobic with a contact angle higher than 90°. Secondly, all passivated surfaces had significantly higher hydrophilicity than untreated control surfaces. Thirdly, the surfaces passivated with Piranha solution produced a significantly higher hydrophilic material than the

surfaces treated with HCl. Water contact angle, as well as polar and dispersive components of SFE, are plotted in Figure 6.

Corresponding with the results for the wettability of the different surfaces, the polar component of the surface free energy in the titanium alloy passivated with Piranha solution was the highest among all tested surfaces. The differences in the dispersive and polar components of the surface free energy for all tested surfaces were statistically significant [33-37].

It is widely accepted that increasing the polar component of a material's surface energy promotes initial adhesion and cell proliferation [17].

Table 3. Contact angles and components of the surface free energy for the differently passivated meshes.

Mesh	Θ Water (°)	Θ Diidomethane (°)	γd (mJ/m2)	γp (mJ/m2)	SFE (mJ/m2)
Control	102.76 ± 7.00	48.40 ± 2.32	35.15 ± 1.28	0.12 ± 0.10	35.28 ± 1.35
HCl	86.37 ± 4.12	53.54 ± 0.92	32.39 ± 0.52	3.31 ± 1.28	35.70 ± 1.60
Piranha	49.05 ± 7.67	34.12 ± 3.94	42.37 ± 1.79	16.52 ± 4.22	58.90 ± 4.11

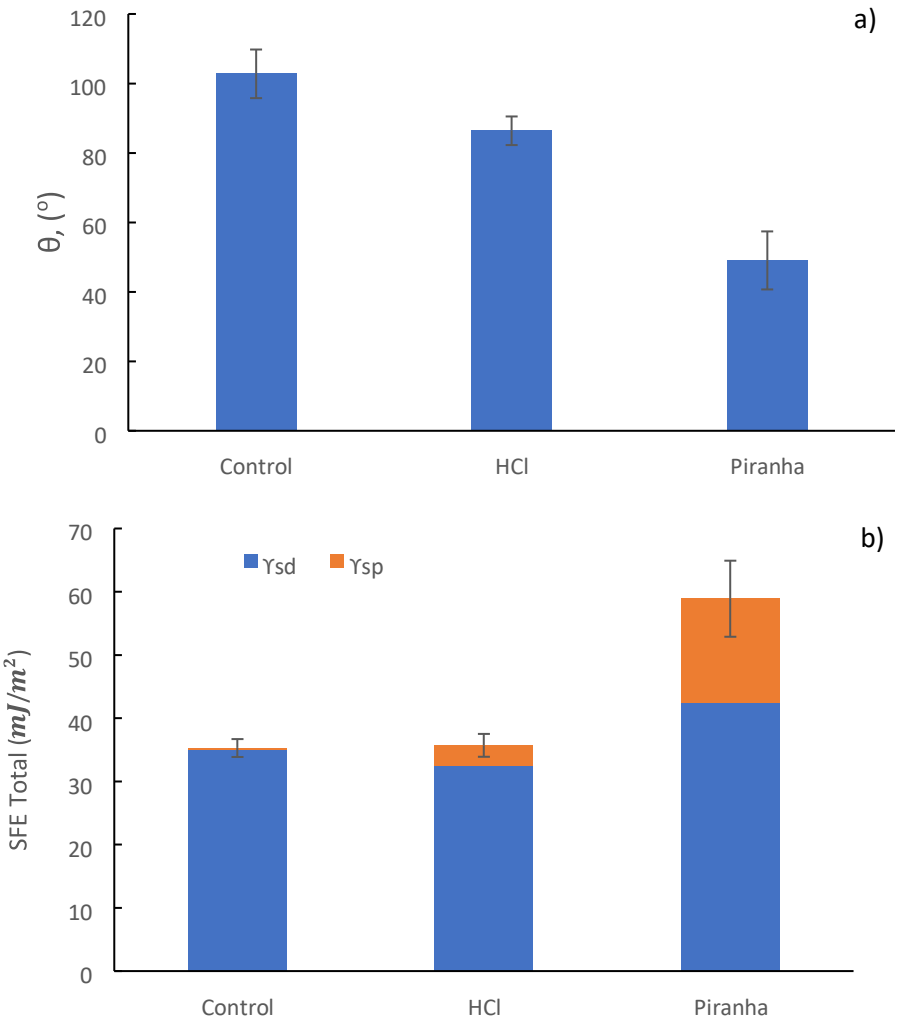

Figure 6. θ values (a) and SFE values (b) of cpTi treated with different passivation conditions.

Table 4 shows that the highest open circuit corrosion potential values (EOCP) were obtained for titanium alloy surfaces treated with HCl. Therefore, HCl passivation produces the surfaces with the least tendency for corrosion, and therefore the best corrosion behavior. Conversely, surfaces treated with the Pirahna solution showed the lowest values in open circuit, which indicated the highest tendency for corrosion. The potentiodynamic studies confirmed that the treatment that produced surfaces with the best corrosion resistance was using HCl, as these passivated surfaces showed the lowest values of corrosion current density (icorr) and corrosion rate (Vc). In addition, the HCl-treated samples show

the highest resistance to polarization (Rp). The Piranha solution should produce the thickest protective TiO2 layer; however, surfaces passivated with Piranha did not have an improved corrosion behavior with respect to the control samples.

Moreover, only in samples treated with Piranha solution pitting corrosion could be observed after the potentiodynamic tests (Figure 7).

Table 4. Electrochemical and corrosion parameters assessed for Ti alloy meshes with different passivation treatments.

Mesh	EOCP (mV)	icorr (μA/cm2)	Rp (□□/cm2)	Ecorr (V)	Vc (□m/year)
Control	−196 ± 01	0.027 ± 0.008	2.428 ± 0.390	−361 ± 14	0.233 ± 0.066
HCl	−145 ± 11	0.018 ± 0.005	2.479 ± 0.083	−536 ± 39	0.176 ± 0.048
Piranha	−206 ± 27	0.056 ± 0.006	1.102 ± 0.149	−447 ± 26	0.488 ±0.047

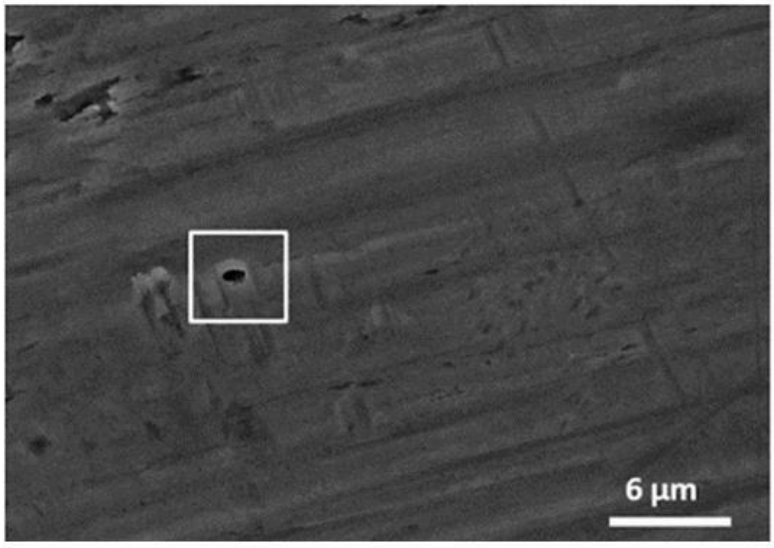

Figure 7. Pitting corrosion marks produced after completing the potentiodynamic test on a Grade 5 titanium alloy surface passivated with Piranha solution.

Table 5 shows the cumulative Ti ion release in parts per billion (ppb) from the passivated meshes in Hank's solution after increasing days of incubation, as can been observed in Figure 8. Analogous to the highest electrochemical stability, Ti ion release was the lowest from surfaces passivated with HCl, with a total cumulative concentration after 21 days of incubation of 4.1 ± 0.4 ppb, although with no statistically significant difference with respect to the untreated control group (7.0 ± 0.6 ppb). Differences are statistically significant when comparing Ti ion release from surfaces passivated with Pirahna solution and with HCl. Ion release from Piranha-treated titanium alloy meshes (10.3 ppb ± 0.9) more than doubled the ion release values from HCl-treated surfaces.

Table 5. Ti ion release (ppb) at different incubation times in Hank's solution.

Mesh	1 day	3 days	7 days	14 days	21 days
Control	1.3 ± 0.2	2.7 ± 0.5	2.8 ± 0.3	4.5 ± 0.4	7.0 ± 0.6
HCl	1.0 ± 0.3	2.0 ± 0.2	2.1 ± 0.2	3.7 ± 0.3	4.1 ± 0.4
Piranha	2.2 ± 0.7	3.8 ± 0.2	4.2 ± 0.1	7.4 ± 0.9	10.3 ± 0.9

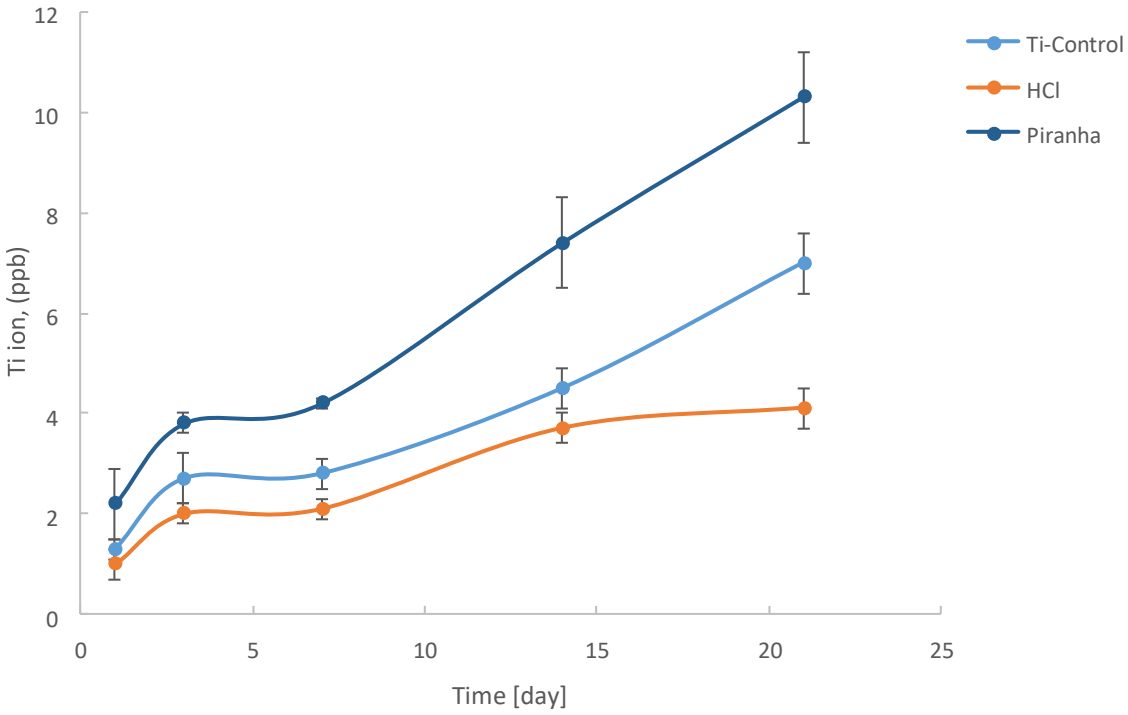

Figure 8. Ti ion release at different immersion times in Hank's solution of different passivation treatments on cpTi.

The higher ion release from surfaces treated with Piranha solutions with respect to the control and HCl-treated ones could be related to the higher corrosion rate and current density values, as previously presented. Corrosion phenomena are most likely the main cause of the degradation of the passive layer and the subsequent release of ions into the medium.

The higher ion release from surfaces treated with Piranha solutions with respect to the control and HCl-treated ones could be related to the higher corrosion rate and current density values, as previously presented. Corrosion phenomena are most likely the main cause of the degradation of the passive layer and the subsequent release of ions into the medium.

Quantitative analyses of the bacterial adhesion test performed with the Gramnegative P. aeruginosa and for the Gram-positive S. sanguinis show that

there are no significant differences in the number of bacteria adhering to the surface of the control and HCl-treated surfaces, but there were significant differences with meshes treated with Piranha solution (Table 6). Indeed, for both bacterial strains, the Piranha-treated titanium alloy surfaces drastically reduced (at least one order of magnitude) bacterial adhesion in comparison to all other groups (Figure 9 and 10). The bacteria adhered on the differently-treated surfaces can be observed in Figure 10 for P. aeruginosa and in Figure 11 for S. sanguinis, which supported the quantification differences assessed for bacterial adhesion. The LIVE/DEAD imaging revealed that differences in bacterial number were mainly related to prevention of bacteria colonization of the Piranha-treated surfaces as almost none of the bacteria remaining on the surfaces had their membranes compromised (red color).

Table 6. Quantitative analysis of number of P. aeruginosa and S. sanguinis adhered on Grade 5 titanium alloy surfaces with different passivation treatments.

Mesh	P. aeruginosa (Number of bacteria/mm2)	S. sanguinis (Number of bacteria/mm2)
Control	7.02 × 105 ± 0.52 × 105	3.52 × 105 ± 0.48 × 105
HCl	5.75 × 105 ± 0.33 × 105	2.25 × 105 ± 0.13 × 105
Piranha	1.23 × 104 ± 0.02 × 104	5.03 × 103 ± 0.10 × 103

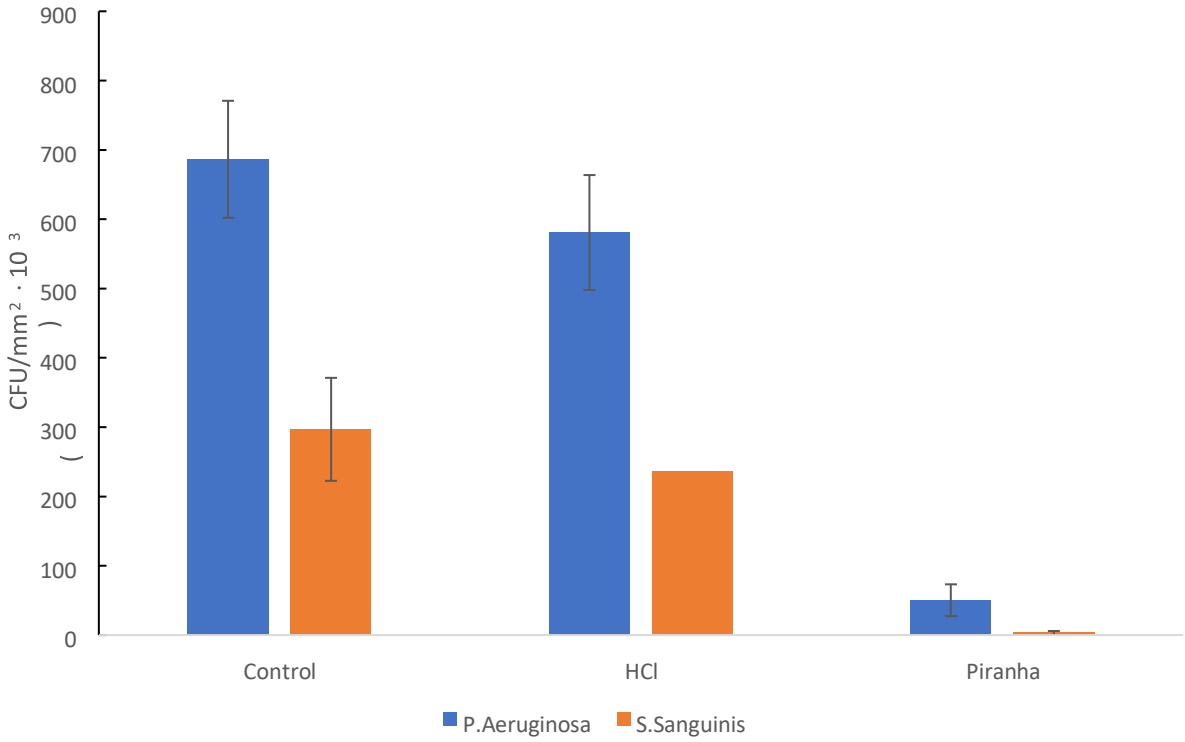

Figure 9. Analysis of P. aeruginosa and S. sanguinis adhesion for the three different conditions.

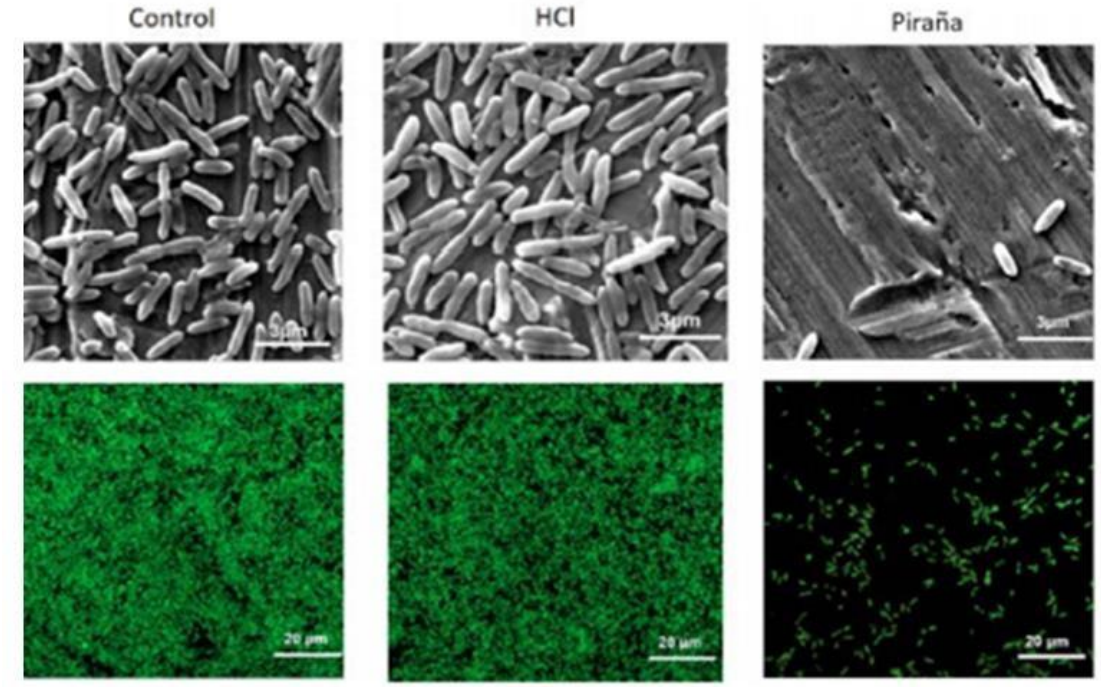

Figure 10. SEM (top row) and fluorescence (bottom row) images of P. aeruginosa stained by LIVE/DEAD.

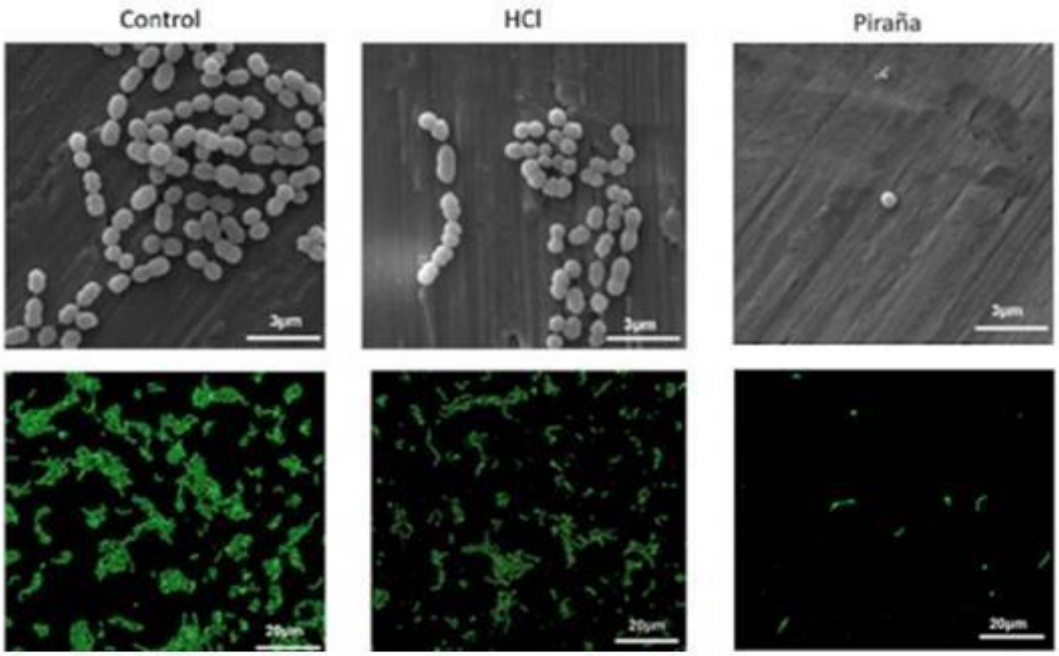

Figure 11. SEM (top row) and fluorescence (bottom row) images of S. sanguinis stained by LIVE/DEAD.

4. Discussion

The characteristic nanotexture [15, 35–37] resulting from the passivation treatment of titanium alloy meshes with Pirahna solution (Figure 12) was a relevant surface property achieved with Piranha treatment in comparison to HCl treatment. Meshes treated with Piranha solution showed a submicrotexture with superimposed nanoporosity ranging from 9–20 nm. This surface topography was homogeneous and without cracks, which suggest a good toughness of the oxide layer formed. The presence of furrows on the treated surfaces might be related to a preferential etching process in areas with high internal energy, such as grain

boundaries, dislocation pile-ups or other metallurgical or crystallographic singularities.

Notably, all passivation treatments tested increased hydrophilicity and surface free energy (Table 3). This suggests that passivating titanium meshes would not only produce a protective oxide layer but could also increase the meshes' interactions with the biological environment, favoring water, water-mediated and cellular–bacterial interactions. In most cases, protein adsorption and cell adhesion and proliferation have been correlated with an increase in surface hydrophilicity and the polar component of the surface free energy [37-38]. In particular, fibroblasts are sensitive to variations in wettability, and cell spreading increases when cells grow on more hydrophilic surfaces [14, 31]. In the case of bacterial adhesion, the effects of wettability have not been so widely explored and conclusions are more diverse, as they depend on many experimental factors, among which it is worth noting the high diversity in membrane properties of different bacterial strains.

Several studies using XPS analysis allowed to determine the chemical composition of the Ti6Al4V alloy surface after the Piranha etching [39–43]. This analysis confirmed that the atomic concentration of TiO_2 did not vary dramatically and the presence of suboxides such as TiO and Ti_2O_3 were observed. These observations are consistent with the model for the oxide layers proposed by McCafferty et al. [44], which is composed by three different layers, namely TiO (inner layer in contact with the metal), Ti_2O_3 (intermediate layer), and TiO_2 (outer layer). The superficial layer thus comprises a mixture of amorphous TiO_2, Al_2O_3, and small quantities of V_2O_5. This behavior is chemically plausible and can be explained by assuming that suboxides such as TiO and Ti_2O_3 are transformed into TiO_2 in the oxidative medium of Piranha solution [45-46], and by assuming that the etching solution penetrates the nanopits and reaches the underlying metal [46-47]. When the solution reaches the suboxides, they are further oxidized into TiO_2, thereby increasing the thickness of the dioxide nanoporous layer in a

manner consistent with ellipsometric measurements [48-49]. This porosity increases the rate of penetration of the oxidant, and the loss of material from the surface occurs at similar rates, increasing the corrosion. In addition, the reduction in electrochemical resistance of surfaces treated with Piranha solution might have been favored by the increase in real surface area and thus, reactive surface provided by the presence of the surface nanotexture generated with this treatment. These facts, in turn, might result in decreased corrosion resistance and associated increased Ti ion release of the titanium meshes treated with Piranha solution in comparison to the HCl-treated ones. This is a potential limitation for the translation of this treatment to a clinically-used mesh and should be further studied and optimized in future work.

We focused here on assessing the effects of the passivation treatment on bacterial adhesion, as infection is an increasing concern in the case of dental meshes. We assessed that the titanium alloy surfaces with Piranha solution prevented bacterial adhesion in a notably more effective way than non-treated and HCl-treated surfaces. It is known that bacterial adhesion is significantly hindered by surface nanotextures, typically obtained with Piranha solution treatments, as it manages to alter some structural parameters of the bacteria that determine their invasion potential [33]. Additionally, and most likely in a related way, some studies have also shown that there is a relationship between surface hydrophobicity and bacterial adhesion [36]. Hydrophobic metal surfaces favor adhesion of hydrophobic bacteria. Both strains tested here, S. sanguinis and P. aeruginosa, are hydrophobic bacteria [37]; so, a significant decrease in bacterial adhesion could be expected on Piranha-treated surfaces that had a significantly higher surface hydrophilicity and polar character (Table 3).

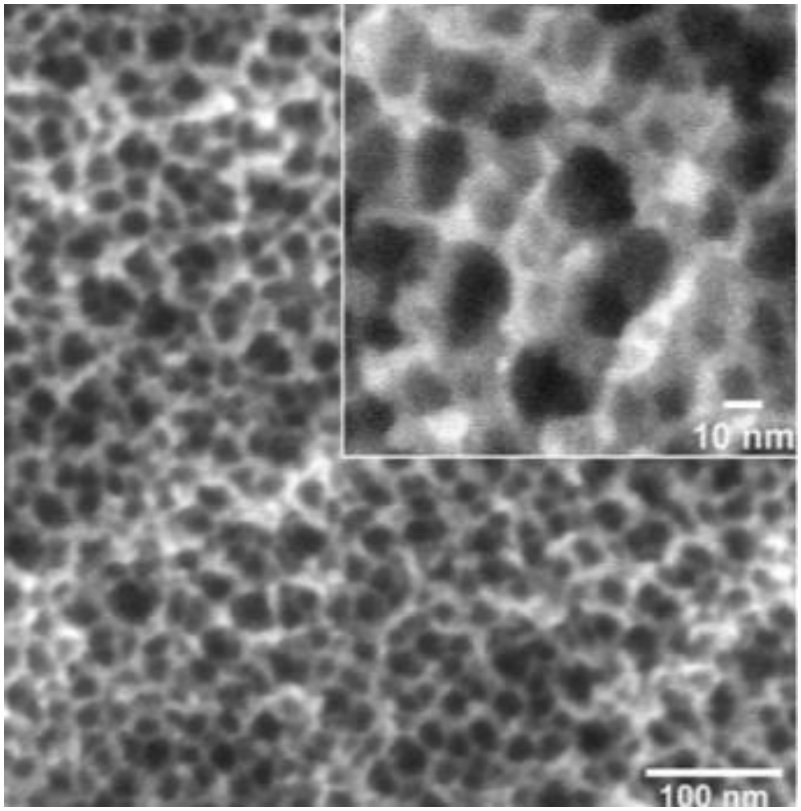

Figure 12. Nanostructure obtained in titanium meshes treated with Piranha.

The nanotexture effect is mainly caused by specific nanostructures of spike-like nanopillars, which have the capacity to mechanically destroy the murein wall of bacteria as it can be observed in titania nanotubes [50–54]. Depending on the general shape in terms of length, width and distances between these pillars, different effects such as penetration and rupture of the membrane through stretching or buckling of the bacterial wall are discussed as the actual antibacterial effect. Titania nanotubes with a diameter of 100 nm could successfully enhance gingival fibroblast proliferation and attachment while reducing the adhesion of P. gingivalis [55]. In this regard, there seem to be different targets in terms of how a nanostructure should be designed, and titanium biomaterials with such surfaces have not yet been introduced into the field. The antibacterial tests on Piranha-treated nanostructured substrates also confirmed

a substantial reduction in bacterial growth over large areas in titanium treated with Piranha, such as E. coli [56] and *S. aureus* [57-58].

According to Seddiki et al., the surface features consist of ‘tips’ that have a sharp aspect ratio [60]. These take advantage of the fact that bacterial cells have a more rigid cell wall than eukaryotic cells. Hence, the proliferation of bacteria and such other pathogenic microorganisms onto the surface is discouraged. There is also a higher ratio of TiO2 on the surface that contributes to the antibacterial activity [57]. Piranha-treated samples showed the highest cell viability after 24 h. This could be attributed to the change in surface morphology that allows for easy attachment of cells. However, there is no significant change in their viability even after 72 h [56]. These bacterial strains are characteristic of infections in orthopedics; in this contribution, we used aerobic and anaerobic bacteria typical in oral surgery.

It should be taken into account that this work has the limitation of ultraviolet treatment that can affect the chemical composition of the surface, but we wanted to be the closest to what actually happens. Ultraviolet light has a significant effect on the antibacterial properties of titanium surfaces. It has been reported that for titanium materials with nanostructures on the surface, when exposed to ultraviolet light for only 15 min, titanium materials show super hydrophilicity and the elimination of surface hydrocarbon pollution. Compared with those without ultraviolet light, titanium materials have lower initial bacterial adhesion and biofilm formation. The response of smooth titanium to ultraviolet light may be different from that of a titanium surface forming a nanostructure. Insufficient control of experimental variables affect the results of bacterial adhesion experiments [59].

5. Conclusions

The use of Piranha solution as an alternative passivation method for Ti6Al4V alloy for dental meshes was introduced. The Piranha treatment produced a nanotextured, hydrophilic, polar surface with anti-adhesion bacterial properties and compromised electrochemical properties. Open circuit potential and potentiodynamic tests show an increase in corrosion rate. In addition, titanium ion release is higher with Piranha treatment than HCl and control. Within the limitations of this work, we conclude that using Piranha solution could be a viable alternative method for passivating titanium dental meshes that merits further validation for its translation as a treatment applied to clinically-used meshes, taking in account the chemical degradation.

Funding: The work was supported by the Spanish Government and the Ministry of Science and Innovation of Spain by research projects RTI2018-098075-B-C21 and RTI2018-098075-B-C22 (co-funded by the European Regional Development Fund (ERDF), a way to build Europe). Authors also acknowledge Generalitat de Catalunya for funding through the 2017SGR-1165 project and the 2017SGR708 project.

Institutional review board statement: Not applicable.

Informed consent statement: Not applicable.

Data Availability Statement: The authors can provide details of the research requesting by letter and commenting on their needs

Ethical approval: This article does not contain any studies with human participants or animals performed by any of the authors.

Acknowledgments: The authors kindly acknowledge the collaboration of Archimedes and Meritxell Molmeneu who contributed to the development of the project.

Conflicts of interest: The authors do not have any conflict of interest.

5.3. Optimization of Titanium Dental Mesh Surfaces for Biological Sealing and Prevention of Bacterial Colonization

Published in

Journal	Materials
DOI	https://doi.org/10.3390/ma15072651
Website link	https://www.mdpi.com/1996-1944/15/7/2651
Publishing year	2022
Impact Factor	3.623 (2020) ; 5-Year Impact Factor: 3.920 (2020) JCR - Q1 (*Metallurgy & Metallurgical Engineering*) / CiteScore - Q2 (*Condensed Matter Physics*)

References

1. Bassir SH, Alhareky M, Wangsrimongkol B, Jia Y, Karimbux N. Systematic Review and Meta-Analysis of Hard Tissue Outcomes of Alveolar Ridge Preservation. Int J Oral Maxillofac Implants. 2018; 33(5):979-994. doi: 10.11607/jomi.6399.
2. Cruz N, Martins MI, Domingos Santos J, Gil Mur J, Tondela JP. Surface Comparison of Three Different Commercial Custom-Made Titanium Meshes Produced by SLM for Dental Applications. Materials (Basel). 2020;13(9):

2177. doi: 10.3390/ma13092177.

3. Bosshardt D, Schenk R – Biologic Basis of Bone Regeneration. In Buser D – 20 years of Guided Bone Regeneration in Implant Dentistry. (Hanover, Germany): Quintessence Publishing Co,2009

4. Elgali, I., Omar, O., Dahlin, C., Thomsen, P. Guided bone regeneration: materials and biological mechanisms revisited. Eur. J. Oral. Sci. 2017; 125: 315–337.

5. Retzepi, M., Donos, N. Guided bone regeneration: biological principle and therapeutic applications. Clin. Oral. Implants Res. 2010; 21: 567–576.

6. Guillem-Marti J, Delgado L, Godoy-Gallardo M, Pegueroles M, Herrero M, Gil FJ. Fibroblast adhesion and activation onto micro-machined titanium surfaces. Clin Oral Implants Res. 2013 Jul;24(7):770-80. doi: 10.1111/j.16000501.2012.02451.x.

7. Xie Y, Li S, Zhang T, Wang C, Cai X. Titanium mesh for bone augmentation in oral implantology: current application and progress. Int J Oral Sci. 2020 Dec 30;12(1):37. doi: 10.1038/s41368-020-00107-z.

8. Uehara S, Kurita H, Shimane T, Sakai H, Kamata T, Teramoto Y, Yamada S. Predictability of staged localized alveolar ridge augmentation using a micro titanium mesh. Oral Maxillofac Surg. 2015;19(4): 411-416. doi: 10.1007/s10006-015-0513-6.

9. Mounir, M., Shalash, M., Mounir, S., Nassar, Y., El Khatib, O. Assessment of three dimensional bone augmentation of severely atrophied maxillary alveolar bridges using prebent titanium mesh vs customized poly-ether-etherketone (PEEK) mesh: A randomized clinical trial. Clin. Implant Dent. Relat.
Res. 2019; 21, 960–967.

10. Sagheb K, Schiegnitz E, Moergel M, Walter C, Al-Nawas B, Wagner W. Clinical outcome of alveolar ridge augmentation with individualized CADCAM-produced titanium mesh. Int J Implant Dent. 2017; 3(1):36. doi: 10.1186/s40729-017-0097-z

11. Rakhmatia YD, Ayukawa Y, Furuhashi A, Koyano K. Current barrier membranes: titanium mesh and other membranes for guided bone regeneration in dental applications. J Prosthodont Res. 2013; 57:3–14.

12. Watzinger F, Luksch J, Millesi W. Guided bone regeneration with titanium membranes: a clinical study. Br J Oral Maxillofac Surg. 2000; 38:312.

13. Rakhmatia YD, Ayukawa Y, Atsuta I, Furuhashi A, Koyano K. Fibroblast attachment onto novel titanium mesh membranes for guided bone regeneration. Odontology. 2015;103(2):218-26. doi: 10.1007/s10266-0140151-8.

14. Elias, C., Lima, J., Valiev, R. & Meyers, M. Biomedical applications of titanium and its alloys. JOM 2008; 60: 46–49.

15. Sidambe, A. T. Biocompatibility of advanced manufactured titanium implants—a review. Materials 2014; 7: 8168–8188.

16. Cucchi, A., Sartori, M., Aldini, N. N., Vignudelli, E. & Corinaldesi, G. A proposal of pseudo-periosteum classification after GBR by means of titanium-reinforced d- PTFE membranes or titanium meshes plus crosslinked collagen membranes. Int. J. Periodontics Restor. Dent. 2019; 39: 157– 165.

17. Her, S., Kang, T., Fien, M. J. Titanium mesh as an alternative to a membrane for ridge augmentation. J. Oral. Maxillofac. Surg. 2012; 70: 803–810.

18. Ciocca L, Lizio G, Baldissara P, Sambuco A, Scotti R, Corinaldesi G. Prosthetically CAD-CAM-Guided Bone Augmentation of Atrophic Jaws Using Customized Titanium Mesh: Preliminary Results of an Open Prospective Study. J Oral Implantol. 2018 ;44(2):131-137. doi: 10.1563/aaid-joi-D-1700125.

19. Roccuzzo, M., Ramieri, G., Bunino, M. & Berrone, S. Autogenous bone graft alone or associated with titanium mesh for vertical alveolar ridge augmentation: a controlled clinical trial. Clin. Oral. Implant Res. 2007; 18: 286–294.

20. Torres J, Tamimi F, Alkhraisat MH, Manchón A, Linares R, Prados-Frutos JC, Hernández G, López CabarcosTorres, J. Platelet-rich plasma may prevent titanium-mesh exposure in alveolar ridge augmentation with anorganic bovine bone. J. Clin. Periodontol. 2010, 37: 943–951.

21. Behring J, Junker R, Walboomers XF, Chessnut B, Jansen JA. Toward guided tissue and bone regeneration: morphology,attachm ent, proliferation, and migration of cells cultured on collagen barrier membranes: a systematic review. Odontology. 2008; 96:1–11.

22. Warrer K, Sanchez R, Karring T. Guided tissue regeneration in recession type defects using a bioabsorbable Resolut or non bioabsorbable Gore-Tex periodontal material (GTAM) membrane. J Dent Res. 1994; 73:380.

23. Rakhmatia, Yunia Dwi, et al. "Fibroblast attachment onto novel titanium mesh membranes for guided bone regeneration." Odontology 2015; 103.2: 218226.

24. Takata T, Wang HL, Miyauchi M. Attachment, proliferation and differentiation of periodontal ligament cells on various guided tissue regeneration membranes. J Periodontal Res. 2001; 36:322–7.

25. Gil, F.J.; Rodriguez, A.; Espinar, E.; Llamas, J.M.; Padulles, E.; Juarez, A. Effect of the oral bacteria on the mechanical behavior of titanium dental implants. Int. J. Oral Maxillofac. Impl. 2012, 27: 64–68.

26. Mombelli, A.; van Oosten, M.A.; Schurch, E.; Land, N.P. The microbiota associated with successful or failing osseointegrated titanium implants. Oral Microbiol. Immunol. 1987, 2: 145–151

27. Punset, M.; Villarrasa, J.; Nart, J.; Manero, J.M.; Bosch, B.; Padrós, R.; Perez, R.A.; Gil, F.J. Citric Acid Passivation of Titanium Dental Implants for Minimizing Bacterial Colonization Impact. Coatings 2021, 11: 214. https://doi.org/10.3390/ coatings11020214

28. Godoy-Gallardo, M.; Manzanares-Céspedes, M. C.; Sevilla, P.; Nart, J.; Manzanares, N.; Manero, J. M.; Gil, F. J.; Boyd, S. K.; Rodríguez, D.,

Evaluation of bone loss in antibacterial coated dental implants: An experimental study in dogs. Mater Sci Eng C Mater Biol Appl 2016, 69: 538-45.

29. Gil FJ, Rodríguez D., Planell JA. Grain growth kinetics of pure titanium". Scripta Met. Mat. 1995; 33(8): 1361-1366.

30. Gil FJ, Manero JM, Ginebra MP, Planell JA. The effect of cooling rate on the cyclic deformation of □-annealed Ti6Al4V. Mater. Sci. Eng. A. 2003, 349: 150155.

31. Gil FJ, Planell JA. Behaviour of normal grain growth kinetics in single phase titanium and titanium alloys Mater. Sci. & Eng. A, 2000; 283: 17-24.

32. Brunette DM, Chehroudi B. The effects of the surface topography of micromachined titanium substrata on cell behavior in vitro and in vivo. J Biomech Eng 1999: 121: 49-57.

33. Bobbert FSL, Lietaert K, Eftekhari AA, Pouran B. Additively manufactured metallic porous biomaterials based on minimal surfaces: A unique combination of topological, mechanical, and mass transport properties. Acta Biomater., 2017, 53: 572-584. ISSN 1742-7061, https://doi.org/10.1016/j.actbio.2017.02.024.

34. Khodaei M, Fathi M, Meratian M et al. The effect of porosity on the mechanical properties of porous titanium scaffolds: Comparative study on experimental and analytical values. Materials Research Express, 2018, 5(5). https://doi.org/10.1088/2053-1591/aabfa2.

35. McAnulty RJ. Fibroblasts and myofibroblasts: their source, function and role in disease. Int J Biochem Cell Biol 2007; 39: 666-671.

36. Tomasek JJ, Gabbiani G, Hinz B, Chaponnier C, Brown RA. Myofibroblasts and mechano-regulation of connective tissue remodelling. Nat Rev Mol Cell Biol 2002, 3: 349-363.

37. Mutsaers SE, Bishop JE, McGrouther G, Laurent GJ. Mechanisms of tissue repair: from wound healing to fibrosis. Int J Biochem Cell Biol 1997; 29: 5-17.

38. Variola, F., Lauria, A., Nanci, A., & Rosei, F. Influence of Treatment Conditions on the Chemical Oxidative Activity of H2SO4/H2O2Mixtures for Modulating the Topography of Titanium. Advanced Engineering Materials, 2009: 11(12), B227–B234.

39. Bagno, A.; Di Bello, C. Surface treatments and roughness properties of Tibased biomaterials. J. Mater. Sci. Mater. Med. 2004, 15, 939–945.

40. Kasemo, B., Gold, J. Implant Surfaces and Interface Processes. Advances in Dental Research, 1999: 13(1), 8–20.

41. Sorsa T, Tjäderhane L, Konttinen YT, Lauhio A, Salo T, Lee HM, Golub LM, Brown DL, Mäntylä P. Matrix metalloproteinases: contribution to pathogenesis, diagnosis and treatment of periodontal inflammation. Ann Med 2006; 38: 306-321.

42. Antoszewska J, Raftowicz-Wójcik K, Kawala B, Matthews-Brzozowska T. Biological factors involved in implant-anchored orthodontics and in prosthetic-implant therapy: a literature review. Arch Immunol Ther Exp (Warsz) 2010; 58: 379-383.

43. Chou L, Firth JD, Uitto VJ, Brunette DM. Substratum surface topography alters cell shape and regulates fibronectin mRNA level, mRNA stability, secretion and assembly in human fibroblasts J Cell Sci 1995; 108: 15631573.

44. Amoroso PF, Adams RJ, Waters MG, Williams DW. Titanium surface modification and its effect on the adherence of Porphyromonas gingivalis: an in vitro study. Clin Oral Implants Res 2006; 17: 633-637.

45. Gristina AG. Biomaterial-centered infection: microbial adhesion versus tissue integration. Science 1987; 237: 1588-1595.

46. Subbiahdoss G, Kuijer R, Grijpma DW, van der Mei HC, Busscher HJ. Microbial biofilm growth vs. tissue integration: "the race for the surface" experimentally studied. Acta Biomater 2009; 5: 1399-1404.

Optimization of titanium dental mesh surfaces for biological sealing and prevention of bacterial colonization

Nuno Cruz[1,2], João Paulo Tondela[3], Maria Inês Martins[4], Eugenio VelascoOrtega[5] and F Javier Gil[1,2,*]

[1] School of Dentistry, Universitat Internacional de Catalunya (UIC), C. Josep Trueta s/n, 08195 Sant Cugat del Vallès, Spain. nuno.cruz@orismed.pt, xavier.gil@uic.es

[2] Bioengineering Institute of Technology, International University of Catalonia, Josep Trueta s/n. 08195-Barcelona, Spain.

[3] CIROS from the Faculty of Medicine, University of Coimbra, FMUC; jtondela@fmed.uc.pt

[4] Faculty of Engineering. University of Porto (FEUP), 4200-465 Porto, Portugal; up201305982@fe.up.pt,

[5] Master in Implant Dentistry. Faculty of Dentistry, University of Seville, Spain; (evelasco@us.es)

***** Correspondence: xavier.gil@uic.es. FJG .jtondela@fmed.uc.pt. JPT.

Abstract: Titanium dental meshes have a wide application in order to the retention of calcium phosphate-based biomaterials to regenerate bone tissue. These meshes are temporary and must grow a soft tissue to prevent bacterial colonization and provide stability. In this work we have tried to optimize the roughness of the meshes to obtain a good biological seal while maintaining a behavior that does not favor bacterial colonization. To this end, six types of surface have been studied: machined as a control, polished, sandblasted with three different alumina sizes and sintered. The roughness, contact angles and

biological behavior using fibroblast cultures at 7, 24 and 72 hours were determined, as well as cytotoxicity studies. Cultures of two very common bacterial strains in the oral cavity were also carried out: *Streptococcus sanguinis* and *Lactobacillus salivarius*. The results showed that the samples treated with alumina particles by sandblasting at 200 micrometres were the ones that performed best with fibroblasts and also with the number of bacterial colonies in both strains. According to the results, we see in this treatment a candidate for the surface treatment of dental meshes with an excellent performance.

Keywords: dental meshes, titanium, sealing, bacteria, roughness, wettability.

1. Introduction

Nowadays, modern oral rehabilitation focuses in minimal invasive approaches in order to obtain the desired results with regard to patient best interests and less discomfort possible.

However, when it comes to oral surgery involving soft and hard tissue reconstruction, the idea of minimal invasive approach relies on the complexity of the diagnosis and correspondent(s) treatment plan(s). Moreover, when complex bone losses, combining horizontal and vertical defects, or atrophic maxillary/mandibular need volume improvements in order to rehabilitate function and aesthetics with fixed teeth, we can only expect higher challenges that end in a more demanding treatment for both patient and clinician.

The success of dental implant treatments depends on the bone quality as well as the alveolar volume for the proper placement of dental implants. Implant

design, biomaterials, good primary fixation with cortical bone and good soft tissue healing also play an important role [1].

Permanent prostheses fixed by dental implants for the rehabilitation of the oral cavity do not mean a simple fitting following the shape of the bone tissue. Nowadays, surgeons must make treatment plans for each patient and must analyse bone defects, suitable spaces for placement by computed tomography (CT)/cone beam computed tomography (CBCT) [2].

Several studies have been conducted to regenerate alveolar bone tissue after tooth loss. These surgical regeneration procedures will be key to the success of the treatment [2-3]. These report that almost half of the rehabilitations with dental implants need some kind of bone regeneration procedure. The procedure can be before or during implant placement [3].

Different methodologies and clinical procedures have been developed to restore bone defects in the alveolus. One of the most prominent is guided bone regeneration (GBR), as well as bone grafting, bone extrusion, new bone generation by distraction.

Due to the simplicity of the technique, its ability to create new bone tissue in different directions and its stability, GBR is currently the most widely used technique for the repair of alveolar bone defects [4]. The Resorbable Barrier Membrane (RBM) technique consists of preventing epithelial cells and connective tissue cells from proliferating in the area of the bone defect by using the barrier membrane. The different migration rate of the different cells allows osteoblastic cells to preferentially enter the bone defect area to induce and regenerate new bone tissue [5].

There are two different types of barrier membranes used, in most cases, for Barrier Membrane (BR): resorbable or non-resorbable. Both have the same mission, which is to act as a mechanical barrier to calcium phosphate-based materials. These BR differ in the chemical composition and macro and microdesign, but always have the same retentive function [6]. To fulfil this main objective, the meshes must have good biocompatibility and mechanical strength in order to have a good retentive capacity [7].

In the presence of significant bone tissue defects, both vertical and horizontal, titanium or Ti6Al4V alloy meshes are ideal, as demonstrated by several clinical studies, given their good mechanical properties and osteogenic capacity [8-10].

Recently, new designs of titanium mesh membranes and titanium alloys (Ti6Al4V) have been studied with the aim of facilitating the formation of new bone tissue, stabilising bone grafts beneath the membrane while minimising the possibility of fibrous tissue growth and/or preventing collapse [11-12].

The optimal membrane should facilitate cell activity (adhesion, proliferation, migration and differentiation cellular) on the membrane surface, in order to isolate the defect from the presence of bacteria, in addition to the main function of the membrane. This biological sealing produced by the cells of the connective tissue will stabilize the blood clot causing the integration of the soft tissue in the membrane. However, fibroblasts must be prevented from penetrating the membrane, since it could be biologically harmful [13].

In addition to its good biocompatibility and mechanical properties, titanium and Ti6Al4V also has an excellent corrosion behavior due to the formation a passive and inert oxide film [14-15]. In addition, *the reconstruction of* alveolar ridge produced by metallic mesh, a thin 1-2 mm thick soft tissue layer can be

observed on the regenerated bone tisuue on the surface, called "pseudoperiosteum. The mission of the pseudoperiosteum is the bone graft protection, prevention of graft bacteria colonization [16].

However, exposure rates and consequent healing complications of the use of titanium meshes in bone regeneration remains as a major concern. The incidence of mesh exposure is mostly 20% to 30% and the highest reported exposure rate is 66% [17-20].

As known, primary wound closure and soft tissue stability during the remaining healing period play a crucial role in order to avoid early and late exposure of the titanium mesh. As it has been mentioned, the difference in the superficial properties, and the porosity characteristics (number, sizes, distribution) may produce different behavior on cell adhesion, migration, proliferation and differentiation. Furthermore, it is suggested that cell adhesion to surfaces is produced by the protein interactions of the body environment, and also that the properties of this layer depend on characteristics such as surface electrical charge, chemical elements and the internal energy of the titanium [2122].

Results from Rakhmatia and collaborators work evaluated the difference in fibroblast adhesion and morphology in relation to the exposition to different design and structures of GBR barrier membranes [23]. Several factors such as: membrane material, topography, design, adhesion behavior, protein-binding ability, debris released during degradation, wettability, internal energy, texture, and duration of barrier function may influence GBR outcomes has not yet been completely understood [24].

The aim of this contribution is to determine the best conditions of roughness of the surface of the meshes so that they perform the barrier function and for this there is a good adhesion, proliferation and differentiation of fibroblasts in order to obtain a good biological seal that prevents bacterial colonisation. It is also very important that the topography does not favour the activity of osteoblastic cells to prevent osseointegration. Once these meshes have performed their function of bone regeneration, they must be removed and therefore it is not good for them to remain anchored in the bone tissue. For these reasons, the best conditions for the surface topography of the meshes should be studied, which we are trying to clarify in this work.

2. Materials and Methods

2.1. Materials

120 grade 5 titanium alloy (Ti6Al4V) meshes (BoneEasy, Arada, Portugal) were used. In Figure 1 shows the mesh design used.

Figure 1. Ti6Al4V mesh used in this study

Cylindrical shape samples (5 mm diameter, 2 mm width) were cut and six different surfaces were evaluated:

- (Mech): as-received lathe cut titanium samples (control samples). Mech samples used in the study correspond to the same material, roughness and mesh conditions as shown in Figure 1. The samples are extracted from the same material with the same mesh conditions.
- (Smooth): samples were treated with 220 to 4000 grit SiC paper in water medium, deburred, and after polished by SiO_2 suspension.

  Sand-blasted: the surfaces were sand-blasted at a pressure of 2.5 MPa with:

- (Al2): Al_2O_3 small size particles (212-□m)□□□
- (Al6): Al_2O_3 medium size particles (425-600 □m)
- (Al9): Al_2O_3 big size particles (1000-1400 □m)
- (Sinter): Ti6Al4V spheres sintered from 10-50 □m□ of diameter.

After treatment, all samples were cleaned with deionized water, ethanol and acetone, dried at 25ºC and sterilized by autoclave at 120 °C for half an hour.

2.2. Characterization of the surfaces

Roughness parameters were obtained by means of a white light interferometer microscope (Wyko NT1100, Veeco Instruments Inc., USA) and proprietary software (Vison32, Veeco Instruments Inc., USA). The measurements were realized in 10 samples to determine the average roughness (Ra), which represents the mean height of the peaks indicated by the arithmetic average of the absolute values of all points of the profile, and the real surface area (Ar), larger than the nominal area (70.7 mm^2) due to the surface roughness.

Hydrophilic and hydrophobic characters were measured using a contact angle video-based system (Contact Angle System OCA15plus, Dataphysics, Germany) and analyzed with proprietary software (SCA20, Dataphysics, Germany). The analysis was performed under conditions of 100% relative humidity and controlled temperature.

The topography of the samples was observed by scanning the electron microscopy (SEM) using the Phenom XL Desktop SEM microscope (PhenomWorld, Eindhoven, The Netherland) using a voltage of 20 keV to accelerate the electrons and to achieve a good resoluction (7 nm). This microscope has a EDX microanalysis in order to atomic chemical analysis with a sensitivity around 0.1%.

2.3. Cell culture and cell seeding

Primary human foreskin fibroblast cells (Millipore, Billerica, MA, USA) were cultured in Dulbecco's minimal essential medium (DMEM; Invitrogen, Carlsbad, CA, USA) and the addition of 10 % fetal bovine serum (FBS), L-glutamine (2 mM) and penicillin/streptomycin (50 U/ml and 50 g/ml, respectively) at 37 °C in a humidified incubator at 5% CO_2. The culture medium was changed every 48 hours. Subconfluent fibroblasts were trypsinised, centrifuged and seeded with 6

x 10^3 cells/disc with DMEM without serum and phenol red in the different Ti6Al4V samples placed in a 48-well microplate. An agarose film was introduced (in order to inhibit fibroblast adhesion) in order to have a negative control and can determine the adhesion behavior. Tissue culture polystyrene (TCPS) and polished Ti6Al4V (Smooth) were used as reference substrates. Fibroblast analyses were carried out at 4 hours, 24 hours and 72 hours.

2.4. Cell morphology

Field Emission Scanning Electron Microscopy (FESEM), (JSM-7001F JEOL Ltd., Tokyo, Japan) was used to characterized the cellular morphologies. For this objective, the discs cultured were cleaned by means of 0.1M phosphate buffer (PB) and fixed with 2.5% glutaraldehyde solution in PB, 4 hours at 4ºC. The samples were immersed 2 hours at room temperature in a 1% solution of osmium tetroxide in order to improve the observation. Fixed samples were then dehydrated in 50, 70, 90, 96 and 100% ethanol series three times followed by a hexamethyldisilazane (HDMS) drying procedure.

2.5. Cell proliferation – WST-1

HFF fibroblasts were cultured on the different surfaces studied, analyzing adhesion and proliferation using WST-1 (Roche Applied Science, Penzberg, Germany). This colorimetric determination quantifies cell activity by formazan staining. The mechanism is that mitochondrial dehydrogenases in living cells cause the separation of tetrazole salts and the colour of the soluble formazan is measured spectrophotometrically. The absorbance increases and can be correlated with increasing cell number. For the determination of cell viability, cell viability was determined at the different specified culture times by incubating for

2 h with WST-1 1:10 in DMEM without serum and phenol red. The optical density (OD) at 440 nm of the cell supernatant was measured with the ELx800 universal microplate reader (Bio-Tek Instruments, Inc., Winooski, VT, USA). Three different samples were studied for each surface type and two different experiments were performed in parallel. The optical density (OD) at 440 nm of the cell supernatant was determined with the ELx800 universal microplate reader (Bio-Tek Instruments, Inc., Winooski, VT, USA). Three samples were studied for each surface type and two tests were performed. A curve was obtained using different number of cells from 3 x 10^3 to 50 x 10^3.

2.6. Cell viability – LDH

Lactate dehydrogenase (LDH) enzyme release at culture times was the methodology used for quantification of non-viable cells.The supernatant liquid was extracted from the cell-free culture. This broth was centrifuged at 250 x g for 5 minutes and subsequently detected by the Cytotoxicity Kit LDH (Roche Applied Science). The decrease of tetrazolium compounds in formazan staining by LDH activity was determined spectrophotometrically using 490 nm. TCPS was used as a minimum control and lysed cells (maximum LDH activity) as a maximum control. Two experiments were realized in order to evaluate the cytotoxicity of three samples of each series.

2.7. Microbiological behavior

The bacteria strain *Streptococcus sanguinis* (CECT 480) and *Lacobacillus salivarius* (CECT 4063) (Colección Española de Cultivos Tipo, Valencia, Spain) were tested in this research. Strains were cultured in Todd-Hewitt broth at 37 ºC in a 5 % CO_2-enriched atmosphere. Microbial Adhesion to Solvents (MATS)

assay [25] was followed to determine bacterial adhesion in physiological medium is the MATS test based on the electronic exchange of bacteria (donor/acceptor) [26-28].

Bacteria were collected when proliferation was in exponential growth function. Bacteria were collected after centrifugation at 4500 g for 15 minutes at a temperature of 4 ºC. Once obtained, the bacteria were washed with Phosphate Buffer Solution (PBS) at 0.15 M. The bacteria were then suspended in PBS and their optical density was determined at a wavelength of 550 nm (A_0). The MATS test was performed in hexane, chloroform and diethyl ether. 3 ml of bacteria dissolution was extracted into 9 tubes and 400 µl of solvent (3 samples for each solvent) were added. The different suspensions were incubated at 20 °C for 10 minutes and mixed in a vortex shaker for 1 minute. Phase separation was performed after 15 minutes by measuring the optical density of the aqueous phase at the same wavelength (A_1). The resulting bacterial adhesion was determined according to the formula: $(1-A_1/A_0) \times 100$.

Ti6Al4V samples of 5 mm diameter and 2 mm thickness were tested. These were cleaned in 70 % ethyl alcohol, acetone and distilled water, dried at room temperature and autoclaved. These discs were seeded with two bacterial strains frequently present the oral cavity: *Streptococcus sanguinis* (CECT 480) and *Lactobacillus salivarius* (CECT 4063). The bacteria were incubated on the discs for 2 hours at 37 °C and 5 % CO_2. Subsequently, they were washed with PBS and detached in Ringers' solution. Bacterial seedings from the suspension (MRS for *Lactobacillus salivarius* and Todd-Hewitt for *Streptococcus sanguinis*) were incubated at 37 ºC for 2 days. Subsequently, the number of colonies was analysed. The variation of acidity during bacterial growth was also determined.

The discs were cleaned with phosphate buffer (PB, pH 7.2–7.4) for 5 min and then fixed with a 2.5% solution of glutaraldehyde in 0.1 M PB for 30 min at 4 °C.

This washing process was repeated twice. After washing for 5 min with PB thrice, the discs were stored at 4 °C prepared for further treatment according to the MATS.

The samples were dehydrated by 10 min exposure to a graded sequence of aqueous ethanol (30–100%) and finally dried overnight at 25ºC. Then, discs were treated by sputtering in order to coat with a carbon (Emitech k950x, Kent, UK) and can be observed by SEM.

2.8. Statistical analysis

Data were expressed as the mean ± standard deviation. Statistical analysis was performed using MINITAB® (version 18, Minitab Inc.). We used nonparametric test because although the normal distribution of each data population was confirmed by Anderson-Darling normality test, homocedasticity was ruled out (Barlett and Levene's test for homogeneity of variances). Therefore, we used Kruskal-Wallis test for multiple comparisons and U Mann-Whitney test for individual (one-to-one) comparisons. Statistical significance was set at $p<0,01$.

3. Results and Discussion.

3.1.Surface characterisation

Figure 2 shows the studied surfaces observed by electron microscopy. From this figure it can be seen that the values with the lowest roughness are the polished samples, and an increasing roughness can be seen as the size of the

abrasive alumina particles used in the sandblasting process increases. Small abrasive particles (Al2) produced a Ra ≈ 2,02 µm, whereas another size particle (Al6, Al9) let obtain Ra ≈ 4.21 µm and 7.10 µm.

Likewise, the surface of the sintered samples can be observed on the Ti6Al4V surface, showing that the welding processes of the spheres are not very severe, as they maintain the morphology of the spheres at approximately 80% of the initial volume of each sphere. In this case, the roughness is higher than 14 µm. The roughness values obtained are shown in Figure 3, where all the surfaces present statistically significant differences between them with a $p<0.01$.

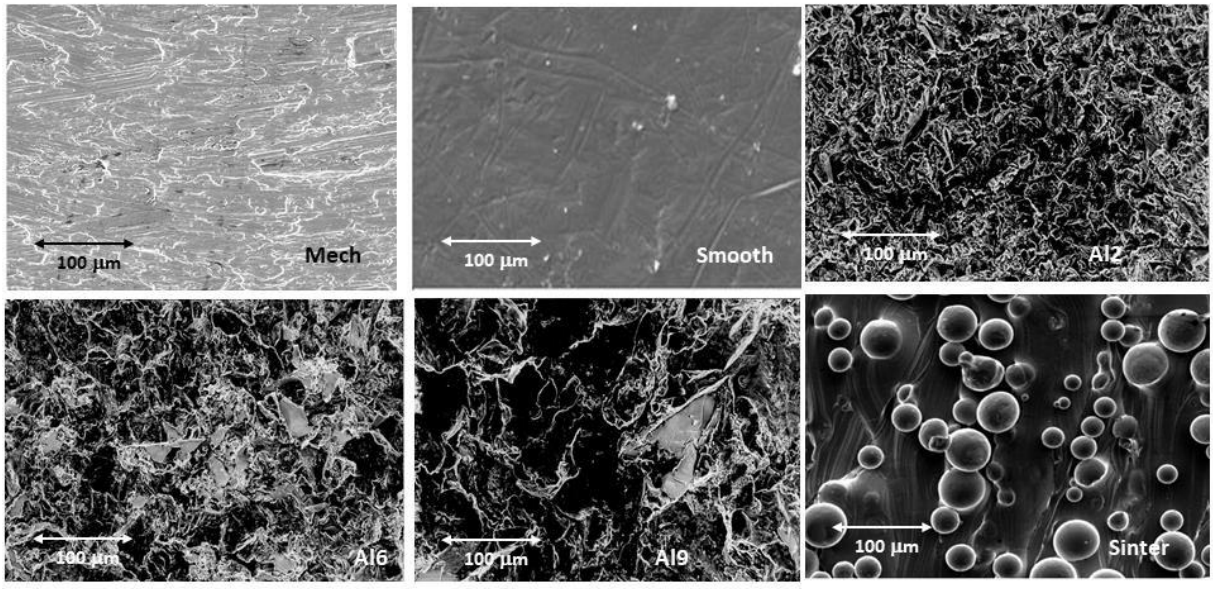

Figure 2. Surfaces observed by Scanning electron microscopy with the same magnification for each treatment studied.

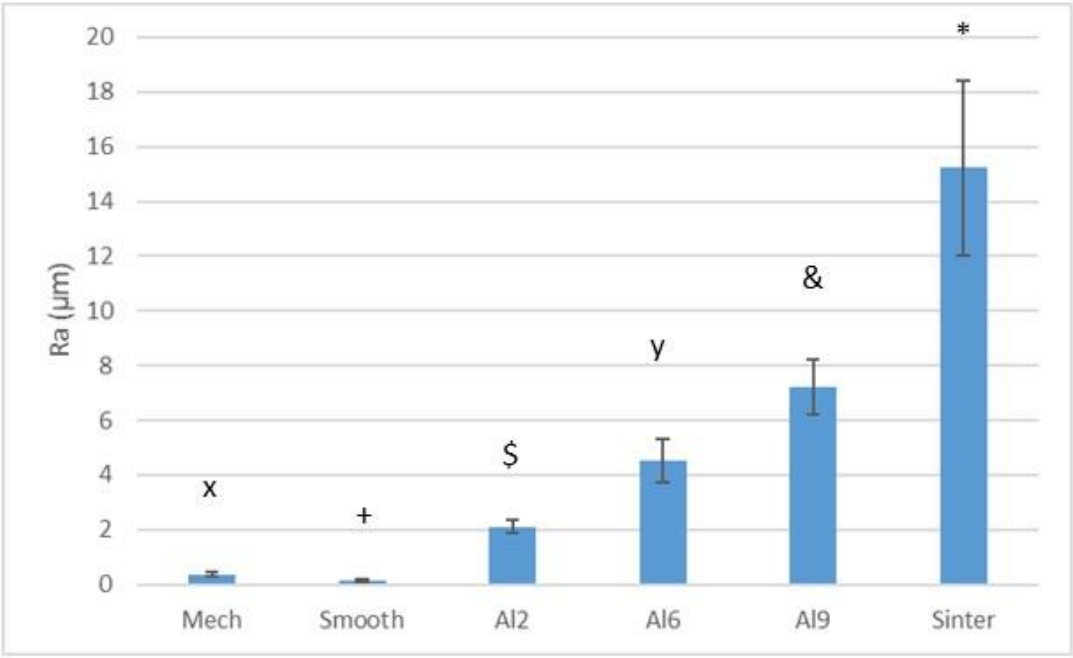

Figure 3. Roughness (Ra) obtained by each treatment. Each symbol means that the results are statistical difference significance with the others symbols. All the results present statistical difference significance with $p<0.01$. For the Ra values the different surface treatments show roughness values that are all statistically different from each other.

The contact angles results are shown in Figure 4. Contact angles values presented a good correlation with the roughness: Smooth and Mech samples (Smooth Ra ≈ 150 nm and Mech Ra ≈ 360 nm) presented a contact angle result

≤80º; while Al2 (Ra ≈2.02 µm) presented a result ≈90 º and Al6 and Al9 presented results ≥98º. The very high values of contact angles of the sintered mesh, reaching values of 150º, i.e. a very hydrophobic character, are noteworthy. This important difference could be due to the fact that the sintering treatment requires reaching very high temperatures, producing microstructural changes in the Ti6Al4V which, besides producing an important grain growth, causes a change of structure from mill annealed to Widmasntatten structures [29-31]. These structural changes could justify this important increase in the contact angle.

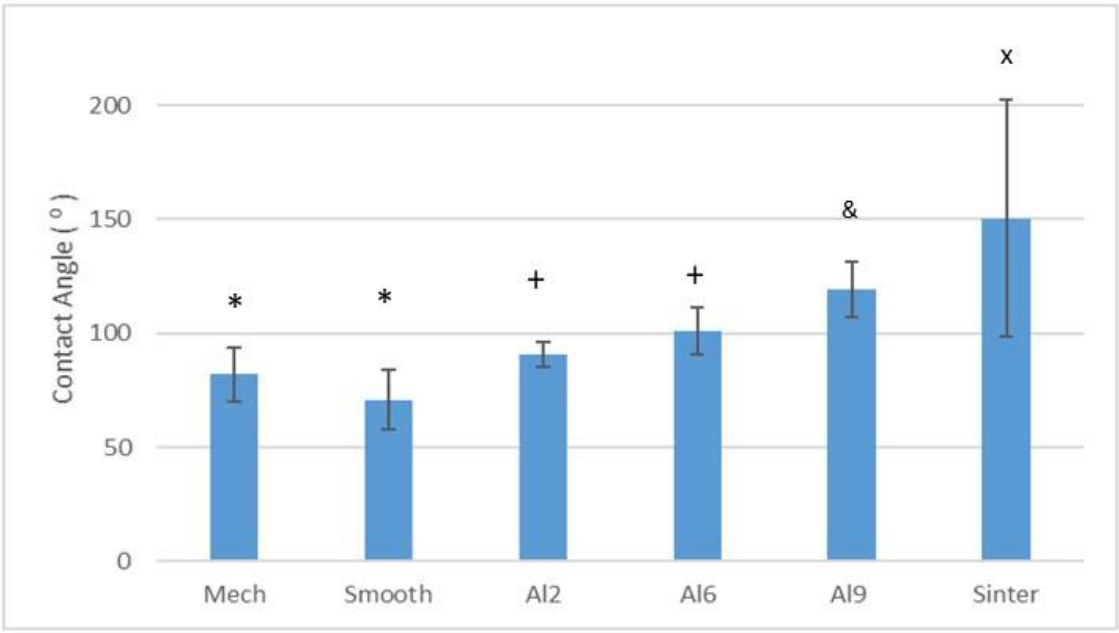

Figure 4. Contact angles obtained by each treatment. Each symbol means that the results are statistical difference significance with the others symbols $p<0.01$. The contact angles of the Sinter and Al9 samples show statistically significant differences between all other surfaces. The Mech and Smooth samples do not show significant differences between them, but they do show significant differences between all the other samples. The same is true for the Al2 and Al6 samples, which do not differ statistically from each other but do differ from the rest of the samples.

Table 1 shows the atomic compositions of the different samples studied. Ten measurements were performed for each one. The slight presence of aluminium can be observed in the samples that have been sand blasted with alumina. Also in the titanium, some traces of iron can be observed, which is a common impurity in medical grade titanium. It can be said that the samples do not have a clean surface with very little contamination.

Table 1. Chemical composition of the different surfaces analysed by dispersive energy of X-rays.

Samples	Al	V	Fe	Si	C	Ti
Mech	0.11±0.12	-	0.23±0.02	-	0.40±0.03	balance
Smooth	0.12±0.23	-	0.21±0.03	0.20±0.02	0.61±0.04	balance
Al2	1.21±0.22	-	0.30±0.04	-	0.71±0.02	balance
Al6	1.41±0.24	-	0.21±0.07	-	0.81±0.07	balance
Al9	1.63±0.35	-	0.32±0.05	-	0.51±0.03	balance
Sinter	6.40±0.52	3.80±0.12	0.51±0.04	-	0.72±0.09	balance

3.2. Cell proliferation and cytotoxicity

Fibroblast proliferation was quantified measuring the conversion of tetrazolium salts into soluble formazan dye by metabolically active cells. HFFs were cultured onto different surfaces and the absorbance at 440 nm after WST1 addition was measured at 4 hours, 1 and 3 days after cell seeding. A standard curve using serial dilutions of cell numbers was prepared to extrapolate absorbance sample values. The number of living cells after the different times for each surface can be seen in Figure 5a. As can be observed, after 4 hours of culture, there were no statistically significant differences in cell viability between any of the tested surfaces. In addition, after 72 hours there were statistically more living cells on Al2 surfaces than the other surfaces showing a statistically difference significance ($p<0.01$).

The behaviour of Al2 in which cell proliferation does not stand out at short time is because on that surface the adhesion and proliferation process has gone very fast and at those times the cells are already in the differentiation phase. Subsequently, an increase in the number of living cells is observed [32]. Therefore, we can say that the Al2 surface is the one that shows the best behaviour towards biological sealing.

As is well known, in dental meshes we need soft tissue to cover the mesh to prevent bacterial colonisation and also to prevent osteoblastic cells from adhering. If osteoblastic adhesion, proliferation and differentiation were to occur, the mesh could become osseointegrated and it would be difficult to remove the plaque once the bone regeneration biomaterial had succeeded in increasing the bone volume. This is why the mesh needs the formation of soft tissue that seals the dental mesh from bacterial attack and that this tissue forms quickly to avoid the formation of bone tissue that would make mesh removal difficult. The dentist himself removes it once the bone has regenerated.

The first step of cell adhesion to a surface is the key role for cell viability. This process depends not only on the surface chemistry, but also on the surface

roughness. Despite of its biocompatibility, it is demonstrated that fibroblasts adhere better to sandblasted samples than on Mech and Smooth samples. Although, several studies have been realised on the generation of micro and nano-roughness in order to induce cell orientation, nevertheless, a better adhesion to modified titanium was not demonstrated. Our results demonstrate that cells adhere better and proliferate earlier on Al2 surfaces, as compared with the other tested surfaces. Moreover, these results suggested that initial adhesion is more related to micro-roughness.

Cytotoxicity was assessed measuring the reduction of tetrazolium salts into formazan dye by LDH activity released by damaged cells. In Figure 5b can be observed the cytotoxicity for the different surfaces studied. Although there were only statistical differences between roughened and smooth surfaces at 4 hours, the cytotoxicity was below 10% of the positive control (Mech) result for the different times and type of surface. In no case do the surfaces show cytotoxicity, the most compatible surfaces being those with the least roughness. It is worth noting the significant difference in the sintered meshes, which reach values of almost 9%, probably due to the internal stresses caused by the welding, although this does not affect the good biological behaviour with the fibroblast cells [33-34].

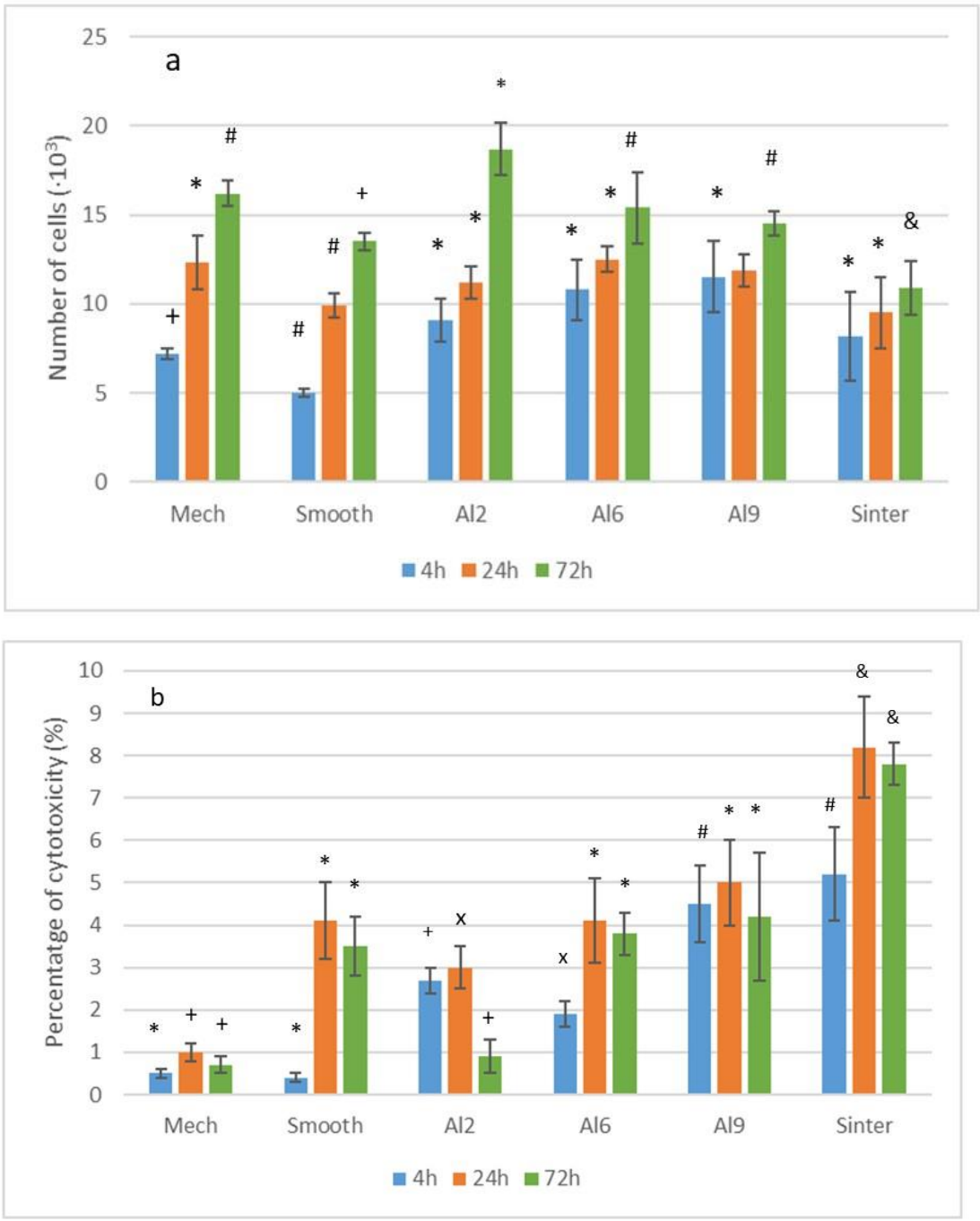

Figure 5. Analysis of cell viability onto the different micro-machined and reference surfaces at 4, 24 and 72 hours. (a) WST-1 cell proliferation tests. (b) Released LDH activity demonstrated that cytotoxic effects were less than 10% of the positive control for all the tested surfaces in all the times analysed. Each symbol means that the results, for each time, are statistical difference significance with the others symbols $p<0.01$. The statistical study was carried out for the six types

of surface for the three times studied. The differences are established for each time.

FESEM observations showed that fibroblasts were flattened and their distribution do not show any preferred orientation when were cultured on Mech and Smooth titanium after 4 hours of culture (Figure 6a). On the other hand, for the micro roughness surfaces Al2, Al6 and Al9, 4 hours after cell seeding, fibroblasts presented an elongated shape and were placed in the valleys. Moreover, cells attached on the Al2 series accommodated entirely inside the valleys, presenting a semi-flattened morphology (Figure 6b), whereas for the Al6 and Al9 series, cells grew up occupying part of the ridges (Figure 6c). At higher magnifications, it was observed that fibroblasts cells adhered to titanium by filopodia-type digitations. In Figure 6d, 6e and 6f can be observed the fibroblasts morphologies after 72 hours for Mech, Al2 and Al9, respectively. It can be seen that the cells are rounded and have different filopodia between the fibroblasts forming the soft tissue.

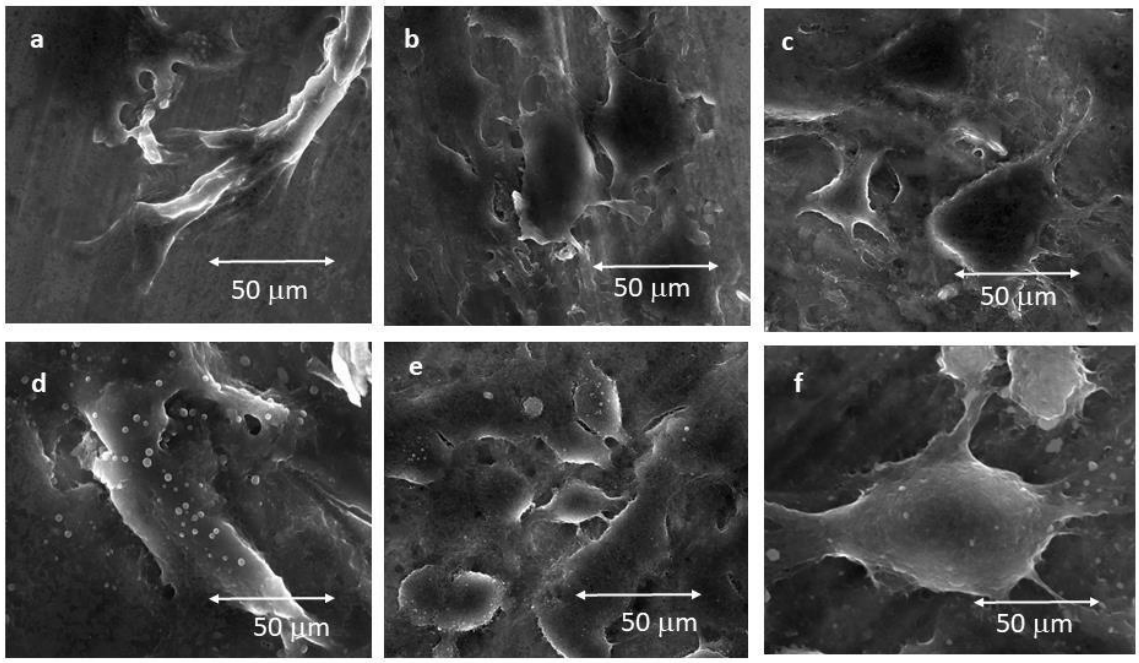

Figure 6. FESEM images of fibroblasts morphologies. a. Mech samples at 4h. b. Al2 samples at 4h. c. Al9 samples at 4h. d. Mech samples at 72h. e. Al2 samples at 72h. f. Al9 samples at 72h.

Subsequently, the possibility of the modified surfaces to activate the seeded fibroblasts was analyzed. In physiological and pathological situations, such as wound healing, fibroblasts are recruited at the injured site and they are activated to a transient state named myofibroblast. In this state, they express -SMA, a characteristic marker of smooth muscle cells that confers cytoskeleton contractility, and synthesize and remodel the extracellular matrix (ECM) until they resolve the wound [35]. After that, it is suspected that myofibroblasts disappear, mainly via apoptotic pathways induced by the mechanical load of the reconstructed ECM [36], and resident fibroblasts colonize the healed zone and proliferate. Otherwise, persistent myofibroblast proliferation and/or survival are considered an aberrant ECM repair that lead to a fibrotic disease or wound repair failure [37]. Meanwhile, after biomaterial implantation, fibroblasts must be

activated to promote fibrointegration. Fibroblasts that colonize the biomaterial, initially adhered by proteins adsorbed on it, activate to a myofibroblastic phenotype and start to remodel and secrete their own ECM until this reconstructed ECM induces their apoptosis. Nevertheless, if this process fails, it could fall into implant lost.

3.3. Microbiological behavior

Samples were observed by Scanning Electron Microscopy to determine if bacteria adhered on the different Ti6Al4V surfaces. Figure 7a shows the usual morphology of “necklace of pearls” of *Streptococcus sanguinis*, this shape demonstrates the adhesion on Ti6Al4V surface. The observed size of the bacteria ranges from 0.7 to 2.2 micrometres in diameter. It is common for two *Streptococcus sanguinis* to join at the hemispheres but they do not form large clusters or colonies as is the case with *Lactobacillus salivarius*. For this strain the “number” of bacteria has been higher on all surfaces studied in comparison with *Streptococcus sanguinis*. Besides, *Lactobacillus salivarius* shows the same configuration on the different surfaces observing small agglomerations and short chains (Fig. 7b). The size of the Lactobacillus rods is smaller than for *Streptococcus sanguinis* with values of 0.4 to 1.2 micrometres in length of the major axis. The morphologies of both bacterial species are not modified by topography.

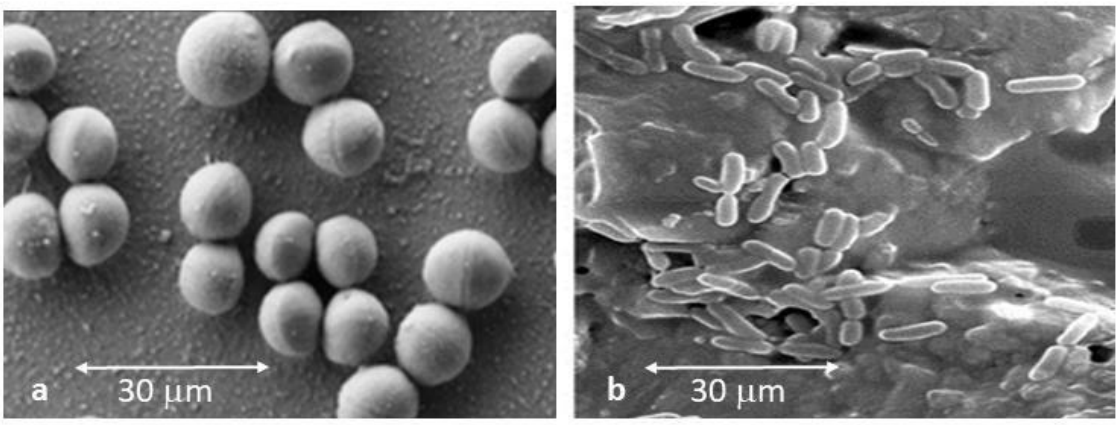

Figure 7. Bacteria strains tested in this research. a. *Streptococcus sanguinis*. b. *Lactobacillus salivarius*.

The evaluation of Colonies Forming Unities (CFU´s) per square millimeter ($p<0.005$) can be observed in Figure 7, the two bacteria strains showed low tendency to adhere on Smooth (*Lactobacillus salivarius* ~4.27 x 10^1/mm^2, *Streptococcus sanguinis* ~8.02 x10^3/mm^2) than rougher surfaces. However, on rougher surfaces Al2 can be observed the less quantity of bacteria attached in two bacteria strains studied (*Lactobacillus salivarius* ~9.73 x 10^1/mm^2, *Streptococcus sanguinis* ~5.03 x 10^3/mm^2), at the same time. These results are very significant, as a slightly rough surface such as Al2 performs slightly better than the polished surface for at least one of the strains studied. That is, sometimes the nanotextures of the surfaces can generate bactericidal behaviours, as it has been exposed in different articles when titanium samples are treated with chemical agents such as Piranha [35]. Rougher samples increase the number of CFUs: Al6 presented few CFU´s with *L. Salivarius* (~3.14 x 10^2/mm^2), whereas *Streptococcus sanguinis* (~1.03 x 10^4/mm^2) showed almost the same bacteria attached on Al9 *(Streptococcus sanguinis* ~2.50 x 10^4/mm^2) although the quantification with *Lactobacillus salivarius* was higher in Al9 (~2.90 x 10^3/mm^2). The sintered samples show the worst behaviour towards both bacterial strains of the surfaces studied. Values were obtained for *Lactobacillus*

salivarius of and *Streptococcus sanguinis* were 6.12 x 10^3/mm^2 and 9.59 x 10^4/mm^2

One aspect to be taken into consideration is that alumina sandblasting treatments have been found to have a bactericidal character. This is due to the fact that the alumina residues remaining on the surface cause a change in the surface energy of the titanium as well as its wettability characteristics in the polar and dispersive components, making the surface less favourable to bacterial colonisation [38-40].

The CFU cultured on both types of bacteria were determined and compared under the same conditions (because the actual area on the different discs is not the same). Initially, the results of CFU/mm^2 on MRS and Todd-Hewitt suspension showed a correlation with topography (rougher surfaces showed more CFU/mm^2, resulting in minimal CFU/mm^2 on the smooth surface) due to the possible effect on the interaction of the bacteria with the rough surface and the hydrophilic and/or hydrophobic character. This hydrophobic tendency is evident in the quantifications of *Streptococcus sanguinis*, where Smooth and Mech samples showed a high number of CFU/mm^2 compared to rougher surfaces such as Al2.

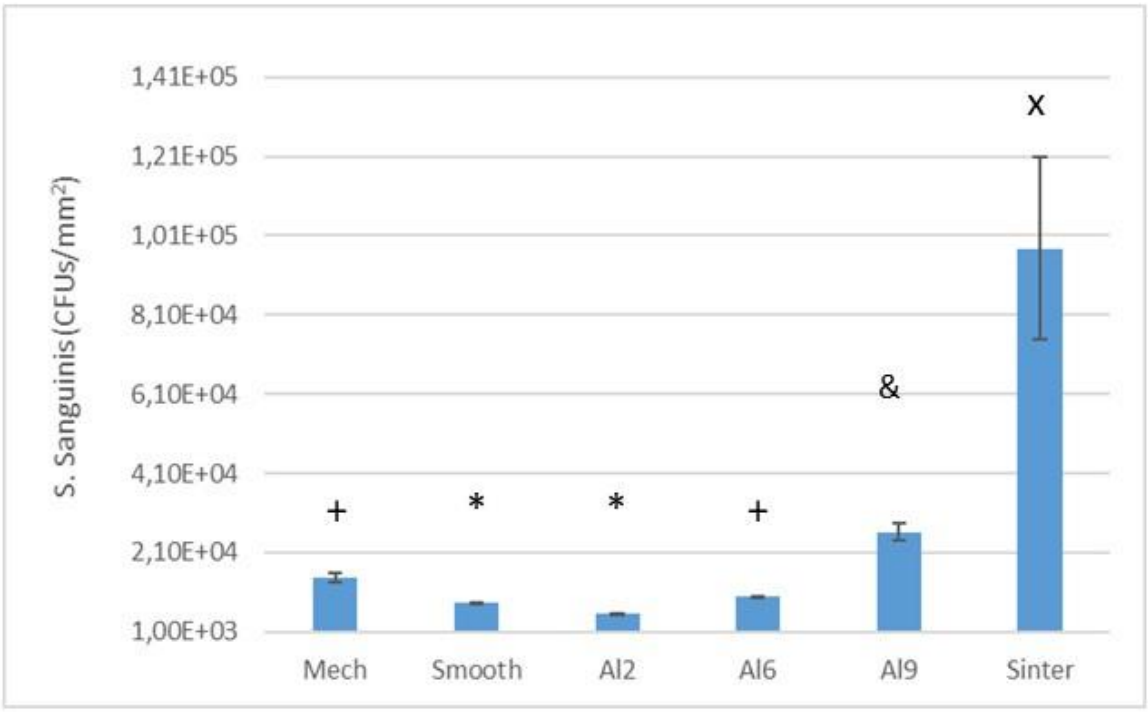

Figure 7. CFUs /mm^2 of Streptococcus sanguins for the different treatments studied. Each symbol means that the results are statistical difference significance with the others symbols $p<0.01$. For this bacterial strain, the Sinter and Al9 surfaces show statistically significant differences between them and the rest of the samples. The Al6 and Mech surfaces do not show any differences and neither do the Al2 and Smooth surfaces, but there are differences between the other surfaces.

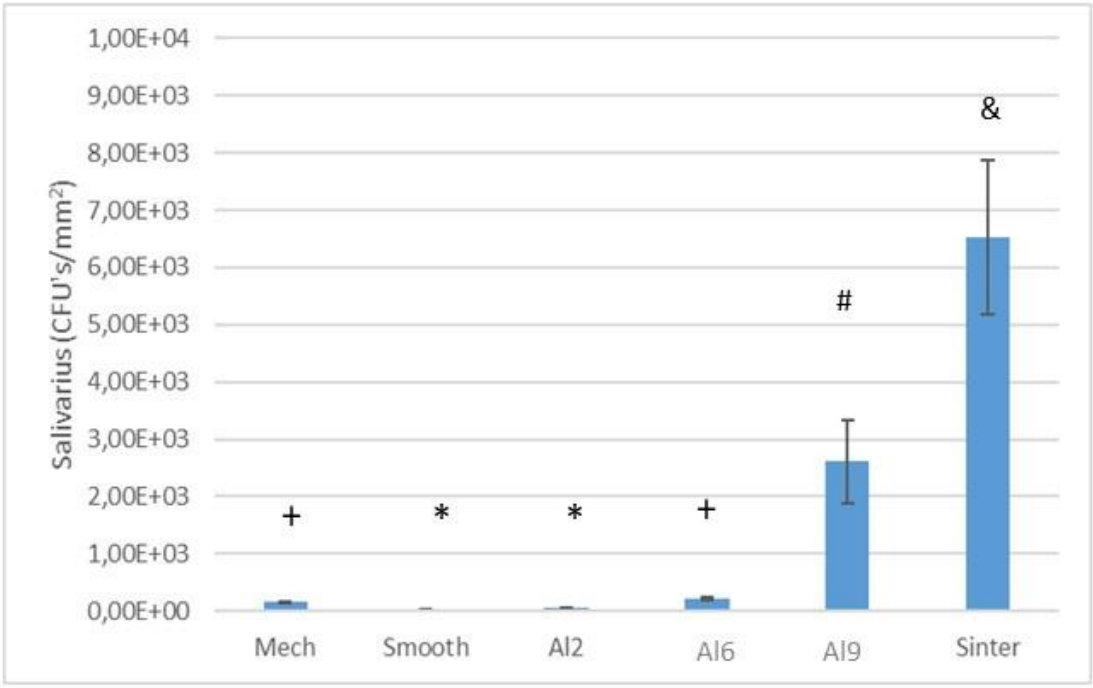

Figure 8. CFUs /mm^2 of Lactobacillus salivarius for the different treatments studied. Each symbol means that the results are statistical difference significance with the others symbols $p<0.01$. For this bacterial strain, the Sinter and Al9 surfaces show statistically significant differences between them and the rest of the samples. The Al6 and Mech surfaces do not show any differences and neither do the Al2 and Smooth surfaces, but there are differences between the other surfaces.

In cellular behavior, prevention of bacterial proliferation plays a key role in implant osseointegration. It has been stuied that microbiological infection can produce fibrosis of connective tissue around the implant, mainly via inflammatory reactions, triggering the dental implant lost [41-42]. Surface properties, such as roughness or surface free energy, are important in bacterial adhesion, formation of biofilms and development of pathologies. Generally, it is explained that bacterial adhesion is favoured on roughened surfaces, such as surface valleys,

depressions, pits and edges [43], but few studies have analysed bacterial adhesion on micro and nano-roughness combined surfaces.

These values were in accordance with Amoroso et al, who suggested a lower surface roughness cutoff value (between 34 and 155 nm) for reduced bacterial adhesion [44]. In that work, they confirmed that an increase in the roughness did not improve the attachment of P. gingivalis, because the increased size of surface irregularities was then too large to offer increased bacterial retention. Although smooth surfaces diminished bacterial adhesion, the generation of a biological seal, stimulated by microroughness surfaces, might be more critical for bacterial colonization prevention and mesh successful integration, balancing the race for the surface to greater tissue integration [45-46].

This work presents some limitations since the study of the microbiological behavior has been carried out with only two bacterial strains and no biofilm has been produced that would have allowed a better understanding of the influence of the different topographies. Also, we have taken two types of bacteria, widely used in studies since they are aerobic and anaerobic, but there are some strains with pathogenesis. Throughout the study we have followed international protocols to be able to compare with other investigations.

5. Conclusions

Six surfaces with different roughness have been studied with the aim of obtaining good fibroblast growth in order to achieve a good biological sealing in the dental mesh. In addition, the osteoblastic capacity is intended to be as small as possible to avoid osseointegration of the mesh. We have been able to determine that alumina sandblasted samples of sizes between 212 and m give the best compromise between fibroblasts and osteoblasts. Microbiological studies have determined that the roughness generated by these particles

presents a behavior very similar to the polished samples with minimal bacterial colonies on their surface. It has been shown that increased roughness leads to increased contact angles by studying wettability and thus makes the surfaces more hydrophobic.

Furthermore, this treatment shows a low bacterial adhesion (*Streptococcus sanguinis* and *Lactobacillus salivarius*) comparable to polished surfaces. We can also conclude that the increased roughness favours bacterial growth. The meshes obtained by sintering do not show good biological behavior, having the highest cytotoxicity indexes and their surface favours bacterial colonisation. Therefore, this treatment is highly recommended for dental meshes as it produces a good biological seal, does not favour osseointegration and has an excellent behaviour against bacteria.

Supplementary materials: There are no supplementary materials.

Funding: The work was also supported by the Spanish Government and the Ministry of Science and Innovation of Spain by research projects RTI2018098075-B-C21 and RTI2018-098075-B-C22 (co-funded by the European Regional Development Fund [ERDF], a way to build Europe). Authors also acknowledge Generalitat de Catalunya for funding through the 2017SGR-1165 project and the 2017SGR708 project.

Institutional review board statement: Not applicable.

Informed consent statement: Not applicable.

Ethical approval: This article does not contain any studies with human participants or animals performed by any of the authors.

Acknowledgments: The authors kindly acknowledge the collaboration of Archimedes and Meritxell Molmeneu who contributed to the development of the project.

Conflicts of interest: The authors have not any conflict of interest.

6. Conclusions

Regarding our secondary objectives, we concluded that:

1. The electropolished BoneEasy's mesh was the one that presented the lowest Ra value and was the mesh that got the closest to the reported optimal roughness degree that enhances the osteoblasts' affinity to the surface, reported as 0.5 µm. The reported differences between the surfaces were due to the divergent post-production superficial treatments applied. Mesh4U endured an electropolishing treatment of high quality that was able to deliver flawless smooth surfaces. Contrastingly, the BTK produced mesh also withstood the same polishing process but its surface displayed countless non-polished pits, exposing the less perfect treatment application.

2. Evidences of stainless-steel contamination were found on this mesh surface. The Yxoss CBR® mesh suffered a sandblasting treatment that, apart from introducing alumina and silicon impurities onto the surface, was responsible for the very high roughness values that were reported.

Regarding our primary objectives, we concluded that:

1. Piranha solution is a viable alternative method for passivating titanium dental meshes with beneficial antibacterial properties that merits further validation for its translation as a treatment applied to clinically used meshes.

2. The passivation of titanium meshes with Piranha solution improved their hydrophilicity and conferred a notably higher bactericidal activity in comparison with the meshes passivated with HCl. This unique

response can be attributed to differences in the obtained nanotextures of the TiO_2 layer. However, Piranha solution treatment decreased electrochemical stability and increased ion release as a result of the porous coating formed on the treated surfaces, which can compromise their corrosion resistance.

3. The samples treated with alumina particles by sandblasting at 200-300 micrometres give the best compromise between fibroblasts and osteoblasts. Microbiological studies have determined that the roughness generated by these particles presents a behavior very similar to the polished samples with minimal bacterial colonies on their surface. It has been shown that increased roughness leads to increased contact angles by studying wettability and thus makes the Surface more hydrophobic. Furthermore, this treatment shows a low bacterial adhesion (*Streptococcus sanguinis* and *Lactobacillus salivarius*) comparable to polished surfaces. The increased roughness favors bacterial growth. This treatment is highly recommended for dental meshes as it produces a good biological seal, does not favor osseointegration and has an excellent behavior against bacteria.
4. The meshes obtained by sintering do not show good biological behavior, having the highest cytotoxicity indexes and their surface favors bacterial colonization.

Finally, since sintered custom-made titanium meshes are already available for clinical use with good results and due to the fact that our findings merits validation for further clinical appliance, it could be promising to develop a new surface treatment protocol to sintered meshes in order to reduce exposure rates and increase better clinical outcomes. Moreover, it could also be established a line of investigation in order to apply similar surface treatments to prosthetic components.